1997-03

Diurnal variation over the tropical monsoon regions during northern summer 1991

Jiminez, Greg M

Monterey, California. Naval Postgraduate School

NAVAL POSTGRADUATE SCHOOL
Monterey, California

THESIS

DIURNAL VARIATION OVER THE TROPICAL MONSOON REGIONS DURING NORTHERN SUMMER 1991

by

Greg M. Jimenez

March 1997

Thesis Advisor: Chih-Pei Chang
Co-Advisor: Peter C. Chu

Approved for public release; distribution is unlimited.

DUDLEY KNOX LIBRARY
NAVAL POSTGRADUATE SCHOOL
MONTEREY CA 93943-5101

REPORT DOCUMENTATION PAGE

Form Approved OMB No. 0704-0188

1. AGENCY USE ONLY *(Leave blank)*	2. REPORT DATE March 1997	3. REPORT TYPE AND DATES COVERED Master's Thesis

4. TITLE AND SUBTITLE DIURNAL VARIATION OVER THE TROPICAL MONSOON REGIONS DURING NORTHERN SUMMER 1991

5. FUNDING NUMBERS

6. AUTHOR(S) Jimenez, Greg M.

7. PERFORMING ORGANIZATION NAME(S) AND ADDRESS(ES)
Naval Postgraduate School
Monterey CA 93943-5000

8. PERFORMING ORGANIZATION REPORT NUMBER

9. SPONSORING/MONITORING AGENCY NAME(S) AND ADDRESS(ES)

10. SPONSORING/MONITORING AGENCY REPORT NUMBER

11. SUPPLEMENTARY NOTES The views expressed in this thesis are those of the author and do not reflect the official policy or position of the Department of Defense or the U.S. Government.

12a. DISTRIBUTION/AVAILABILITY STATEMENT
Approved for public release; distribution is unlimited.

12b. DISTRIBUTION CODE

13. ABSTRACT *(maximum 200 words)*

This study examines diurnal variation of convection over western India, the Bay of Bengal, Indochina and the northern South China Sea during the 1991 northern summer monsoon using combined Japanese (GMS) and Indian (INSAT) geostationary satellite data, ECMWF 850 hPa wind data, and NCEP sea surface temperature analyses.

The diurnal cycle is examined in terms of spatial and temporal structure prior to onset and during the monsoon. The northern South China Sea is examined to determine how different periods of synoptic influences resulted in an anomalously strong diurnal signal during June. The wind and SST data are used to examine the relationship between the diurnal variation of convection and both low-level convergence and vertical latent heat fluxes.

Convection over west India is most common during May and June and starts as a diurnal system over land that becomes organized and propagates westward over the east Arabian Sea. The Bay of Bengal follows the classic land-sea breeze model and convection is modulated by convergence between the land breeze and large-scale monsoon flow. The diurnal cycle is generally enhanced over the ocean during active phases of convective activity. The maximum latent heat fluxes generally occurs prior to maximum convection due to strong monsoon flow enhancing evaporation.

14. SUBJECT TERMS
DIURNAL VARIATION, WEST INDIA, ONSET OF NORTHERN SUMMER MONSOON OVER INDIA, MONSOON CONVECTION

15. NUMBER OF PAGES 175

16. PRICE CODE

17. SECURITY CLASSIFICATION OF REPORT	18. SECURITY CLASSIFICATION OF THIS PAGE	19. SECURITY CLASSIFICATION OF ABSTRACT	20. LIMITATION OF ABSTRACT
Unclassified	Unclassified	Unclassified	UL

NSN 7540-01-280-5500

Standard Form 298 (Rev. 2-89)
Prescribed by ANSI Std. 239-18 298-102

DIURNAL VARIATION OVER THE TROPICAL MONSOON REGIONS DURING NORTHERN SUMMER 1991

Greg M. Jimenez
Lieutenant, United States Navy
B.S., Colorado School of Mines, 1986

Submitted in partial fulfillment
of the requirements for the degrees of

MASTER OF SCIENCE IN METEOROLOGY
MASTER OF SCIENCE IN PHYSICAL OCEANOGRAPHY

from the

NAVAL POSTGRADUATE SCHOOL
March 1997

ABSTRACT

This study examines diurnal variation of convection over western India, the Bay of Bengal, Indochina and the northern South China Sea during the 1991 northern summer monsoon using combined Japanese (GMS) and Indian (INSAT) geostationary satellite data, ECMWF 850 hPa wind data, and NCEP sea surface temperature analyses.

The diurnal cycle is examined in terms of spatial and temporal structure prior to onset and during the monsoon. The northern South China Sea is examined to determine how different periods of synoptic influences resulted in an anomalously strong diurnal signal during June. The wind and SST data are used to examine the relationship between the diurnal variation of convection and both low-level convergence and vertical latent heat fluxes.

Convection over west India is most common during May and June and starts as a diurnal system over land that becomes organized and propagates westward over the east Arabian Sea. The Bay of Bengal follows the classic land-sea breeze model and convection is modulated by convergence between the land breeze and large-scale monsoon flow. The diurnal cycle is generally enhanced over the ocean during active phases of convective activity. The maximum latent heat fluxes generally occurs prior to maximum convection due to strong monsoon flow enhancing evaporation.

TABLE OF CONTENTS

ACKNOWLEDGEMENT

I never would have been able to complete this work without the help of a few key individuals. I would like to thank my two advisors, Professors C.P.Chang and Peter Chu for their guidance, counsel and enthusiasm throughout this entire endeavor.

Most importantly, I thank my wife, Patty for her love, support and patience; and my son, Bradley for keeping me focussed on the important things in life and always making sure I took time to enjoy it.

I. INTRODUCTION

Diurnal variations in deep convection have been observed in many parts of the tropics. In general, the amplitude of the variations is large over land areas, particularly in the vicinity of coastal regions where convergence due to the land-sea breeze further enhances the diurnal heating of the boundary layer over land. From satellite observations, the maximum convection over the land area, as represented by the cloud top black body temperature, generally occurs in the late afternoon or evening. This is because the convective system usually continues to develop after it starts in the afternoon when the surface heating reaches a maximum (Murakami, 1983). The continuous development leads to expanded cloud cover in the evening. This expansion results in the peak time being reflected in the satellite temperature data a few hours after the maximum surface heating in the afternoon. This peak time can also be 1-2 hours after the maximum precipitation (Oki and Musiake, 1994).

However, the diurnal convection maximum over the ocean has been reported to occur at different times. Near the coasts of large tropical islands the ocean diurnal convective peak tends to occur in the morning during both January and July (Nitta and Sekine, 1994). A typical example is the diurnal system over northern Borneo during the northern winter monsoon. During the Winter Monsoon Experiment, Houze et al. (1981) observed that the convection reaches a maximum in the evening inland of the northwestern Borneo coast, and in the early morning about 100 km offshore. They attributed the occurrence of this convection to the convergence produced by the northeast monsoon winds and the land breeze. Similar morning ocean convection maxima were reported by Murakami (1983), Chen

and Takahashi (1995) and others near other large islands in the maritime continent during both January and July. Nitta and Sekine (1994) also stressed the importance of the large-scale onshore wind in the production of the morning convection peak over the coastal ocean. They noted that in November the mean wind is onshore and can provide a convergence mechanism with the land breeze at night. This is when a strong morning peak of convection is observed off the northwest Borneo coast. In March the mean wind is easterly and the morning peak is obscure.

In the Bay of Bengal and the South China Sea, maximum diurnal convection was observed to occur near noon or early afternoon (e.g., Nitta and Sekine, 1994). Over the open ocean of the Pacific and Atlantic, diurnal convection peaks have been reported both in the early morning and in the afternoon, (Gray and Jacobson, 1977; Augustein, 1984; Albright et al., 1985; Nitta and Sekine, 1994), leading several investigators to call attention to the existence of semi-diurnal variations. Gray and Jacobson (1977) proposed that differential longwave cooling during the night between cloud clusters and the surrounding clear areas causes subsidence around cloud clusters and enhances convergence underneath, resulting in the maximum early morning convection. However, recently Chen and Houze (1997) noted that radiative processes may play only a minor role in deep convective systems. They argued that since cloud clusters develop in the presence of large-scale forcing, once formed they are largely controlled by non-radiative processes (dynamic, thermodynamic, cloud physical, and boundary layer). The deep convection starts during the day when heating at the ocean surface reaches a maximum, but the large-scale organizing processes cause the convection to

continue and develop well into the night until pre-dawn hours when the life cycle of the convection cannot be sustained any longer. Thus, the convection under the active phase of large-scale forcing reaches its maximum in the early morning. They also proposed that the spatially-small convection systems that develop in the absence of large forcing are in phase with the solar cycle, with maximum convection occurring in the early afternoon.

The possible interactions of the large-scale tropical disturbance and the diurnal variations were also studied by Nitta and Sekine (1994), Chen and Takahashi (1995) and Murakami et al. (1996), especially on the differences between active and inactive phases of the intra-seasonal oscillations. In most cases, their results show that the diurnal cycle becomes more prominent in the active phase, particularly over the open ocean. Chen and Takahashi (1995) reported that the large cloud cover associated with the active phase of the intra-seasonal disturbance may suppress the diurnal amplitude over the maritime continent islands because of the reduction of land-sea thermal contrast. They did not find any significant difference on the phase of the diurnal cycle between active and inactive periods. However, Murakami et al. (1996) reported that the active phase tends to advance the peaking of diurnal convection while the inactive phase tends to delay it.

These previous studies were mostly based on precipitation data and on the geostationary satellite data that provides broad area coverage at high temporal resolutions. Over the western Pacific and vicinity high-resolution cloud-top black-body temperature (Tbb) data have been measured by the Japanese Geostationary Meteorological Satellite (GMS) since 1979. Previous studies of convection over the East Arabian Sea and Indian Ocean have

been possible only with twice daily OLR (outgoing longwave radiation) data. The OLR data is only available at 00Z and 12Z. Therefore, it has not been possible to study diurnal variation over the entire tropical region using continuous high temporal resolution satellite imagery.

Recently, a merged set of three-hourly, 1°x1° resolution Tbb data taken from the Indian INSAT and the GMS from May to August 1991 became available from the Meteorological Research Institute of the Japan Meteorological Agency. This data set provides an opportunity to study the diurnal variation of deep convection in the broad tropical oceans under the influence of the Asian summer monsoon, from the Indian Ocean to the western Pacific.

The availability of this data allows us to document the diurnal cycle across the tropical oceans, especially over the east Arabian Sea, India subcontinent and western Bay of Bengal. Once the diurnal cycle of convection is established from satellite data, other fields such as winds, can be evaluated in terms of the dynamic support provided for the observed convection.

The main purpose of this study is to use this merged INSAT-GMS data, together with the four times per day, 1.125°x1.125° resolution European Center for Medium-range Weather Forecasting (ECMWF) 850 hPa wind analysis, to study the diurnal variation in this area. Since upper air reports are sparse in this region, particularly over the oceans, the diurnal cycle in the ECMWF 850 hPa wind and convergence fields is strongly influenced by model physics.

The northern summer monsoon region will be divided into four sub-regions for more detailed analysis: Western India and the Eastern Arabian Sea, Bay of Bengal, Indochina Peninsula and the northern South China Sea. These sub-regions are diurnally active areas with several kilometers of coastline following the classic land-sea breeze model, but they also deviate from the model due to influences by topography, coastline geometry and large-scale forcing.

Although the diurnal cycle is well documented over the South China Sea and western Pacific, special attention is paid to the northern South China Sea during June 1991. An anomaly exists this month where the diurnal cycle is similar in phase but significantly stronger in amplitude when compared to a ten-year climatology. During June, there were two separate large-scale events over the northern South China Sea that either impacted or had an impact on the diurnal cycle.

The second purpose of this study is to evaluate the diurnal cycle in the ECMWF wind analysis, based on comparisons with the diurnal cycle of Tbb-inferred convection. We will focus on regions of land masses and their surrounding oceans where the convection is more active and the ECMWF analysis has somewhat better observational basis than wide-open oceans. If the model fields adequately represent low-level convergence prior to convective maxima over both land and coastal ocean regions as expected, then the diurnal cycle may be described by both convective index and low-level wind fields. The relationship between convergence and convection will also be examined in terms of diurnal and monthly mean fields of convective index and convergence.

A good correlation is expected over land and between the monthly mean convective index and mean convergence. Cases where convergence and convective index fields disagree may be due to poor data (over the ocean) and other influences such as tropical cyclones, topography, sub-grid scale or meso-scale processes and complex land-sea breeze circulations.

The third purpose is to examine air-sea interaction by looking at the relationship between convective activity, latent heat fluxes and sea surface temperature. Murakami et al. (1995) looked at the combined INSAT-GMS IR data set along with split window SST data and found active convection corresponded with cool SST over the Arabian Sea in 1988 while weak convection corresponded with warm SST in 1987. However, water vapor over the Arabian Sea corresponded positively with convective activity. Regardless of SST, strong southwesterly monsoonal flow enhanced evaporation, increasing convective activity over southern India.

Rao et al. (1981) found well-marked diurnal variations in wet-bulb depression and sea surface temperature over the Arabian Sea and Bay of Bengal during May-June, June-July, and August of 1977. They were unable to detect any diurnal signal in the winds. The most rapid evaporation occurred prior to monsoon onset due to the relatively dry air at both locations.

Pisharoty (1965, 1981) studied latent heat fluxes in the northern Indian Ocean from May through September using ten years of data. He computed weekly latent heat fluxes across the west coast of India from the Arabian Sea. He found that a drop in areal averaged sea surface temperature occurred with the onset of southwesterly winds and a large, negative

latent heat flux from the adjacent waters had a positive correlation with the onset of strong convection over the Indian sub-continent.

Additional studies (Cornejo-Garrido and Stone, 1977; Ramage and Hori, 1981; Rasmussen and Carpenter, 1982) suggest that convective activity in the tropics is closely associated with sea surface temperature anomalies, which in turn govern the transfer of latent heat to and from the atmosphere. Prior to monsoon onset, the highest average sea surface temperatures observed in the northern Indian Ocean were between 30.5 and 31.0° C. After onset, the average sea surface temperatures were between 28.0 and 29.0 °C, demonstrating a drop of approximately 2.0 °C during onset of the monsoon. Our specific objectives are:

1. To describe the diurnal variations in the vicinity of the India subcontinent, from the eastern Arabian Sea to the Bay of Bengal, and compare the structures over land and sea with those in other parts of the tropical monsoon region.

2. To examine the extent that the diurnal variations in convection determined from Tbb can be represented by the ECMWF wind analysis.

3. To compare the diurnal variations during different periods of synoptic influences in the northern South China Sea.

4. To examine the relationship between the diurnal variations in latent heat fluxes and convection over the oceans in each sub-region.

II. DATA AND METHODOLOGY

A. SATELLITE IMAGERY

The combined 3-hourly IR TBB (infrared equivalent black body temperature) data set for May through September of 1991 are derived from the Geostationary Meteorological Satellite (GMS) of Japan and the INSAT of India imageries at 1° x 1° grid points. This data was provided by Dr. Matsuto Murakami of the Meteorological Research Institute (MRI) in Tsukuba, Japan. The INSAT was located above 82°E over the equator and its observation footprint covered the latitudinal range roughly from 40°E to 120°E. The GMS was located above 140°E over the equator covering the longitudinal range roughly from 80°E to 160°W. The inter-calibration between GMS and INSAT was carried out by MRI utilizing the overlapping area from 110°E-115°E. The composition of these two geostationary satellites resulted in full coverage of the entire Asian monsoon region (40°E-160°W, 50°N-50°S) providing finer spatial and temporal resolution than the generally available OLR (Out-going Longwave Radiation) data used in many previous studies.

A sub-section of the initial data coverage was chosen to concentrate on the western Pacific to Indian Ocean portion of the 1991 northern summer monsoon. The longitudinal range (63°E-153°E) and the latitudinal range (18°S-27°N) were chosen to match boundary grid points of subsequent data sets used in these investigations. Quality control of each data point was necessary (particularly in the case of the INSAT data, which has more missing

data than the GMS). Approximately ten percent of the INSAT data was bad or missing each month. These data were removed prior to computing convective indices.

Deep convective activity is represented by the following convective index (CI) (Nitta, 1983) at each grid point.

$$CI=255-T_{bb},\ if\ T_{bb}<255°K \tag{1a}$$

$$CI=0,\ if\ T_{bb}>255°K \tag{1b}$$

where 255° K represents the mean air temperature around 400 hPa. The convective index, CI, corresponds to deep convective activity above 400 hPa. Use of this convective index also eliminates the effects of surface temperature as all the land surfaces are below the level of 500 hPa.

The CI for each month was composited with respect to the eight three-hourly observation times each day. The monthly mean CI, ($\overline{CI}$) is then removed from the composites resulting in a diurnal convective index anomaly seen in equation 2.

$$CI'=CI-\overline{CI} \tag{2}$$

Following McGarry and Reed (1978), Fourier analysis is applied to each of the eight three-hourly composites to determine the phase and amplitude of the first or diurnal component. Each phase is adjusted to the local time. The results are used to represent the mean phase and amplitude of the diurnal cycle for each month.

B. WIND DATA

The model data used is from the European Center for Medium Range Weather Forecasting (ECMWF) Advanced Operational Data Set, four times daily (00Z, 06Z, 12Z, 18Z GMT), fields. These are un-initialized analyses of geopotential, temperature, u and v components of horizontal wind, and relative humidity at fourteen pressure levels in the troposphere. The data was converted from spherical harmonics to a Gaussian grid, yielding a final horizontal resolution of 1.125°. Over regions where elevations exceed the 850 hPa level, the ECMWF surface wind is substituted for the 850 hPa wind.

Monthly mean and six-hourly composite 850 mb wind fields (V850) and anomaly composites have been constructed for each of the 4 times of the day using the same technique described above for CI. Plots of wind anomaly composites contain vectors that have been normalized so the largest magnitude represented is consistent for each of the four times of the day. Plots of mean wind fields have not been normalized.

Divergence was computed from the gridded data using finite differencing techniques with the following equation:

$$D850=\overline{\nabla}\cdot\overline{V}=\partial u/\partial x+\partial v/\partial y \qquad (3)$$

Monthly mean and six- hourly composite 850 mb divergence fields (D850) have been constructed for each of the four times of the day as well. The departure from the mean or low

level divergence composite anomaly was computed using the same techniques as above:

$$D850' = D850 - \overline{D850} \tag{4}$$

Fourier analysis was also applied to each of the four six-hourly composites to determine the phase and amplitude of the first or diurnal component. Each phase is adjusted to the local time. The diurnal cycle phase and amplitude of divergence are compared with those of CI.

C. OCEANOGRAPHIC DATA

Optimum interpolation (OI) global sea surface temperature (SST) data set from the National Center for Environmental Prediction (NCEP) was used, together with ECMWF gridded data, to study air-sea thermal interaction. The analyses use in situ and satellite SST, produced weekly on a one-degree grid. Satellite data were adjusted for biases using the method of Reynolds (1988) and Reynolds and Marsico (1993). The bias correction adds a small amount of noise in time, which was eliminated using a 1/4-1/2-1/4 binomial filter. The weeks were defined to be centered on Wednesday at 0000Z, in agreement with the definition used for ocean modeling. Each data point was linearly interpolated in time between weeks to match the temporal frequency of the ECMWF data (0000Z, 0600Z, 1200Z, and 1800Z daily). More exact interpolation schemes were not used due to small SST variance.

To study the exchange of heat across the air-sea interface, and its possible effect on convective activity, the vertical latent heat fluxes were computed as detailed below. Gridded data were converted from the one-degree by one-degree grid of the original NCEP SST data

set to the Gaussian grid used by ECMWF by using an OI scheme and finite difference methods described by Schlatter (1975). The remainder of this chapter describes the method used to calculate the latent fluxes. The magnitude of total velocity (W_{10}) at 10 meters was calculated from individual components of velocity as:

$$W_{10}=\sqrt{U_{10}^{2}+V_{10}^{2}} \quad . \qquad (5)$$

Surface latent heat flux was computed using the method of Buck (1981), beginning with the following equation for saturation vapor pressure (e_s):

$$e_s=6.1121\exp\left(\frac{17.502T_{sfc\ air}}{240.97+T_{sfc\ air}}\right)(1.0007+3.46E{-}6\ P_{SFC}) \quad . \qquad (6)$$

$T_{sfc\ air}$ is the air temperature in °C just above the ocean surface; and P_{SFC} is surface pressure in hPa. The saturation mixing ratio (w_s) was then defined as:

$$w_s=.622\frac{e_s}{p-e_s} \quad . \qquad (7)$$

Relative humidity (r) was available in the ECMWF data, so the mixing ratio (w) was approximated as:

$$w\approx rw_s \quad . \qquad (8)$$

The specific humidity of air at the surface of the water and the specific humidity in the air above the surface (q_s and q, equations (9) and (10), respectively) were then derived as:

$$q_s = \frac{w_s}{w_s + 1} \qquad (9)$$

$$q = \frac{w}{w + 1} \; . \qquad (10)$$

The air density was calculated using the virtual temperature (T_v) and the ideal gas law:

$$T_v = T_{sfc\ air} \frac{(1 + 1.60779w)}{(1 + w)} \qquad (11)$$

$$\rho_{air} = 3.4838 \; x \; 10^{-4} \frac{P}{T_v} \; . \qquad (12)$$

The neutral value for the drag coefficient of momentum was taken from Garratt (1977):

$$C_{DN} = 7.5 \; x \; 10^{-7} W_{10} \; . \qquad (13)$$

The transfer coefficient for latent heat exchange was assumed to be constant (C_{EN}=.0014). The variation of the transfer coefficient with wind speed is much smaller than that of the drag coefficient, and there will only be significant error at wind speeds exceeding 25 m/s.

The stability correction to the neutral drag coefficients was taken from Kondo (1975), starting with a stability parameter (S) defined as:

$$S=S_O\frac{|S_O|}{|S_O|+0.01} \qquad (14)$$

where

$$S_O=\frac{T_{SST}-T_{SFC\ AIR}}{W_{10}^{\ 2}},\quad for\ z=10m\ . \qquad (15)$$

Applying the stability correction to the neutral transfer coefficients yields the transfer coefficients for diabatic conditions (SI units):

(a) *for stable conditions* (T_{SST}-$T_{SFC\ AIR}$ < 0):

$$C_{DN\ corrected}=C_{DN}[0.01+0.03S+0.9e^{4.8S}],\quad for\ -3.3<S<0 \qquad (16)$$

$$C_{EN\ corrected}\approx C_{EN}[0.01+0.03S+0.9e^{4.8S}],\quad for\ -3.3<S<0 \qquad (17)$$

$$C_{DN\ corrected} \approx C_{EN\ corrected} \approx 0, \quad for\ S \leq -3.3 \qquad (18)$$

(b) *for unstable conditions* (T_{SST}-$T_{SFC\ AIR} > 0$):

$$C_{DN\ corrected} \approx C_{DN}[1.0+0.47S^{0.5}] \qquad (19)$$

$$C_{EN\ corrected} \approx C_{EN}[1.0+0.63S^{0.5}] \qquad (20)$$

The magnitude of the surface wind stress (τ) was then computed using:

$$\tau = \rho_{air} C_{DN} W_{10}^{\ 2} \qquad (21)$$

The vertical latent heat flux (Q_E) was computed using the standard bulk formula (after Wyrtki, 1965) as follows:

$$Q_E = -\rho_{air} C_{EN} L(q_s - q) W_{10} \qquad (22)$$

This formula utilizes the convention that negative (positive) values represent a heat transfer from (to) the ocean to (from) the atmosphere. The fluxes were composited as detailed above and Fourier analysis was applied to each of the four six-hourly composites to determine the phase and amplitude of the first or diurnal component. Each phase is adjusted to the local time. The diurnal cycle phase and amplitude of the latent heat flux are compared with those of CI.

D. REMARKS

When the comparison of different fields shows inconsistencies, we assign different confidence levels on the data. The CI is based on direct satellite measurements and therefore receives the highest confidence. This is followed by V850 where we expect the EC assimilation system gives reasonable analysis especially over the land areas. The D850 is most uncertain both due to the difficult nature of observing and computing divergence and also the dominance of model dynamics. We further expect that the CI is almost equally reliable in representing deep convection both for the monthly means and the diurnal cycles, although the diurnal amplitude and phase calculations depend on the Fourier decomposition and are not as quantitatively accurate as the diurnal cycles represented by the three-hourly interval composites. The diurnal cycles of the V850 and D850 both represent a higher degree of uncertainty than their monthly means. This is because the upper air reports are generally available no more than twice a day, so the diurnal cycle of the V850 and D850 are strongly influenced by the diurnal cycle of the EC model. And again, the diurnal amplitude and phase calculations are less reliable than direct composites at different local time. This is more so than the CI as wind data are available only four times a day.

The lead/lag phase relationship contour plots summarize the time difference between wind data (divergence, fluxes) and CI. Since the wind and CI data sets have different spatial resolutions, these time estimates are crude approximations based on comparing the closest common grid points.

Because of the strong influence by the local topography (Figure 1) , the diurnal cycle of convection is highly location dependent and shows mesoscale spatial structures. Therefore, the results will be discussed according to different sub-regions within the area of study.

Each of the sub-regions spans two time zones. The convention throughout the text will be to use the western local time when referring to the diurnal cycle of events. Since each sub-region is a subset of the original dat set, vectors along boundaries may have been truncated so there magnitudes may be questionable. For clarification, the term Indian subcontinent refers to the region of India bounded by the east Arabian Sea and Bay of Bengal.

In this study, the diurnal cycle as determined from the CI and the 850 hPa divergence for each of the four months, May, June, July and August will be discussed for each of the sub-regions. The sub-regions are: Western India and Eastern Arabian Sea, Bay of Bengal, Indochina Peninsula and the northern South China Sea. August turns out to be less interesting for diurnal variation in western India as the convection has all moved to the north (foothills of the Tibetan Plateau). The discussion will be organized as follows. First, the monthly-mean fields of CI, 850 hPa wind (V850) and 850 hPa divergence (D850) will be reviewed. We will note possible associations between the deep convection distribution with the general 850 hPa flow pattern. This will be followed by the presentation of the diurnal cycles of CI and D850. The discussion will focus on the spatial and temporal structure of the diurnal cycle of CI, its relationships with the diurnal cycle of D850, and the mean distributions of convection and winds. The mean convection and flow patterns vary from one month to another as the northern summer monsoon evolves. The month-to-month variations of the

diurnal cycle relative to the intra-seasonal changes provides an analysis of the effect of the active regime and inactive regime to the diurnal cycles in each sub-region.

III. WESTERN INDIA AND EASTERN ARABIAN SEA

A. MAY 1991

Figure 2 shows the mean V850 of May 1991. This is in the late boreal spring transition season prior to the onset of the South Asian summer monsoon and northerly winds at 850 hPa prevail over most of the eastern Arabian Sea and western India. Two nearly perpendicular trough (cyclonic vorticity) systems are connected near the tip of the Indian subcontinent. The near-meridional one extends northward from the southern tip of the Indian subcontinent towards northeastern India. This is the trough between the subtropical highs over the Arabian Sea and the Bay of Bengal. The near-zonal trough extends westward along the northern equatorial Indian Ocean, which is a manifestation of the Intertropical Convergence Zone (ITCZ) between 5°N-10°N.

Figure 3 shows the distribution of the monthly mean CI, which for May is generally concentrated in the lower latitudes as the monsoon convection has not started. The two CI maxima, one in southwestern India and another in the northern equatorial Indian Ocean to the southwest of India, basically near the cyclonic shear regions in the monthly-mean V850 (Figure 2). Relative to the meridional trough, the western location of the southern India convective region appears to be influenced by the high terrain there (Figure 1). The CI values of 4-5° K in both CI maximum regions are relatively modest compared to the monthly mean maxima that will be shown elsewhere in other areas of this study. Convection in both the

trough and the northern equatorial ITCZ are also much less active compared to the western Pacific ITCZ or the South Pacific Convergence Zone.

The mean D850 is shown in Figure 4. The strongest 850 hPa convergence occurs over the interior of India in the cyclonic trough region. This convergence may be expected from heating over the land and is basically consistent with the location of the trough. However, it overlaps with only the northeastern perimeter of the mean CI maximum over southwestern India. The western perimeter of the CI maximum is actually occupied by a weak divergence center, raising questions on the quality of the D850 analysis along the west coast of India. The maximum divergence regions are over northwest India centered at 22°N, 73°E and northeastern India near 18°N, 80°E (off the diagram).

A convergence maximum is not observed along the northern equatorial Indian Ocean ITCZ southwest of India. This is over open ocean with nearly no upper air data. A global assimilation model would need to be able to properly simulate the location of the ITCZ in late Spring over the Indian Ocean to give a corresponding low-level convergence maximum.

Figure 5 shows the amplitude and phase distribution of the diurnal cycle of CI with a vector convention, where the vector length is proportional to the amplitude and the direction indicates the local time in a 24-hour clock with midnight pointing northward. The amplitude is also plotted in Figure 6 where the distribution of all four months are compared. The largest amplitude of diurnal cycle is in the western half of the India Subcontinent with the maximum convection occurring in late evening between 9 and 11 p.m. Local Time (LT). The amplitude decreases offshore to the west and the maximum convection phase undergoes a

continuous shift, first to late night near the western coast, then to early morning over the water near shore, and eventually turning to late morning or noon around 68°E where the diurnal system appears to end.

The nearly 180° out-of-phase relationship between this longitude and the western interior seems to suggest that this is related to a land-sea breeze circulation. Compared to the diurnal cycle observed near the northwestern coast of Borneo during northern winter monsoon, which is also strongly influenced by a significant land sea breeze circulation (Houze et al., 1981), the area covered by the western India diurnal cycle is significantly larger. The Indian system has a horizontal dimension normal to the coast of about 1000 km, almost three times that of the Borneo system. In the Borneo system the northeast monsoon winds enhances the convergence with the land breeze at night, leading to maximum ocean convection to occur in the early morning only about 100 km from the coast. This close proximity of the ocean convection center to land causes the Borneo system to appear as a diurnal dipole with alternating land convection in the evening and near-coast ocean convection in the early morning. In the western India system the offshore extension of the diurnal system shown in Figure 5 is about 500 km from the coast. Although the total phase change between the land and ocean convection centers is closer to 12 hours which is larger than the land-to-sea phase difference in the Borneo system, the phase shift is more gradual. This gradual phase shift and the continuous decay of the amplitude offshore portray a scenario that is quite different from the dipole variation in the Borneo system. As is true in most land areas, increased heating causes convection to begin in the western interior of India in the

afternoon. The convective clouds continue to develop, resulting in maximum high cloud coverage over land in late evening. Afterward, convection moves westward to the eastern Arabian Sea with its magnitude continuing to decrease, until it disappears around the local noontime 500 km off the coast.

The above sequence may be visualized by examining the time and spatial structures of the CI diurnal cycle. This is done by constructing a diurnal sequence of the CI anomalies, First, the CI throughout May is composited with respect to the eight three-hourly observation times each day. The monthly mean CI (Figure 3) is then removed from the composites. The result is shown in Figure 7a. A diurnal convection anomaly of up to 6 °K begins to develop in the interior about 100 km to the east of the monthly-mean maximum (Figure 3) at 4 p.m. LT (12Z). It grows quickly to reach maximum of 12°K at 7 p.m. LT near the center of the monthly CI maximum. This coincidence of the maximum diurnal CI anomaly and the monthly-mean CI in western India indicates that the mean convection system has a large diurnal component, and it is conceivable that the location of the monthly mean maximum is due to the largest diurnal development. The westward movement of the diurnal anomaly continues with a decrease in the diurnal anomaly over the ocean, and eventually disappears at 1 p.m. LT (the data time closest to local noon) in the southeastern Arabian Sea.

Figure 8a shows the four times daily composite of the V850 anomalies. The mean V850 near the western Indian coast is prevailing northerly. At 4 p.m. LT (12Z) a meridionally oriented, extensive convergence zone is clearly indicated in the western interior of the subcontinent. This is consistent with the initial development of convection there. Over

the eastern Arabian sea northwesterly anomalies are prevalent, roughly consistent with a large-scale sea breeze. The exceptions occur near and to the southwest of the coast where the westerly component is absent. At 10 p.m. LT (18Z) the sea breeze pattern reverses into a land breeze pattern over the eastern Arabian Sea, with divergence in the western interior and easterly winds of about 1 m/s near the western coast. This is slightly after the time of maximum convection over land, and the easterly component is in the same direction of the observed westward movement of the convection. The 4 a.m. LT wind anomaly is very weak and at 10 a.m. LT the anomalies are southeasterly near 11°N, 70°E in the southeastern Arabian Sea where the maximum CI anomaly center is observed in Figure 7a. The comparison of the diurnal cycle of CI and V850 anomalies indicates that the convection, once developed in the southern Indian trough due to afternoon land heating, moves westward from late evening to morning. Unlike the winter Borneo convection, there are no prevailing onshore winds in May to provide a convergence with the land breeze in this case, but the degree of convection over ocean is not less than that off Borneo, and the life cycle of the convection as it moves offshore is even longer.

The westward movement of the diurnal CI center is clearly not just a westward drifting of the cloud mass in view of the long time and spatial scale of the downstream travel. The more likely possibility is a westward migration of the environmental condition that favors a condition, such as a westward movement of a large meso-scale (or a synoptic-scale) organization of the convection. If this is the case, a synoptic-scale convective system

develops diurnally in the afternoon in the interior of the subcontinent and then drifts westward for about 1000 km and decays in the southeastern Arabian Sea around noon LT.

In Figure 9 the centers of the diurnal CI anomaly are plotted in the May mean CI field. The diurnal CI centers are along the mean CI maximum and fairly close to the mean troughs. The diurnal center appears to propagate from the meridionally oriented South India trough to the northern equatorial trough, with the oceanic region of the westward movement located just to the north of the equatorial trough. Since the sea-surface temperature (SST) in May over the Arabian Sea is already very warm (Figure 10), conditional instability is available to develop deep convection over the ocean. During the afternoon and evening heating over the land surface causes deep convection to develop in the interior of the subcontinent. Most of the ocean area near the coast during this time is under subsidence, and convection is suppressed. After the sea breeze changes to land breeze in late evening, the subsidence is reduced and the presence of a synoptic-scale organization will be able to maintain convection.

During May 1991 the monthly mean 850 hPa wind (Figure 2) is primarily northeasterly in the southeastern Arabian Sea west of 72°E with an average speed around 8-9 m/s, which may account for the west-southwestward movement of the diurnal CI centers. However, east of 72°E the prevailing wind is northerly and does not explain the westward movement of the diurnal CI center. During night the land breeze does provide an easterly component, but the CI center moves westward at about 1° per three hours, which is nearly ten times faster than the easterly land breeze indicated in the V850 diurnal cycle. Thus, the

westward movement cannot be explained by the advection of a convergence system in the boundary layer.

On the other hand, the monthly mean winds at 700 and 500 hPa (Figure 11) are around 10 m/s in the southern part of the subcontinent and the Arabian Sea south of 17°N. (At 300 hPa the summer upper easterly jet has not developed and the pre-monsoon wind is very weak.) Thus, advection in the lower-middle to middle troposphere is consistent with the westward movement of the diurnal variations. This suggests that the diurnal variations are the result of westward propagation of synoptically-organized convection systems that are diurnally initiated in the afternoon in the western interior of the subcontinent. Synoptic scale motion is developed with the initialization of the afternoon convection in the interior and begins a life cycle that carries it across the coastal zone in the late night and early morning, and vanishes in the southeastern Arabian Sea and the northern equatorial Indian Ocean nearly 500 km from the coast around noontime.

The D850 anomaly (Figure 12a) shows maximum convergence in the interior of India at 4 p.m. LT, in areas fairly close to where the diurnal CI anomaly begins to develop at that time. However, at the other three times (at 10 p.m., 4 a.m. and 10 a.m. LT) the D850 anomalies are not consistent with the CI anomalies. No D850 anomaly diagrams show convergence centers that correspond to the CI anomaly centers, and the diurnal convergence anomalies in various parts of northern India do not have corresponding CI patterns to support them. Since divergence data in the initial analysis is most difficult to be properly represented, particularly in this case when it is associated with the diurnal cycle and is mostly over the

ocean area with no observations, the ECMWF analysis probably has significantly underestimated the land breeze. Therefore, we cannot rule out the possibility that the land breeze may play a supplemental role to advect the western India convection westward at night and in the morning.

A secondary amplitude maximum of the CI diurnal cycle in Figures 5 and 6 is located about 1200 km west-southwest of India with its center located at 7°N, 64°E south of the Arabian Sea. There are no corresponding 850 hPa convergence signals in Figure 12a over this open ocean region, apparently due to lack of upper air data reports. Since this maximum is over the ocean the CI amplitude is considerably smaller than the west India diurnal system. Its phase indicates an evening peaking around 9 p.m. LT south of 8°N, where the convection is in the northern equatorial Indian Ocean trough, and an afternoon peaking time to the north where the area of diurnal influence is even smaller (Figure 6). These diurnal phases are interesting in light of the previous investigations of open ocean diurnal convection. The area south of 8°N may be considered to have modest large-scale forcing as it is in the equatorial trough or a weak ITCZ. As discussed in the Introduction, Chen and Houze (1997) suggested that open ocean diurnal convection should start during the day due to solar heating of the water surface. Spatially-small, unorganized convection would peak sometime around noon or early afternoon, but organized convection under large-scale forcing will continue through the night and peak in the early morning. Radiative processes at the cloud top that have been used to explain night time or early morning ocean convection maximum, such as heating-stabilization during the day and differential cooling during the night, may have only

minor effects. The result south of the Arabian Sea in May partially supports their thesis. Under modest large-scale organization the diurnal convection in the equatorial trough lasts a few hours longer into the evening than the convection to the north, where the forcing should be smaller. It does not lead to more extensive development into the early morning in this case, perhaps because the forcing is only modest. In the meantime, radiative processes will not be able to explain the afternoon or evening peaks at all.

Figure 13 is the amplitude and phase distribution of the diurnal cycle of the 850 hPa convergence (-D850). Here, the amplitude is large in the interior of the subcontinent and the phase mostly indicates a maximum around 6-7 p.m. LT, two to four hours earlier than the time of maximum CI over land. This is consistent with the continuous development of convective clouds over land after maximum afternoon heating. The result may also be affected by the coarse time resolution of the D850 data which is available only every six hours. The convergence phase 300-600 km away from the western coast in the eastern Arabian Sea indicates convergence peaking near local noon. This is also consistent with the local diurnal CI phase where the weaker oceanic convection may not last much longer after it starts. However, there are plenty of areas where the diurnal cycle of 850 hPa convergence is not supported by the CI data, including the western coastal zone where a graduated transition of diurnal phase from land to sea is not seen. Overall, a reasonable correspondence between the two diurnal cycles can be seen in most places where the diurnal amplitude of CI is large, This fact is summarized in Figure 14 which shows the phase difference between the diurnal cycles of CI and 850 hPa convergence in May 1991. Here the phase difference is

plotted only if the CI anomaly exceeds 10°K. In both the western India and the southern Arabian Sea diurnal regions, the convergence mostly leads CI by 6 hours or less as expected. The main exception occurs on the west coast of India between 11°N-15°N, where the inconsistency of the D850 data was noted previously in Figure 12a.

Figure 10 shows the mean sea surface temperature (SST) in the Arabian Sea along the west coast of India is 30.0 °C. Latent heat fluxes associated with the convection off the west coast of India (Figure 15) occur at various times but are most prominent after the time of significant convection. Further off the coast, maximum latent heat fluxes are predominantly found after the time of maximum convection.

B. JUNE 1991

Figure 2 shows the mean V850 of June 1991. This is the first month of the Indian summer monsoon with westerlies established throughout the domain, the typical speed is near or slightly above 10 m/s over the Arabian Sea. The zonally-confined South India trough in May is now replaced by a broad trough with cyclonic vorticity covering eastern Arabian Sea and the subcontinent. The mean CI (Figure 3) shows a strong and broad maximum CI area with center values greater than 12°K just southwest of the subcontinent, more than twice the magnitude of the mean CI maximum in May 1991. This high CI region covers an expanded area of the southeastern Arabian Sea and extends into the northern equatorial Indian Ocean and all of India. The center is in the vicinity of maximum 850 hPa cyclonic vorticity, where strong convection persists through June 1991 and corresponds to a region of minimum SST surrounding southern India (Figure 16).

The mean D850 (Figure 4) shows again a divergence zone along and inside of the western coast of India. Mean convergence shows up to the east of the this coastal divergence zone. There is little evidence to support a correspondence between mean D850 and mean CI distribution over India. To the southwest of India another 850 hPa convergence area exists in the general vicinity of the southeastern Arabian Sea CI maximum. Although the convergence and CI patterns do not closely resemble each other, this collocation is a relatively good agreement between the two fields, in view of the generally questionable divergence data in the Indian Ocean region.

The amplitude and phase distribution of the diurnal cycle of CI is shown in Figure 5. Large amplitude can be observed over most of India and the southeastern Arabian Sea. Figure 6 clearly shows this expanded coverage of active diurnal convection compared to May 1991, both over land and over sea. In June, the entire northwest India becomes active, and a much larger area of the Arabian Sea southeast of India is under diurnal convection. The diurnal phases over the subcontinent and the southeastern Arabian Sea are nearly the same as in May 1991, indicating an evening convection maximum in the interior and a westward propagation towards the Arabian Sea. In contrast to the May 1991 pattern where the diurnal amplitude decreases to the west, the amplitude in June remains large over the ocean. There is even a slight amplification 500-800 km away from the coast after the maximum diurnal convection has traveled past the maximum mean CI center in the southeastern Arabian Sea shown in Figure 3. Furthermore, between 9°N-15°N the speed of westward propagation is

appreciably faster than May, with the maximum phase reaching local noon time at 64°E-65°E, about 1000 km west of the coast.

The three-hourly sequence of composited CI anomalies (with the monthly mean removed) is shown in Figure 7b. Starting from 4 p.m. LT (12Z), convection develops over a large area across the northern foothill of India, as well as smaller areas on the central western coast and in the southern interior of the subcontinent. At 7 p.m. LT the northwestern and central coast systems appear to merge and to extend westward over the coastal ocean, with the maximum CI anomaly center located on the northwest coast around 17°N. The southern interior system grows as a separate, smaller system. Three hours later, by 10 p.m. LT, both systems continue to extend toward the west but the northwest system weakens considerably while the south system continues to expand. At 1 a.m. LT the northwest system decays significantly over the ocean and loses its identity to become the northern part of the south system, which by this time has moved offshore. The west-southwestward propagation of the CI anomaly continues through the night and morning, and by early afternoon the convection anomaly reaches the southeastern Arabian Sea nearly 1000 km from the coast.

Since the mean 850 hPa wind is westerly for the entire domain, the westward movement of the diurnal CI center is again not due to the advection of a meso- or synoptic-scale disturbance by the boundary layer tropospheric wind. The June mean winds at 700 hPa and 500 hPa (not shown) are also westerly in the southern India and Arabian Sea region. However, an examination of the animation loops of the diurnal CI anomalies show that the diurnal variations near the western coast of the subcontinent are important only in the

first half of June, when the monsoon probably has not started and the basic low and middle tropospheric flow is similar to that of May.

In fact, analyzing the first two weeks and second two weeks of June separately, we see (Figure 17) that strong diurnal signals only exist in early June and the phase and amplitude are similar to that of May. The strong diurnal amplitudes influence the monthly mean CI where the maximum CI is 6°K higher for the first two weeks (Figures 18 and 19). These diurnal amplitudes are also strong enough to dominate the monthly mean phase and amplitude.

Figure 20 shows the track of the westward migration of the CI anomaly center overlaid on the June 1991 mean CI. Here the diurnal center passes to the northwest of the mean CI center with no discernible decrease in intensity. Thus, in this case, the amplitude of the diurnal cycle in deep convection is more or less independent of the intensity of the total convection, giving a near constant-amplitude modulation to the large convective system shown in the mean CI field (Figure 3). It is almost as if the maximum CI anomalies of around 4°K are determined at 7 p.m. LT while the center is in the southern interior of the subcontinent, and then maintained throughout the 18 hour journey westward to the southeastern Arabian Sea.

Figure 8b shows the four times daily composite of the V850 anomalies. As in May 1991, the eastern Arabian Sea shows northwesterly anomalies at 4 p.m. LT and a north-east oriented convergence zone occurs in the interior of the subcontinent, consistent with the maximum surface heating. Compared to May 1991 where the convergence zone exists only

in the subcontinent south of 20°N, in June it extends into northern India, reflecting the fact that the monsoon convection is active over the entire region. Similar to May 1991, the V850 anomaly in western India turns to offshore at 10 p.m. LT, and a southerly component begins to develop in the eastern Arabian Sea at 4 a.m. LT. There is no good relationship between the diurnal variations of CI and V850 other than the afternoon convergence. This is true with the D850 anomaly charts (Figure 12b), again calling question to the diurnal cycle of the wind analysis. The diurnal phase of the 850 hPa convergence (Figure 13) does show a general lead time over the CI phase by a few hours in the interior of the subcontinent and in the coastal waters to the west, but the relationship is not consistent on the west coast and further into the southeast Arabian Sea. The phase difference between 850 hPa convergence and CI is summarized in Figure 14.

Sea surface temperatures are now 2 °C cooler over the Arabian Sea except for the cold pool surrounding the southern tip of India (Figure 16). This region of cooler temperature (27 °C) can be attributed to the extensive area of convection overhead, resulting in lower solar heating. Figure 15 shows the CI- latent heat flux relationship similar to May along the southern coast but fluxes lead convection further north and over the ocean.

C. JULY 1991

The July 1991 monthly mean CI is shown in Figure 3. With the advance of the summer monsoon season the main convective activity has shifted to northern Indian with the maximum around 8-10°K, and the subcontinent itself is under a minimum. The coastal water within about 200-300 km from the western coast of the subcontinent is a more active

convection zone with maximum CI around 6°K, probably due to the prevailing 850 hPa westerlies (Figure 2) against the western mountains. The mean speed is around 15-20 m/s over the Arabian Sea, which is about 50% higher than June. The mean D850 (Figure 4) is qualitatively in agreement with the high CI areas, with convergence off the western coast and in the northern India. However, the maximum location on the coastal ocean convective zone is too far to the north, and the magnitude in general do not correspond to the mean CI intensity, with the convergence relatively too weak in northern India. The western coastal land region again shows 850 hPa divergence.

Figure 5 shows the amplitude and phase of diurnal cycle of CI, which is now active over the eastern two thirds of northern India, and southern India is almost dormant. There is also some diurnal activity off the northwest coast of the subcontinent, as can be seen in Figure 6. There appears to be a systematic phase change along a southwestward track originating from the maximum diurnal region in northeastern India. Here the convection peaks in the evening (around 9 p.m. LT), followed by midnight peaking in the north-central and northwest region of the subcontinent, to early morning in the Gulf of Cambay. The amplitude decreases along the way until middle morning peaking time in the coastal region northwest of the subcontinent, where the amplitude is increased. The diurnal signal then decays again as the peaking time shifts to noon hours in the eastern Arabian Sea.

This southwestward propagation of the diurnal variations is also evident in the three-hourly composites of the CI anomalies shown in Figure 7c. In this sequence of diagrams the decay of the diurnal amplitude downstream appears more rapid. The

re-enhancement of the amplitude in the northwest coastal ocean region shown in Figure 5 appears to be due to a slower movement of the anomaly between 4 a.m.-10 a.m. LT, rather than an actually larger-amplitude diurnal variation. Thus, the southwestward migration of the diurnal convection pattern is less systematic than the westward propagation from the western interior of the subcontinent to the equatorial Arabian Sea observed in May and early June.

The diagram overlaying the diurnal CI anomaly centers (Figure 21) and the monthly mean CI indicates that the diurnal center passes through the maximum mean convection region in northern India in late evening. It becomes semi-stationary off the northwest coast of the subcontinent and appears to break down. By 1 p.m. LT it re-emerges near 20°N, 67°E, which is close to the westward extrusion of the mean 2°K isopleth. The indicated amplitude of 2°K is smaller than over land, but its significance is not smaller since this diurnal variation is over open ocean. An interesting feature is another open ocean CI diurnal center at this time around 6°N, 67°E. The same longitude and time suggest that both are open ocean diurnal convection that tends to develop in the early afternoon. Whether the northern one is helped by a southwestward migration of an organized system from the northern India is questionable. Another feature worth noting is that at this longitude the two maximum mean CI locations are close to the two diurnal centers in the early afternoon. Therefore, the diurnal convection in the open ocean seems to contribute to the mean convection.

The six-hourly composites of the V850 anomalies (Figure 8c) show rather strong diurnal variations. At 4 p.m. (12Z) cyclonic circulation centered in northwest India is clearly indicated. East to the cyclonic center confluence of southerlies occurs in the maximum

diurnal center at this time and three hours later (Figure 7c). The circulation quickly disappears at 10 p.m. There is no feature that corresponds to the diurnal CI variations between 10 p.m. and the next few hours. At 4 a.m. LT northern India is under northwest anomalies and the eastern Arabian Sea off the west coast of India is primarily anticyclonic. This again does not seem to relate to the diurnal convection in the coastal oceans for the next six hours. At 10 a.m. LT diurnal confluence centers appear in northwest India and northern Arabian Sea around 20°N and 65°E. The latter center corresponds with the open ocean diurnal convection at 1 a.m. LT, but the first is not reflected in the diurnal CI anomalies. Furthermore, the southern Arabian Sea diurnal center at 1 p.m. appears in a 850 hPa difluent area. Again, it seems that the diurnal V850 variation more or less agrees with the actual convection center only in the maximum surface heating region over the land in the afternoon, and not very much in other situations.

The diurnal variations of divergence anomalies in July shown in Figure 12c bear almost no relationship with those of CI. The model analysis apparently continues to put maximum low-level convergence over the interior of the subcontinent in the afternoon and divergence in the morning, while in the CI field there is not much activity in this minimum (mean) convection region. This point is again obvious when comparing the July diurnal amplitude and phase distribution of D850 (Figure 13) with that of CI (Figure 5). There is no correlation at all. There is thus not much reason for discussing the D850-CI phase difference diagram.

Figure 22 shows a warmer temperature of 30 °C off the west coast of India and cooler temperatures of 28°C over the northeastern Arabian Sea. There is little convective activity over the water since most of the convection has migrated to the northeast. Latent heat fluxes lag convection in the small region over the Arabian Sea in Figure 22. Mean August SST is shown in Figure 23 but here is no significant convection occurring over water during this month over the West India region.

IV. BAY OF BENGAL

A. MAY 1991

Figure 24 shows the mean V850 of May. There is a low-level trough over the northwestern part of the domain. Further east, the winds are zonal. The winds over the southwestern Bay are southerly-southeasterly and become predominantly southwesterly to the north as this area lies between the trough and an area of anticyclonic turning to the southeast.

Figure 25 shows the distribution of monthly mean CI which is concentrated over the head of the Bay of Bengal near Bangladesh. The intensity and location of this CI maximum is a manifestation of tropical cyclones 02B and 03B. Tropical cyclone 02B was a super typhoon that made landfall on 29 April and tropical cyclone 03B made landfall on 02 June as seen in Figure 26. Both cyclones dissipated quickly over land due to the mountainous terrain. The CI value of 10 °K for this maximum is fairly common for this region but will not be the strongest of the season.

Mean D850 is shown in Figure 27. The strongest 850 hPa convergence occurs over the southern extent of the Tibetan plateau, over the northwestern Interior and further east over Myanmar. The first two maxima basically coincide with the position of the trough. Additionally, all three convergence maxima may be expected from heating over land. The northernmost and strongest convergence maximum coincides with the position of the CI maximum. There is no significant convection in the vicinity of the other convergence maxima.

The amplitude and phase distribution of the diurnal cycle of CI is shown in Figure 28. The diurnal amplitude is contoured in Figure 29. The largest amplitudes of the diurnal cycle are found along the northeastern coast of India and the maximum coincides with the position of the mean CI maximum indicating this system has a strong diurnal component. Strong amplitudes are found over the northwestern region near Calcutta and the northern interior near Bangladesh where convection occurs between 6 p.m. LT and 10 p.m. LT.

Strong amplitudes also exist over the Andaman Sea where convection occurs at 10 p.m. LT near the coast and 3 a.m. LT further offshore. This phase relationship suggests a land-sea breeze system (one of many within this domain) in which increased heating over land causes convection to begin in the afternoon. These clouds continue to develop, resulting in maximum high cloud coverage during the evening. The influence of the land breeze then causes the convection to migrate offshore.

The diurnal CI anomaly composite is shown in Figure 30a. Convection over land begins at 5 p.m./6 p.m. LT due to heating. The two maxima to the west and north join later in the evening forming one large cloud shield which dissipates early in the morning.

Convection is present over the Andaman Sea along 93°E during the early afternoon and intensifies at 3 p.m. LT when convection is strong over the northwestern Malay peninsula (NWMP). As the evening progresses, the convection over the Andaman Sea breaks up and convective activity strengthens over the western coast of the Malay peninsula, weakens and migrates to the west over the near-coastal waters.

In Figure 31a, the V850 anomaly indicates northeasterly winds at 5 p.m. LT, indicating that it is the northern CI center that migrates and joins the southwestern center. The easterly component of flow at 11 p.m. LT enhances the land breeze, supporting the westward migration of convection from the Malay peninsula. In fact, the monthly mean flow and 11 p.m. anomalies of the mid-tropospheric flow (not shown) are all easterly as well. Figure 32a is the four times daily D850 diurnal anomaly composite. The D850 anomaly composite shows areas of convergence at 11 a.m. LT in the vicinity of developing CI anomalies along the northern and southwestern coasts of the Bay. The coastal regions become divergent by 5 p.m. LT while the CI anomalies indicate increasing convection. So other than the 11 a.m. LT case, there is not much correspondence between diurnal CI and convergence patterns. The amplitudes of convergence are generally large over land and in the vicinity of strong diurnal CI amplitudes, but no real pattern exists. The relationship is actually worse over water, as expected. However, the area of phase reversal over the Andaman Sea does have a weakly organized pattern, consistently leading convection. The D850 diurnal cycle phase and amplitude is seen in Figure 33. The phase relationship between CI and D850 is summarized in Figure 34. The strong divergence-convergence patterns over the northern part of the domain have little if any, convection associated with them. It is believed that this diurnal signal is due to the cycle built into the model. Furthermore, since this area is also in the vicinity of the Tibetan plateau, the 850 hPa data is unrealistic due to the extreme elevations. Figure 10 shows cooler water of 29 °C over the head of the Bay of Bengal and three smaller cold pools of the same temperature scattered across the southern Bay which is

predominantly 30°C. The only significant convection occurring during May is along the west coast of Myanmar, over the Gulf of Martaban, just north of the southeastern cold pool where latent heat fluxes reach their maximum prior to the convective maximum (Figure 35).

B. JUNE 1991

Mean V850 for June is shown in Figure 24. This represents the post-onset phase of the South Asian summer monsoon. As a result, the entire region is dominated by southwesterly flow. A trough still dominates northeastern India and there is slight cyclonic turning over northwestern Myanmar.

Figure 25 shows a strong CI maximum over the Bay of Bengal during June, partially influenced by tropical cyclone 03B (mentioned previously) which made landfall on 02 June. The location of this intense CI maxima may be attributed to blocking by the coastal mountains. Note that the location of this mean maximum is located over water , whereas most of the convection was over land during May.

Figure 27 shows weak convergence coinciding with the trough over the northwestern interior. The strongest convergence occurs to the northeast over Myanmar in association with the area of cyclonic turning. This may also be an area of large afternoon heating. There are several scattered areas of convergence over the Bay. The primary area of divergence is located to the southeast. There is no correlation between the mean convergence and CI fields.

Figure 28 shows strong amplitudes in the diurnal CI existing over the northwestern interior. The time of convection increases in the westward direction from mid-afternoon to

mid evening (8 p.m. LT). Maximum convection occurs at 10 a.m. LT over the southwestern Bay of Bengal and gradually increases to 1 p.m. LT over the northern half of the Bay. The time of maximum convection is earlier along the west coast of the Bay and becomes later farther off shore, as expected in a land-sea breeze situation.

Convection is still fairly strong over the Andaman sea but has weakened over the western coast of the NWMP. The westward phase shift of convection is still prevalent, but extends further off shore and occurs later (1 a.m. to 10 a.m. LT) during June. Furthermore, there is another phase shift, southward from the Gulf of Martaban from early to late morning. This southward phase shift is more consistent with migration of convection as the northerly land breeze is enhanced during the late evening hours.

The mean and diurnal maxima locations do not agree. The mean maximum coincides with the path of the tropical cyclone whereas the diurnal maximum in Figure 29 is located over the northwestern interior.

It is important to point out that the eastern regions of the Bay are not as diurnally active as the western regions. This trend continues through August. This phenomenon supports the results of Murakami (1983) who found that convection was suppressed in the evening during the summer over the eastern Bay of Bengal. Interestingly, this is the windward side of the monsoon flow over the Indochina peninsula, suggesting a complex interaction between land-sea breeze circulation and large-scale flow. There is added complexity due to the fact that just to the south, the Andaman Sea is a diurnally active region.

In Figure 30b, convection is strong in the afternoon over the northwest interior and dissipates by early morning. Convective activity persists throughout the morning hours and early afternoon over the Bay and is widespread in the early afternoon when convection is also strong over the north central interior. Afternoon convection over the Bay of Bengal migrates to the northeast and there is some weak low-level convergence supporting this activity. Clouds migrate westward from the west coast of the NWMP over the Gulf of Martaban/Andaman Sea and there is a similar eastward migration from the southwestern coast of the Bay.

Figure 31b shows southwesterly flow supporting the migration of convection along the northwestern coast of the Bay at 5 a.m. LT. The cyclonic wind pattern over the head of the Bay also supports intensification and eastward expansion of convective activity at 11 a.m. LT. The eastward phase shift over the southern Bay appears to be a result of convergence between the large -scale flow and the land breeze. This is also a zone of convergence at 500 hPa (not shown). Wind forcing at 850 hPa for the southwestern movement of convection over the Gulf of Martaban can clearly be seen at 11 p.m. LT. However, at higher levels, the 11p.m. LT anomalies are northerly over the Gulf of Martaban and westerly further south. This suggests an enhancement of the land breeze over the Gulf , but convergence of the land breeze and westerly mid-tropospheric flow results in convection off shore. Finally, it is interesting to note that relatively strong (6°K) CI over the Myanmar peninsula region is coincident with strong southwesterly onshore flow, clearly enhancing the sea breeze at 11 a.m. LT.

Figure 32b shows the same diurnal signal mentioned for May exists to the north and the signal is very weak throughout the rest of the domain. Strong convergence is found at 11 a.m./12 p.m. LT along the northwestern coast of Myanmar but the dominant area of strong convection over land lies across the Bay over the northeastern interior of India. Again, correlation between diurnal convergence and CI is slight. Convergence is strong to the northeast (Figure 33) where convection is weak (Figure 28). Although convergence is weak, it does lead convection over limited areas of both land and water in the western half of the domain as seen in Figure 34.

In Figure 16, the SST is 28 °C. over the entire Bay except for the cooler 27 °C water surrounding the southeastern tip of India. Whereas significant convection was associated with the cold pool on the west coast, there is no convection associated with this cold pool on the east coast. The cooler water is upwind of the convective activity along the northwestern section of the Bay. The cool to warm temperature gradient and strong southwesterly flow result in strong convection which is either led by or in phase with the maximum latent heat fluxes as shown in Figure 35.

C. JULY 1991

Figure 24 shows that the Asian monsoon is in full force dominating the entire region. As a resul t, winds over the Bay and continental regions to the east are predominantly southwesterly. There is a cyclone centered over the northwestern interior and there is weak anticyclonic turning over the southeastern corner of the domain.

Figure 25 shows three distinct convective maxima in the mean fields centered over the northeastern coast of India, central Bay of Bengal and Andaman Sea during July. The two northern maxima are located near the cyclonic shear region of the cyclone shown in Figure 24. The three maxima are oriented northwest-southeast, parallel to the coastline indicating that convective activity may result from both geographical and topographical influences on the large-scale southwesterly flow.

Figure 27 shows widespread convergence over the Bay and northwestern coast. Again, convergence is strongest over Myanmar, where there is cyclonic curvature of the winds. The strongest divergence occurs directly south of the strongest convergence. Although there are convergence centers coinciding with the three mean CI maxima, the intensity is weak while the strong convergence maximum coincides with weak CI to the northeast. Hence, there is no mean convergence support for the mean CI maxima.

In Figure 28, strong diurnal convection is occurring over the eastern Bay and Andaman Sea. The pattern over the northwestern interior still shows a westward migration but is not as pronounced as in previous months. The time of maximum convection increases over the northwestern region from 3 p.m. LT in the east to 6 p.m. LT in the west. Nitta and Sekine (1994) determined that maximum convection takes place over the Bay during the afternoon and the diurnal signal may be complicated by the land-sea contrast of the surrounding areas. The time of strong convection over the Bay of Bengal is now increasing from 10 a.m. LT in the west to 3 p.m. LT in the east and 11 a.m. LT in the north to 12 p.m. LT in the south. Strong noontime convection is occurring further south than in June. Strong

amplitudes remain over the Andaman Sea occurring later with less intensity further from shore. The phase relationships indicate movement from west to east over the southern two thirds of the Bay but the amplitudes are small. The westward phase shift off the coast of Myanmar toward the Andaman Sea has virtually disappeared and the dominant phase shift now occurs southward from the Gulf of Martaban. Convection also migrates from north to south over the head of the Bay. The northern and southern mean CI maxima positions agree with those of the diurnal CI. Figure 29 shows the maximum diurnal amplitude occurring over the Andaman Sea.

Figure 30c shows the diurnal CI anomaly series. Convective activity over land starts in the afternoon in response to heating and then dissipates by midnight. Early morning convection moves off the western coast and persists over the Bay for most of the day. Convection forms over the NWMP and coastal waters late in the evening and intensifies. Once it drifts offshore, it migrates south during early morning. This is also seen as a phase reversal in Figure 28. Convection over the water is concentrated along the coast throughout the morning and becomes widespread over the Bay in the early afternoon.

The wind anomalies in Figure 31c show similar support for the evolution and movement of diurnal convection as seen in June. The early morning, middle tropospheric wind anomalies at 700 and 500 hPa (not shown) support the southward migration over the head of the Bay and the wind signals in the vicinity of the Gulf of Martaban are similar to those in June. Figure 32c shows the same diurnal signal mentioned for June exists to the north and the signal is very weak throughout the rest of the domain. Strong convergence is found at

11 a.m. LT along the northwestern coast and the dominant area of strong convection over land still lies over the northeastern interior (Figure 33). There are some coastal areas where low-level convergence leads weak convection. Most of the strong convection over the southwestern Bay is led by convergence. Figure 34 summarizes the phase relationship between convergence and CI.

Figure 22 shows warmer temperatures in the southwest and cooler temperatures over the northeast. Again, convective activity is associated with regions of warmer SST along the western half of the Bay and over the Gulf of Martaban. Referring to Figure 35, the time of maximum latent heat flux leads or is in phase with the time of maximum convection in both cases.

D. AUGUST 1991

Monthly mean V850 is shown in Figure 24. The cyclone over the northwestern interior in July has now moved to the southeast. Northwesterly flow dominates most of the northwestern interior. The flow is southerly and southwesterly over the north central interior and some cyclonic turning in the northeast corner of the domain. Southwesterlies dominate the rest of the domain.

August has two distinct CI maxima in Figure 25. One maximum occurs over the northwestern interior and the other occurs over the Gulf of Martaban/Andaman Sea. The CI maxima over land is in the region of cyclonic shear and the maximum over the Andaman Sea appears to be a result of the strong, zonal cross-coastal flow hitting the coast.

Figure 27 shows several scattered areas of convergence throughout the Bay. The strongest convergence occurs over the northeastern interior and along the southwestern coast. Both areas coincide with areas of cyclonic turning. They may also be areas of large afternoon heating. There are several scattered areas of weak convergence over the Bay. The strongest area of divergence occurs along the northeastern coast. The positions of strong diurnal maxima coincide with the positions of the two mean CI maxima. Figure 29 indicates a third maximum in the southwestern quadrant. Although there are areas of convergence near the areas of mean CI maxima, the relative magnitudes are inconsistent. Therefore, there is no correlation between the mean convergence and CI fields.

Figures 28 and 29 show strong amplitudes are prevalent over the northwest with time of maximum convection increasing from 9 p.m. LT in the west to 2 a.m. LT further east. The time of convection over the western Bay increases from mid-morning in the north to mid-afternoon further south. The Andaman Sea remains a region of strong diurnal signal where the time of convection increases westward, further from the coast than in July.

Referring to Figure 30d, convection begins along the northwest coast early in the morning, weakens and moves offshore, covering much of the Bay by early afternoon. During early afternoon, the land is heating and convective activity increases throughout the interior and coastal regions, including the Malay peninsula. Scattered convection persists until late evening when convective activity is primarily occurring over land.

In Figure 31d, wind anomalies at 5 a.m. LT support the eastward movement of convection over the head of the Bay. The anomalies are generally cyclonic over the Bay at

11 a.m. LT subsequent to the time of maximum cloud coverage over water. The winds at 11 p.m. LT are southerly and easterly , supporting the southwestern migration of convection over the Gulf of Martaban. Furthermore, the winds are convergent over the Andaman Sea, explaining the broader extent. The strong late morning onshore flow over the Myanmar peninsula is now more southerly and convection is weaker over that region.

In Figure 32d, maximum convergence occurs inland and mostly along the coast during the afternoon hours. The primary difference between August and previous months is the lack of widespread convergence over the Bay. In Figure 33, the D850 diurnal pattern is in agreement with the CI pattern (Figure 28) over most of the active oceanic regions and over the north central interior the phase relationship is summarized in Figure 34.

In Figure 23, the SST is predominantly 28 °C except for a small cold tongue north of Sri Lanka and a warm pool of 29 °C over the western half of the Bay. There is strong convective activity associated with the warm pool over the western half of the Bay and over the Andaman Sea, where the SST is still relatively warm. Figure 35 shows all latent heat fluxes leading or in phase with the convection in both areas.

V. INDOCHINA

A. MAY 1991

Figure 36 shows the entire Indochina peninsula under the influence of anticyclonic turning. Winds are mostly southeasterly over the water. Over land, the winds are southeasterly and gradually rotate to southwesterly further north.

Figure 37 depicts mean CI as relatively weak over the Indochina peninsula. There is one large maximum over the Gulf of Thailand. The magnitude of this maximum is 4 °K and is the weakest seen over the four month period. There are two smaller maxima north of the Mekong river delta and over central Thailand.

Figure 38 indicates an inactive period with respect to convergence. The mean convergence is very weak. There are two areas of convergence along the northern coast of Vietnam and over southern Thailand. The area of convergence over Vietnam is associated with the convergence of southeasterly flow over the South China Sea and the southerly flow over Indochina.

Diurnal amplitude and phase are shown in Figure 39. The strongest amplitudes of convection are found over the central interior of the peninsula where convection occurs at 10 p.m. LT and along the southwest coast and coastal waters of the Gulf of Thailand (GOT) where convection occurs between 4 p.m. LT and 7 p.m. LT. There is a weak phase reversal and marked decrease in intensity in the westward direction over the northern gulf indicating

a possible land-sea breeze effect. East coast convection occurs at 7 p.m. LT. It weakens across the bay where the time of convection is 9 a.m. LT along the west coast.

The mean and diurnal CI maxima positions correlate well. Both fields indicate maxima over the GOT which is where the strongest diurnal amplitudes occur in Figure 40. There is no correlation between mean convergence and mean CI. The strongest CI occurs over water and there is no supporting convergence in the vicinity.

The diurnal CI anomaly composite series is shown in Figure 41a. The entire region is quiet throughout the morning and early afternoon until 3 p.m. LT when strong convection is present over the GOT and southern tip of Vietnam. The convection moves southeasterly and broadens until the entire peninsula is under the cloud shield by early evening. High values of CI dominate the coastal regions while lower CI is prevalent over the interior. Convection breaks up throughout the evening and is concentrated primarily over land, where it is dominant over the interior of the peninsula throughout the early morning.

The series explains the phase reversal, showing the migration of weak (slight negative anomaly) convection from east to west over the GOT during the early morning hours.

Figure 42a is the four times daily 850 hPa diurnal wind anomaly composite. There is convergence inland at 12 p.m. LT indicated by onshore flow from the east and west associated with afternoon heating. Winds are southwesterly throughout the evening indicating that convection over the GOT is a result of convergence between the land breeze from the east and the large-scale monsoon flow. There is no wind signal later in the evening supporting the apparent southeastern migration and development of the CI maximum. The

strongest CI (12°K) is associated with the strong onshore flow over the northern gulf, near Bangkok.

Figure 43a shows the interior becoming convergent during 12 p.m. /1 p.m. LT and is slightly divergent early in the morning, providing good low-level support prior to the time of maximum convergence. This pattern is expected as convergence associated with the sea-breeze results from afternoon heating of the land. The convergence pattern in Figure 44 is not as organized as the CI pattern, but strong magnitudes of convergence are mostly coincident with strong CI amplitudes. In Figure 45, convergence leads convection over most of the interior and over the northern GOT where convection is strongest.

Figure 10 shows the Indochina peninsula surrounded by warm 30 °C water in May. In Figure 46, the active area of convection is the eastern Gulf of Thailand and the maximum latent heat fluxes occur prior to the convection.

B. JUNE 1991

Figure 36 shows zonal winds from the west over the southern half of the peninsula. Further to the north, the winds become southwesterly. Wind velocity also increases toward the north.

CI has increased and is prevalent over most of the Indochina peninsula in Figure 37. Maxima are located over the Gulf of Thailand, southern tip of Vietnam and over the South China Sea off the southeastern coast of Vietnam. Convection is weak along the eastern coast.

The strongest convergence follows the geography of the peninsula along the northern and eastern coasts of Vietnam in Figure 38. Strong divergence is aligned northwest -

southeast just inland of the northern coast of Vietnam. Convergence is weaker over the eastern Malay peninsula. There is no correlation between mean convergence and mean CI.

Figure 39 shows a more pronounced diurnal pattern over Indochina. The amplitudes have increased and the phase is delayed, indicating stronger convective activity occurring later in the day. Activity over the GOT has decreased except for the coastal regions. Convection over the southern GOT is now occurring during the late morning (10 a.m. LT) in the west and during mid-afternoon (3 p.m. LT) in the east. The northern GOT experiences the same phase reversal from east to west as seen in May. The mean and diurnal CI maxima positions correlate well indicating this system has a strong diurnal component.

Figure 41b shows there is convective activity over the southern GOT that drifts northeastward and dissipates during the late morning hours. Convection forms along the southern coast and over northern Vietnam in mid-afternoon. As the day progresses, convective activity persists over the entire peninsula except for the east coast. This agrees with the findings of Murakami (1983) who noted that suppressed convection in the evening on the lee side of the Indochina peninsula indicates an interaction between the land-sea breeze circulation and the large-scale southwesterly monsoon flow. Convective activity is suppressed along the east coast during the evening hours. The strongest convection is found over the southern tip of Vietnam. This is also the region of strongest diurnal amplitude in Figure 40. Convection starts to dissipate and most of the peninsula is clear by early morning.

In Figure 42b, the wind anomalies are cyclonic at 6 p.m. LT, lending support to the growing cloud mass with maximum CI values to the north and south. The evening winds are

southwesterly and westerly, resulting in convergence as in May. The CI max of 8°K is associated with a weak southwesterly anomaly indicating enhanced, southwesterly, onshore flow.

The diurnal convergence pattern in Figure 43b is unchanged from May except the afternoon convergence is stronger and located further east. Again, convergence amplitudes are strong over areas of strong convection (Figure 44) and there is good support since low-level convergence generally leads convection where amplitudes are strong (Figure 45).

Figure 16 shows the peninsula is bounded by warm water to the north and southwest. The Gulf of Thailand remains the most active area of convection and is concentrated further to the west, along the Malay peninsula. Again, in Figure 46, the maximum latent heat flux occurs prior to or is in phase with the maximum CI diurnal amplitude.

C. JULY 1991

Winds remain zonal over the peninsula and become southwesterly over northern Vietnam in Figure 36. There has been little change in mean wind fields between June and July due to the large-scale monsoon flow dominating southeastern Asia.

Figure 37 shows moderate values of CI found over the entire peninsula. The lowest CI values are over the eastern coast where convective activity is still suppressed. The Gulf of Thailand becomes active again as the location of the largest maximum of the season.

Referring to Figure 38, the convergence-divergence pattern along the north coast of Vietnam is unchanged from June and there is more convergence occurring over the interior regions and the southern tip of Vietnam. The area of convergence over the eastern Malay

peninsula has broadened over the Gulf of Thailand. Again, there is no low-level mean convergence support for mean CI maxima.

Figure 39 shows amplitudes remain strong over Indochina and convection is stronger and occurs later further north. However, convection is occurring earlier further south over Vietnam. The same phase relationships over the northern and southern regions of the gulf found in June, exist in July. The location of the mean CI maximum over the GOT agrees with the largest diurnal amplitudes in Figure 40 indicating that this convective activity has a strong diurnal signal which is most likely driven by the land-sea breeze circulation.

Figure 41c shows Indochina is relatively quiet during the morning and there is weak convection east of the Malay peninsula and the development moves westward over the land during the afternoon and intensifies. This must be a manifestation of the land-sea breeze effect. Afternoon convective activity is concentrated over the southern half of the peninsula, intensifying and growing in horizontal extent throughout the afternoon and eventually dissipating. Convective activity is prevalent over the GOT and continues to be weak over the east coast during the late evening hours.

Figure 42c shows wind anomalies are southwesterly and the convection must result from land breeze-monsoon flow convergence. July is unique in that there is no evidence of wind support for the strong 10°K CI maximum over Thailand. This maximum is most likely a result of intense heating over land.

The diurnal convergence pattern is unchanged from June (Figure 43c). Although the convergence pattern in Figure 44 is weak and disorganized, convergence generally leads convection where amplitudes are large (Figure 45).

Figure 22 shows the same SST pattern persists in July, except the temperature has increased to 30 °C. Convective activity has increased in July and the most active area is over the Gulf of Thailand along the southwestern coast of the Indochina peninsula. Figure 46 shows latent heat fluxes leading and in phase with convection close to the coast and lagging and out of phase further offshore.

D. AUGUST 1991

The wind pattern in Figure 36 shows little change from July to August. The winds appear to be weaker over the northern part of the domain.

Figure 37 shows the maximum over the gulf of Thailand still remains but has weakened. The strongest convection over land has moved over the northern interior. The convection along the east coast is slightly stronger during August which may be attributed to the weaker westerly flow over the northern part of the domain.

Typhoon Fred crossed the northern peninsula in late August but does not appear to have influenced the mean CI pattern as seen in the Bay of Bengal. Convective index values are 6°K along the northern Indochina peninsula in both July and August.

In Figure 38, the convergence-divergence pattern along the northern and eastern coasts persists but increases in intensity and southern extent. The Malay peninsula is now under a region of convergence.

The diurnal pattern is still prevalent in August in Figure 39. The phase pattern is similar to July with later times of convection to the north but the amplitudes have decreased, most likely due to decreased winds. Amplitudes have decreased along the west coast of the peninsula. The phase of convection over land continues to peak later farther to the north. Convection over the extreme northern GOT is still occurring at 10 p.m. LT. Convection over the central GOT is now an early morning event across the entire gulf. Further south, the eastward phase reversal from late morning to mid-afternoon still exists. The strong phase reversal southward from the northern GOT still exists in August.

The mean and diurnal distribution of CI are in good agreement except the mean maximum in Figure 37 is located over the GOT and the diurnal maximum in Figure 40 is located over western Thailand.

In Figure 41d, convection is located over the GOT throughout the morning, reaching its highest intensity during mid-morning hours. Unlike previous months, the convective activity over Indochina is weaker and less widespread.

The wind anomalies at 6 a.m. LT (Figure 42d) are northwesterly, supporting the southeastern migration of convection from 9 a.m. LT to 12 p.m. Lt over the GOT. Again, convergence between the land breeze and large-scale flow is the most reasonable explanation for convective activity over the GOT. The CI max of 6°K over eastern Vietnam is associated with strong onshore flow.

The diurnal pattern of D850 in Figure 43d shows no change from June and July. Figure 44 shows convergence is generally strong where convection (Figure 39) is weak.

Low-level support is minimal and convergence only leads convection over the GOT (Figure 45).

Figure 23 shows the entire peninsula surrounded by warm 29 °C. water once again. Convective activity has decreased and is concentrated along the southwestern coast of Indochina. The maximum heat fluxes are predominantly in phase with convection over this limited area in Figure 46.

VI. NORTHERN SOUTH CHINA SEA

The diurnal cycle over the South China Sea has been well-documented by previous studies (Murakami, 1983; Nitta and Sekine, 1994) whose results were based on analysis of several years of data. Our documentation of the diurnal cycle over this region in 1991 agrees with the "climatology" established by those studies with the exception of June 1991.

During June of 1991, an anomaly in the diurnal cycle is present over the northern South China Sea between Hainan and Taiwan (Figure 47). The phase in this region occurs in the early afternoon (2 p.m. LT) and is in general agreement with the long term average, but the amplitudes are significantly stronger. After examining animated satellite imagery and 3-hourly CI in this region on a daily basis, we found two separate large-scale systems of six and eight days duration responsible for the increased diurnal amplitudes.

Chen and Takahashi (1995) determined that the diurnal cycle of convection was enhanced (suppressed) over water (land) during active (inactive) periods of 30-60 day intra-seasonal oscillations. We will determine the impact of large-scale systems on the diurnal cycle during active/inactive phases in the synoptic systems with a time scale on the order of one week.

A. JUNE 6-11, 1991

There is a cold front oriented northeast-southwest northwest (off the diagram) of the area of interest at 00Z on the sixth of June (Figure 48a). The southeastern coast of China and the northern South China sea are cloud free except for some minor tropical convection between Vietnam and the Phillippines. A low develops over southeastern China in response to heating at high elevation by the ninth of June and the associated trough extends over most of the South China Sea.

The low associated with the cold front moves off to the northwest over Japan, drawing convection from the south toward the north. Convective activity over land is concentrated along the coast, north of Hainan throughout the morning (Figure 48b). On 8 June the cloud mass extends south at 1 p.m. LT and merges with the tropical oceanic convection located in the trough, which has remained strong throughout the entire day. The maximum CI over water is attained at 2 p.m. LT. The elongated cloud feature breaks from the southern cloud mass at 4 p.m., migrates north and weakens throughout the evening. This process repeats on 9 June except the convection is stronger by 10 - 20°K and the two cloud masses join earlier (10 a.m. LT) and remain as one large cloud mass throughout the day (Figure 48c). The convection is primarily concentrated over water with some weaker activity over China, west of Taiwan during the late evening. Finally, on 11 June, convection dissipates throughout the early morning and the region returns to the sequence of scattered oceanic convection reaching an early morning maximum (7 a.m LT) and convection over land is prominent in the afternoon reaching its maximum at 4 p.m. LT (Figure 48d).

The diurnal cycle between Hainan and Taiwan is enhanced due to the interaction of a synoptic scale front moving off the Asian continent and the oceanic convection associated with a tropical trough located over the South China Sea between Vietnam and the Phillippines. Most of the convective activity is concentrated over water and the maximum CI is attained every day during the early afternoon, coinciding with the phase of the largest diurnal amplitudes. The monthly mean CI in Figure 49 shows the monthly CI maximum coincides with the tropical, oceanic convection which was far more persistent throughout the month. Furthermore, the effects of Typhoon Yunya, which crossed Luzon and then recurved to the northeast (13-17 June) may also be prevalent in the monthly mean.

B. JUNE 19-26, 1991

There is a trough over the northern South China Sea associated with the low over southeastern Asia at 00Z on 19 June (Figure 50a). Convection is present over the SCS between the Phillippines and China throughout the entire day. It is concentrated closer to Luzon in the early morning, reaching peak intensity at 4 a.m. LT. Oceanic convection is maximum between 10 a.m. LT and 1 p.m. LT between Hainan and Taiwan. The oceanic convection retreats back toward Luzon during the evening. Convection is strongest over China during the afternoon, as expected, and persists until early morning. The intense convection northeast of Hainan is associated with a low over southeastern China (deeper than the previous case) and associated troughing (not as widespread as the previous case).

The chain of events for this case is similar to the earlier case in that convection begins over the SCS and is concentrated along the Chinese coast in the early morning (Figure 50b).

The oceanic convection remains strong throughout the morning as the cloud shield breaks and rejoins. Convection over the SCS intensifies, reaching a maximum at 1 p.m. LT and covers more area on 21 June (Figure 50c). Note that convective activity is confined to the coast with very little activity over the interior.

The entire region between China and the Phillippines is dominated by a cloud mass with CI values of 60°K between 1 p.m. and 4 p.m. LT on 22 June (Figure 50d). The cloud mass is oriented northeast-southwest, almost exclusively over water as the influence of the synoptic -scale system draws the clouds northeastward.

The cloud mass decreases in maximum intensity but expands to the north and east, consistent with the evolution of a cold front on 23 June (Figure 50e). Maximum intensity is found over the SCS during the afternoon. The cloud mass size decreases throughout the early morning and peaks at 50 °K over land at 4 a.m. LT (Figure 50f). The cloud mass then moves offshore and expands to the east through the rest of the day.

On 25 June the cloud mass becomes organized into a long narrow band and breaks up in the evening at 7 p.m. LT (Figure 50g). Convection is strong over the Phillippines during the late night and early morning hours and concentrated along the coast of China throughout the day (Figure 50h). After June 26, the northern South China Sea remains relatively cloud-free.

Again, the diurnal cycle between Hainan and Taiwan is enhanced due to the interaction of a synoptic scale front moving off the Asian continent and the oceanic convection associated with a tropical trough located over the South China Sea between

Vietnam and the Phillippines. Most of the convective activity is concentrated over water and the maximum CI is attained every day during the early afternoon, coinciding with the phase of the largest diurnal amplitudes. Although in this case, the large-scale system was more intense, resulting in larger values of CI over the northern SCS. Animated satellite imagery shows the front moving offshore, intensifying as it draws moisture up from the SCS and moving northeast over the subtropical ridge.

Referring to Figures 16 and 23, the mean SST is between 28 °C and 29 °C in June and August, warm enough to sustain convection over the water. Figure 51 shows convective activity is more widespread during June and most of the latent heat fluxes occur in phase with convection. Figure 52 shows convective activity is minimal and occurs after the maximum latent heat flux.

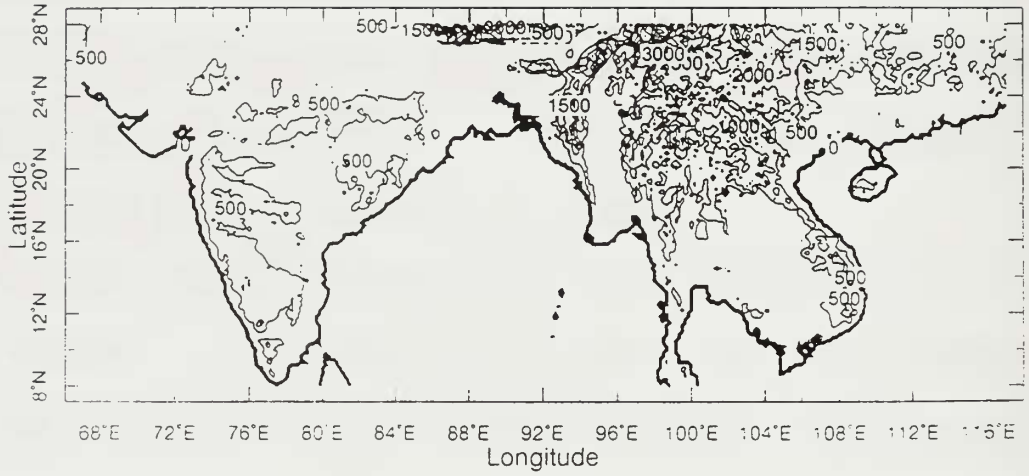

Figure 1. Topography of the northern summer monsoon region. Contour interval is 500 meters.

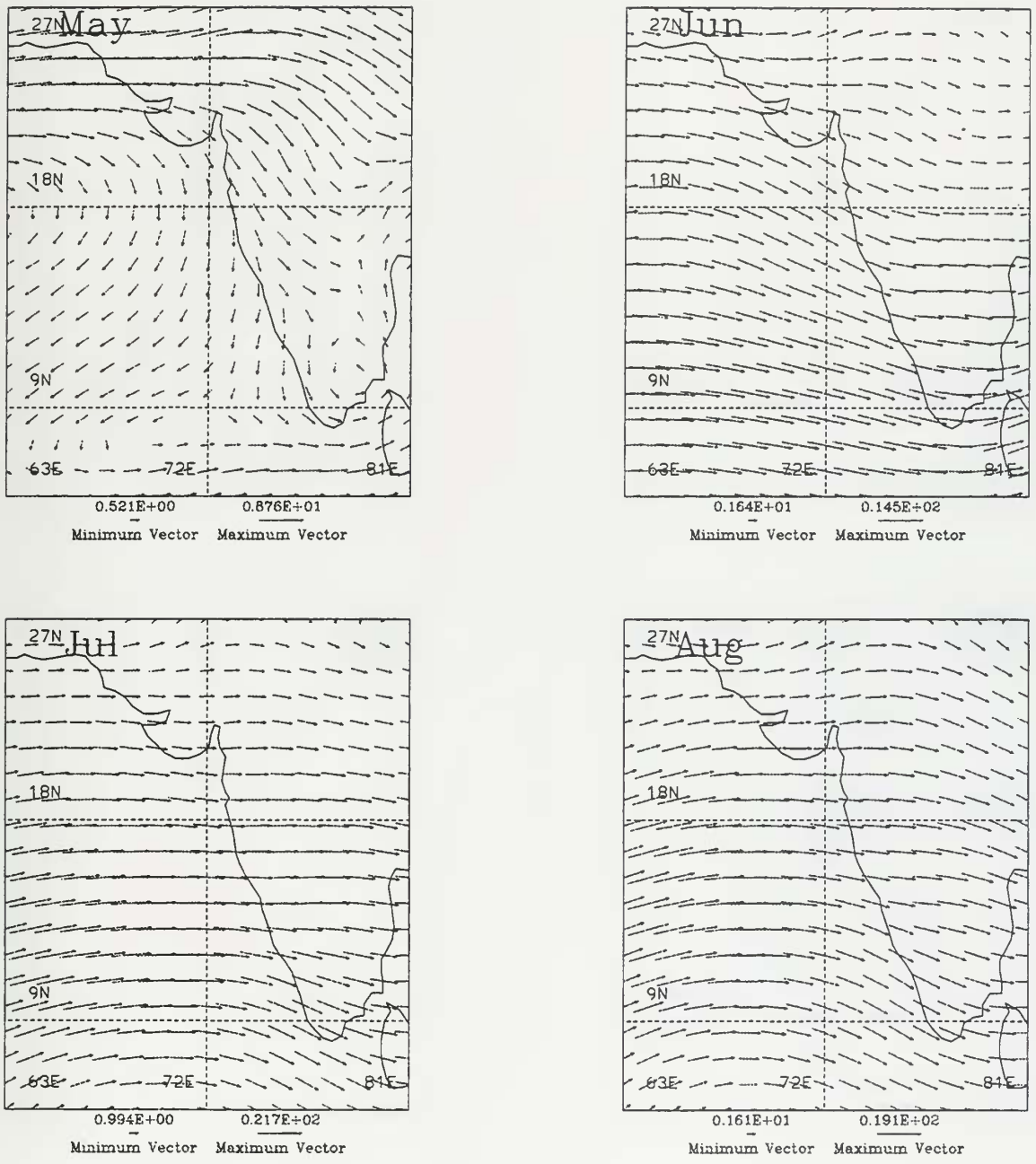

Figure 2. West India 850 hPa monthly mean winds (m/s) for May, June, July and August 1991.

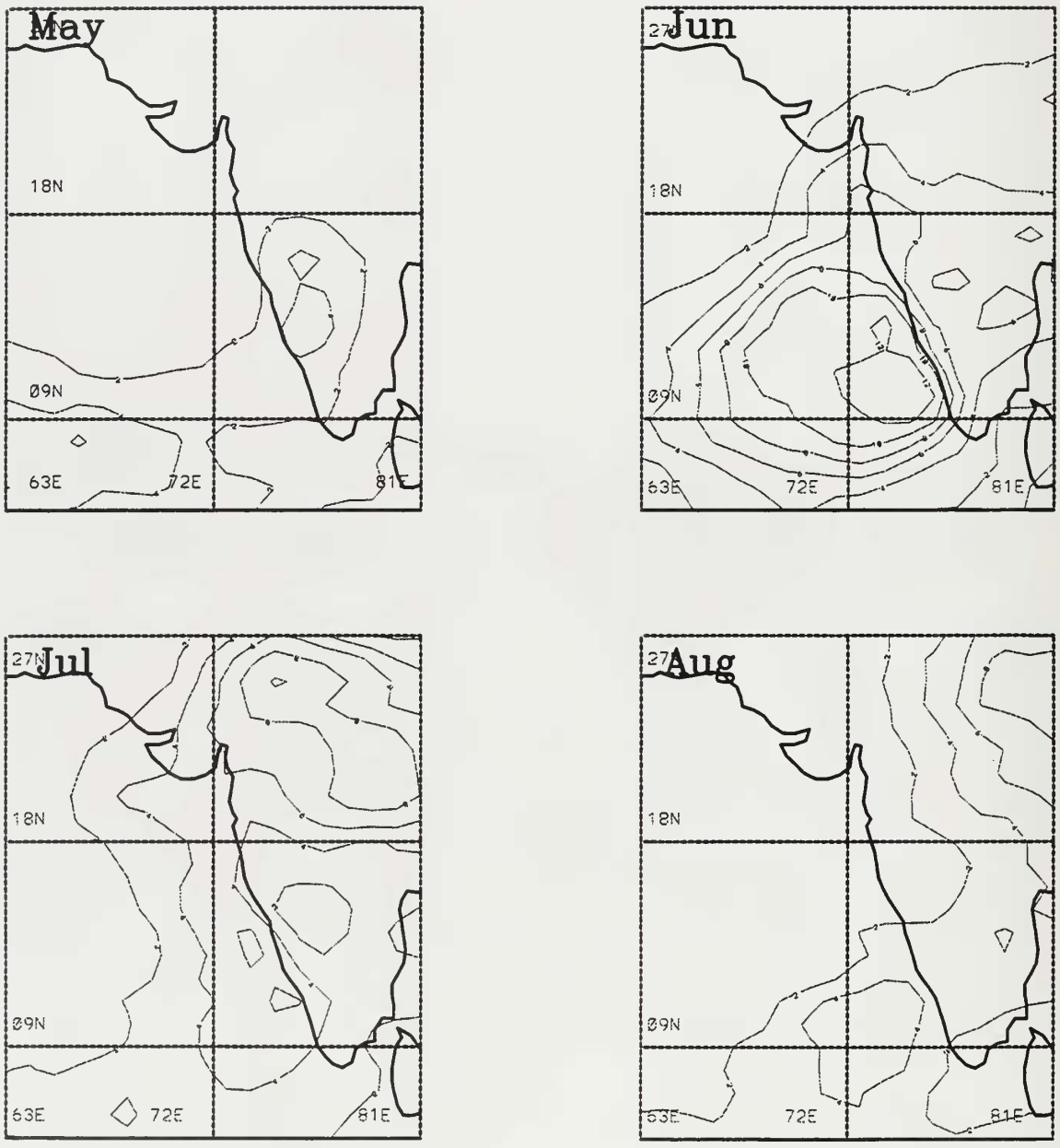

Figure 3. West India monthly mean convective Index (CI) for May, June, July and August 1991. Contour interval is 2 °K.

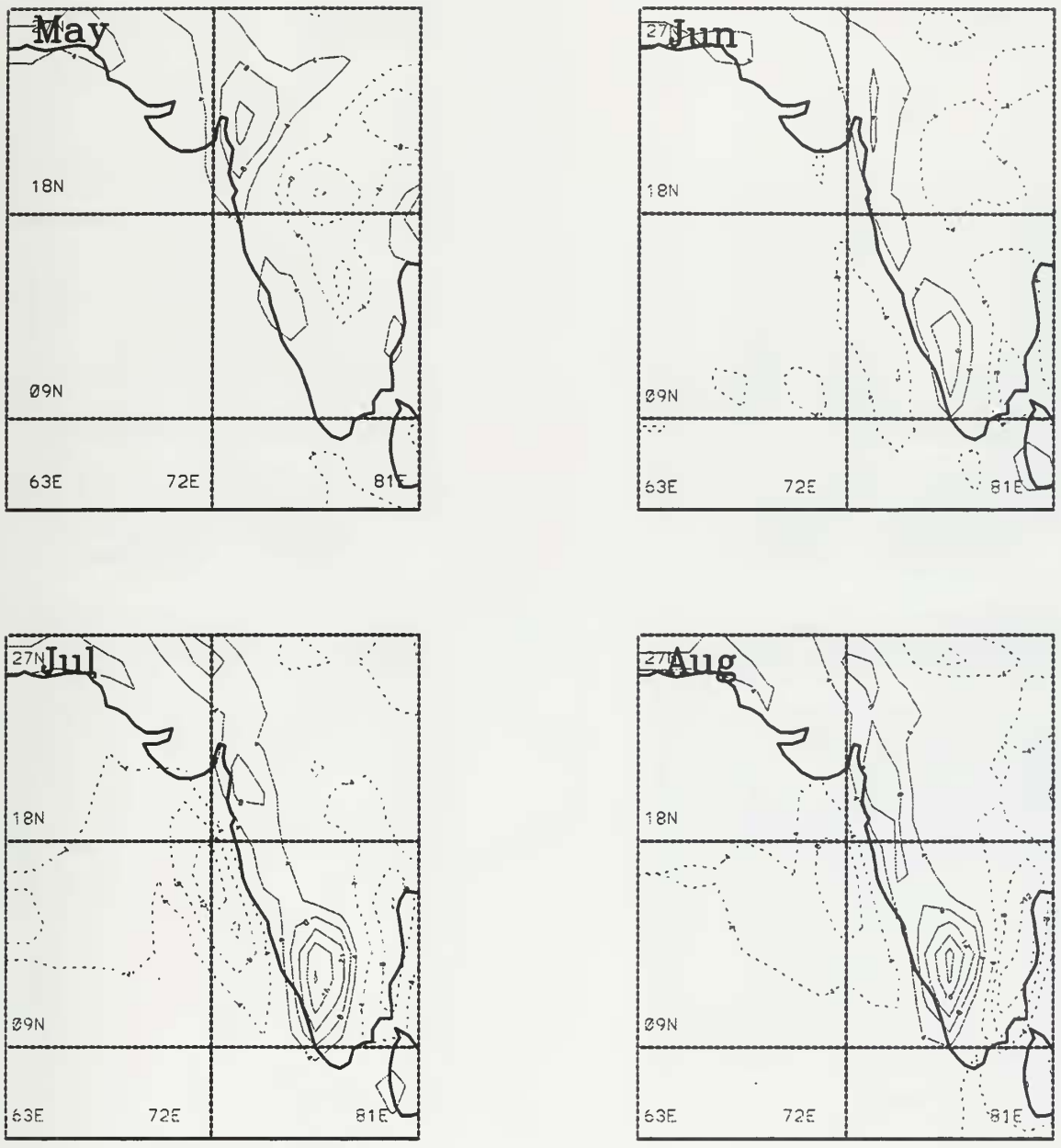

Figure 4. West India monthly mean 850 hPa divergence (10^{-6} s^{-1}) for May, June, July and August 1991. Contour interval is 4x 10^{-6} s^{-1}.

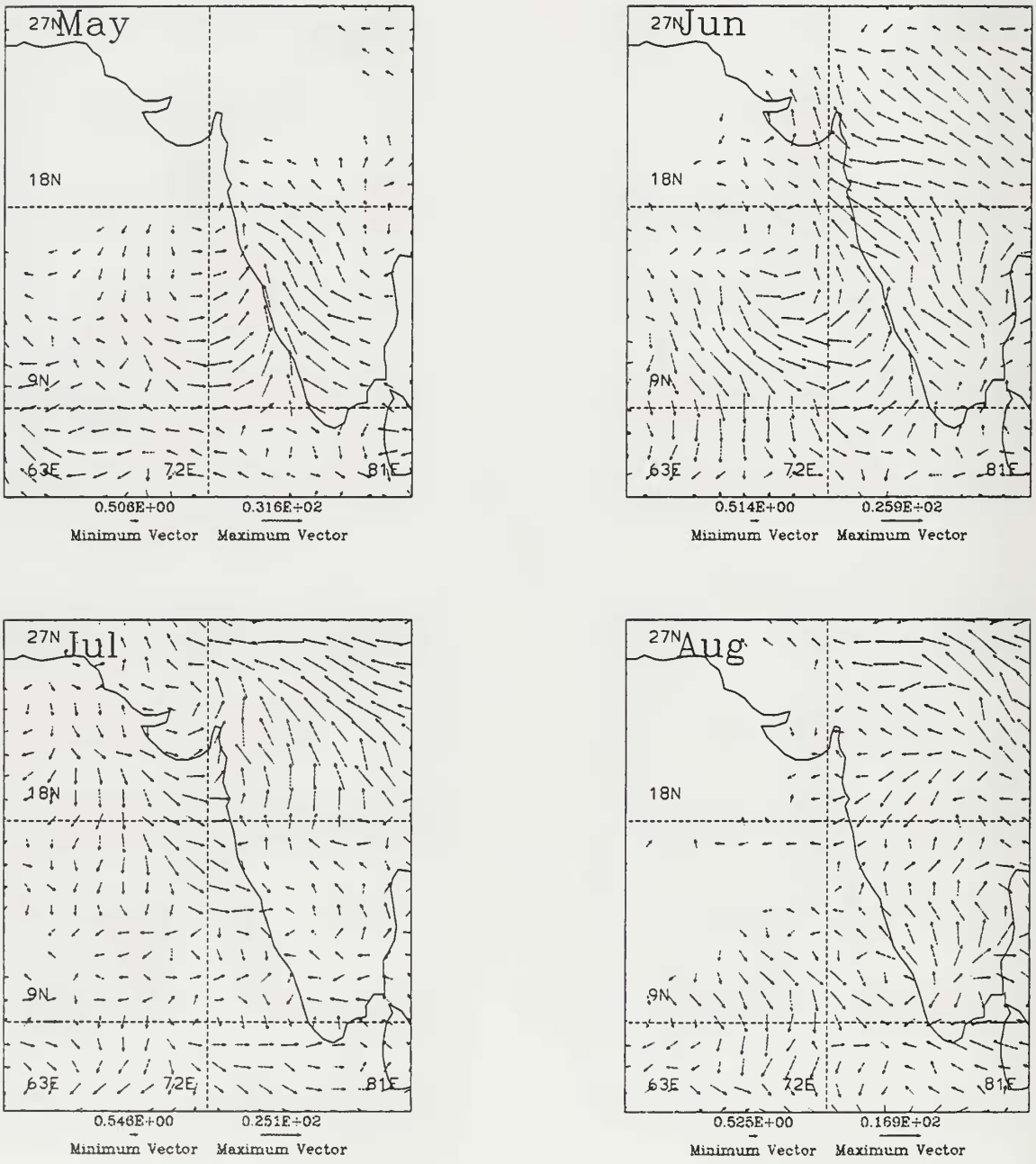

Figure 5. West India CI diurnal components for May, June, July and August 1991. Phase and amplitude are represented in vector form based on a 24 hour clock with 12 midnight pointing north. All times are local time. Vector length indicates magnitude of CI.

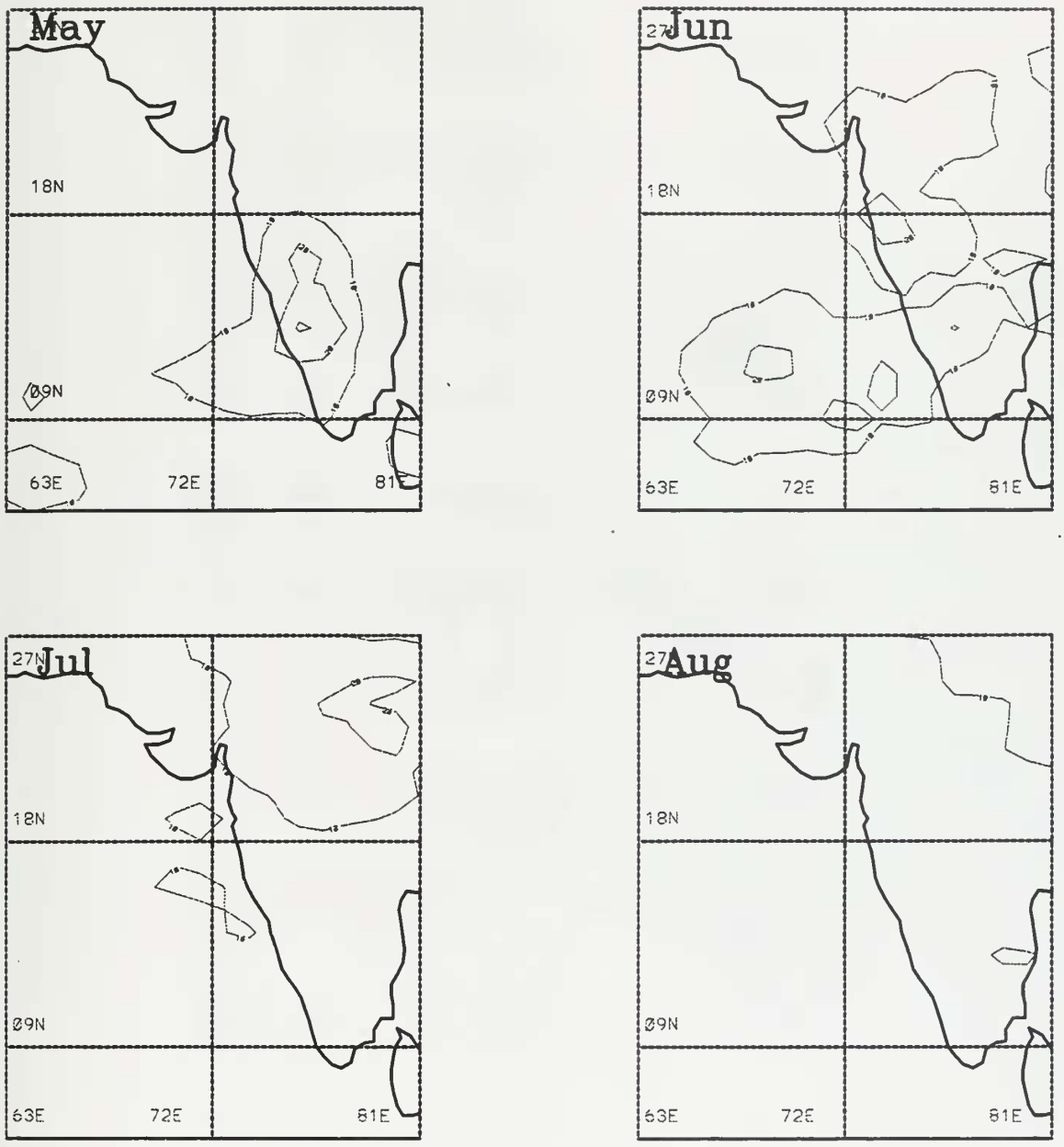

Figure 6. West India horizontal distribution of CI diurnal amplitude for May, June, July and August 1991. Contour interval is 10 °K.

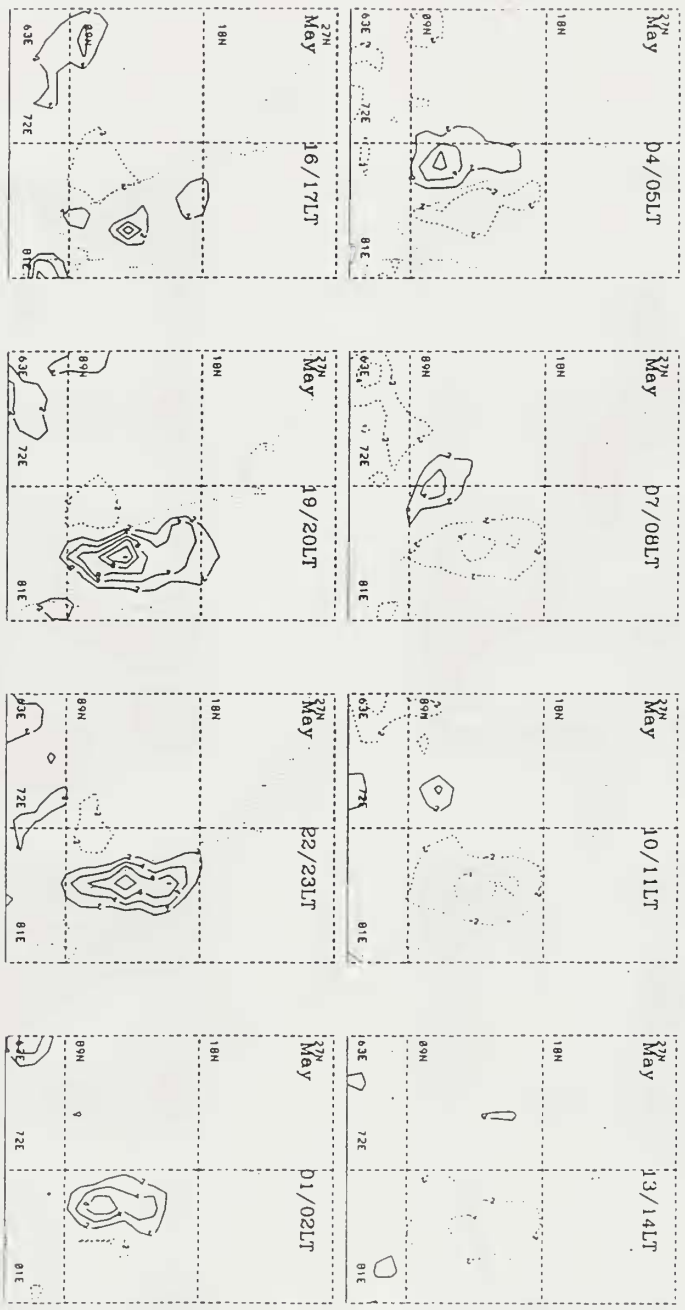

Figure 7a. West India diurnal CI anomaly composite every 3 hours for May 1991. Contour interval is 2 °K. Solid (dashed) contours represent positive (negative) deviations from the monthly mean.

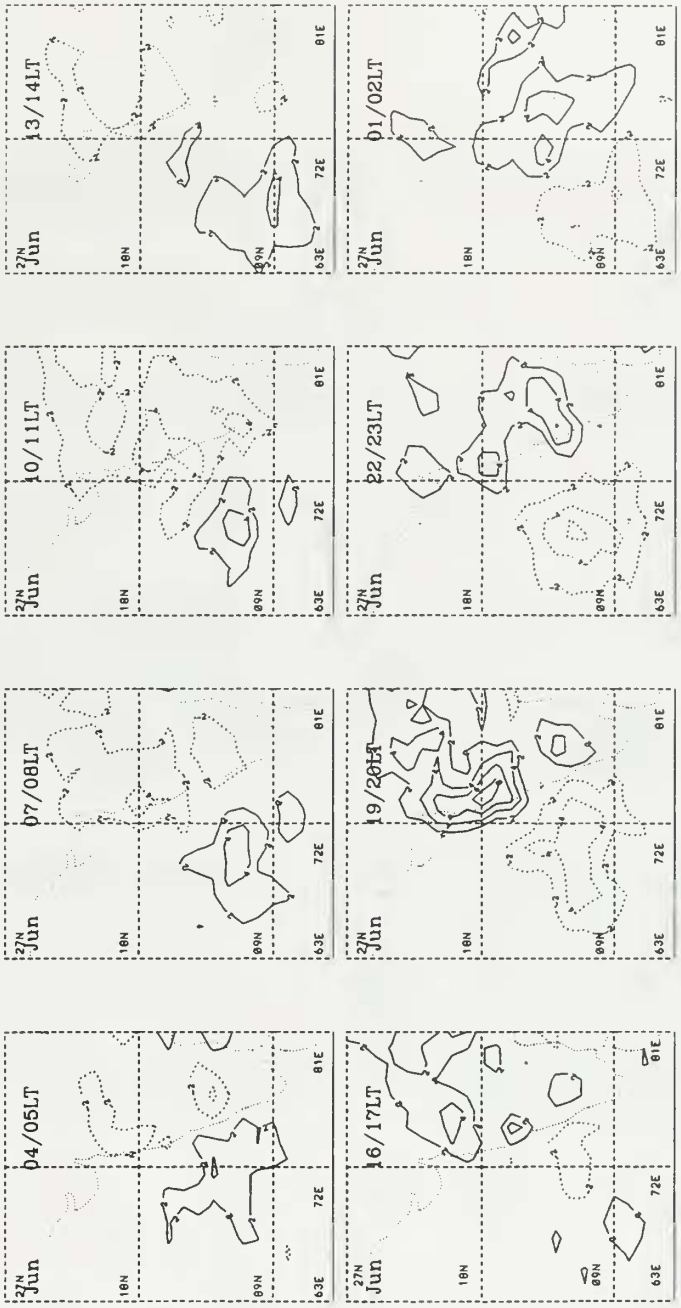

Figure 7b. As in Figure 7a except for June 1991.

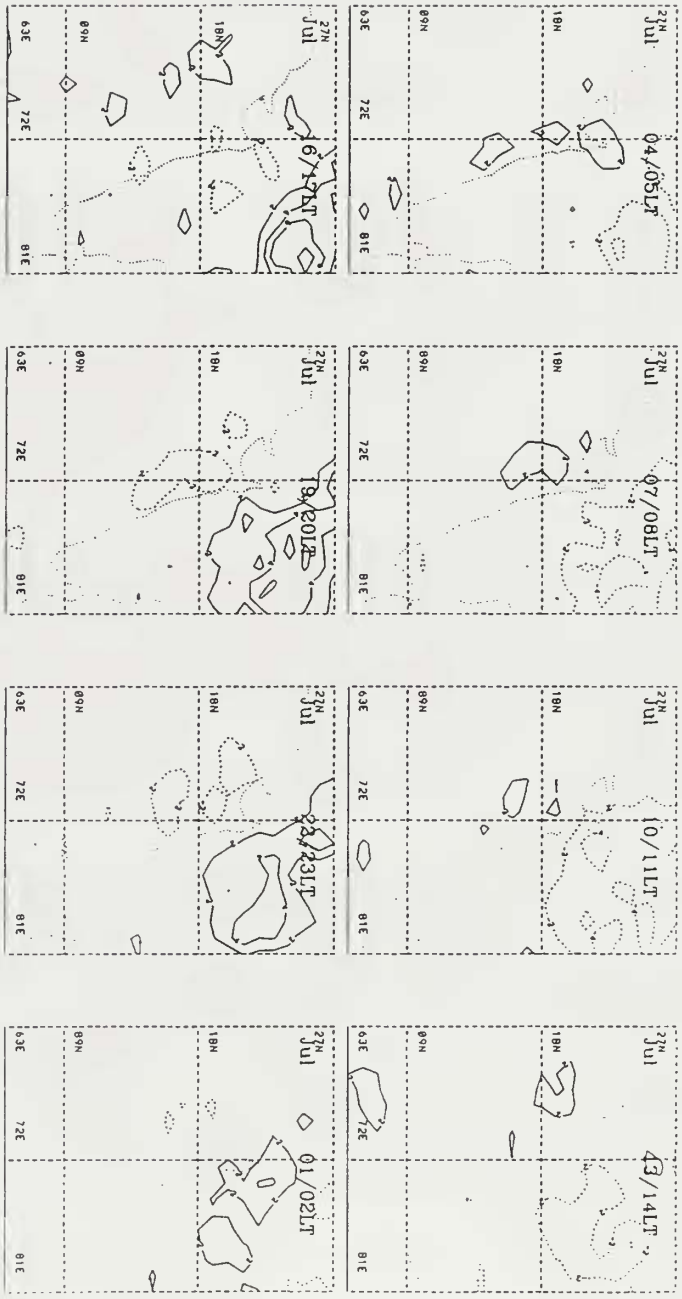

Figure 7c. As in Figure 7a except for July 1991.

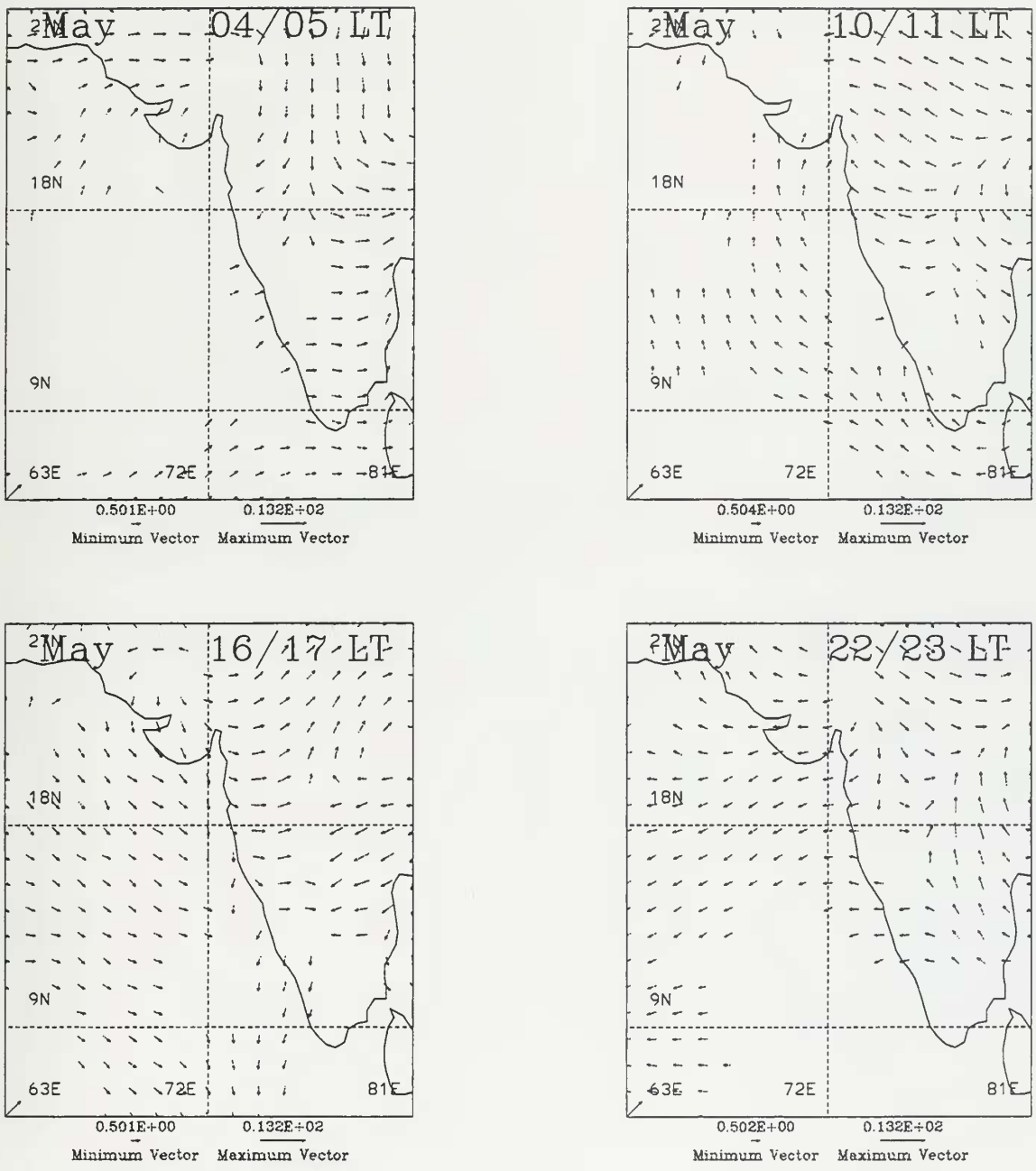

Figure 8a. West India 850 hPa wind anomaly composite every 6 hours for May 1991. Vector direction and size represents direction and magnitude of the deviation from the mean.

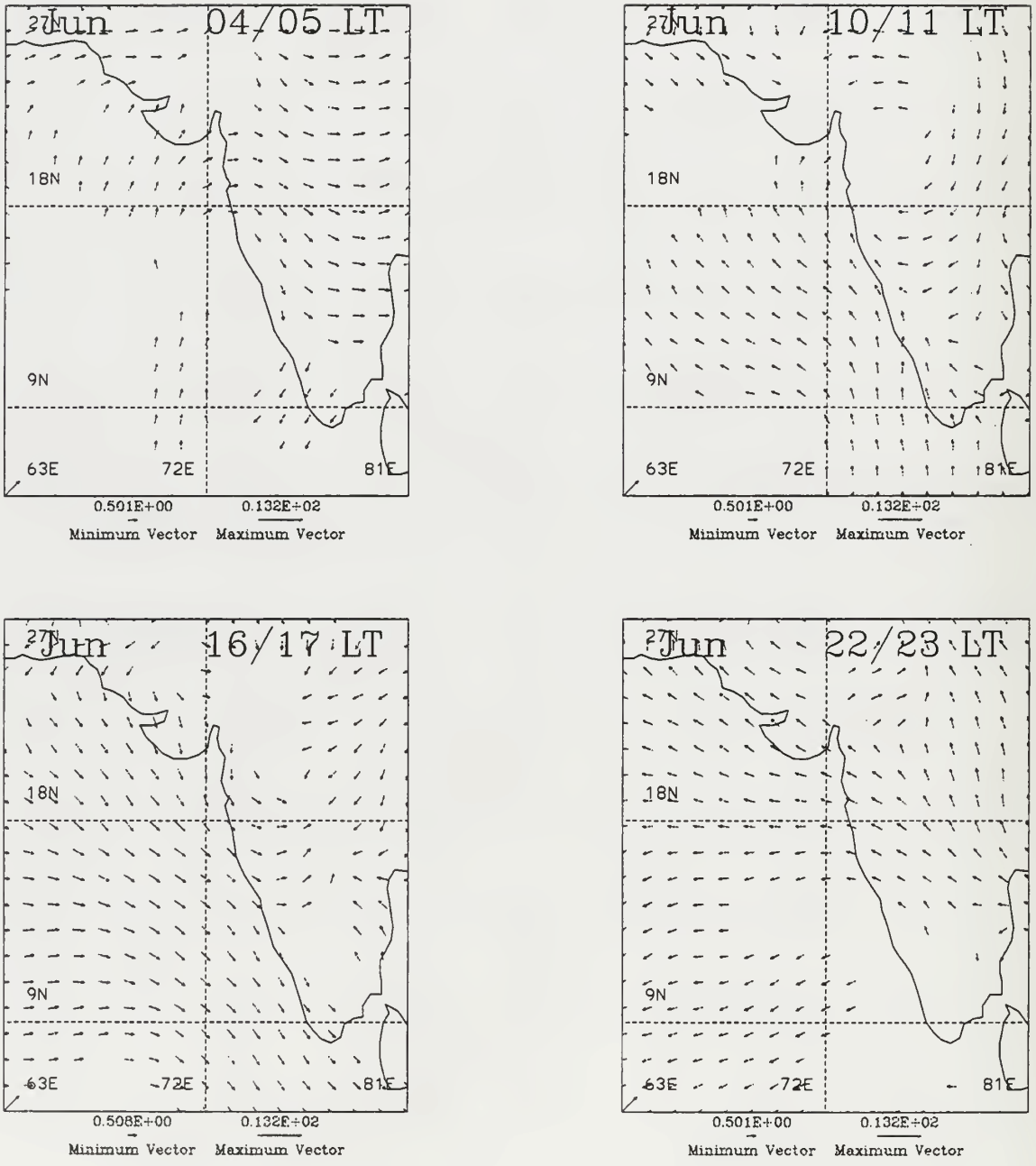

Figure 8b. As in Figure 8a except for June 1991.

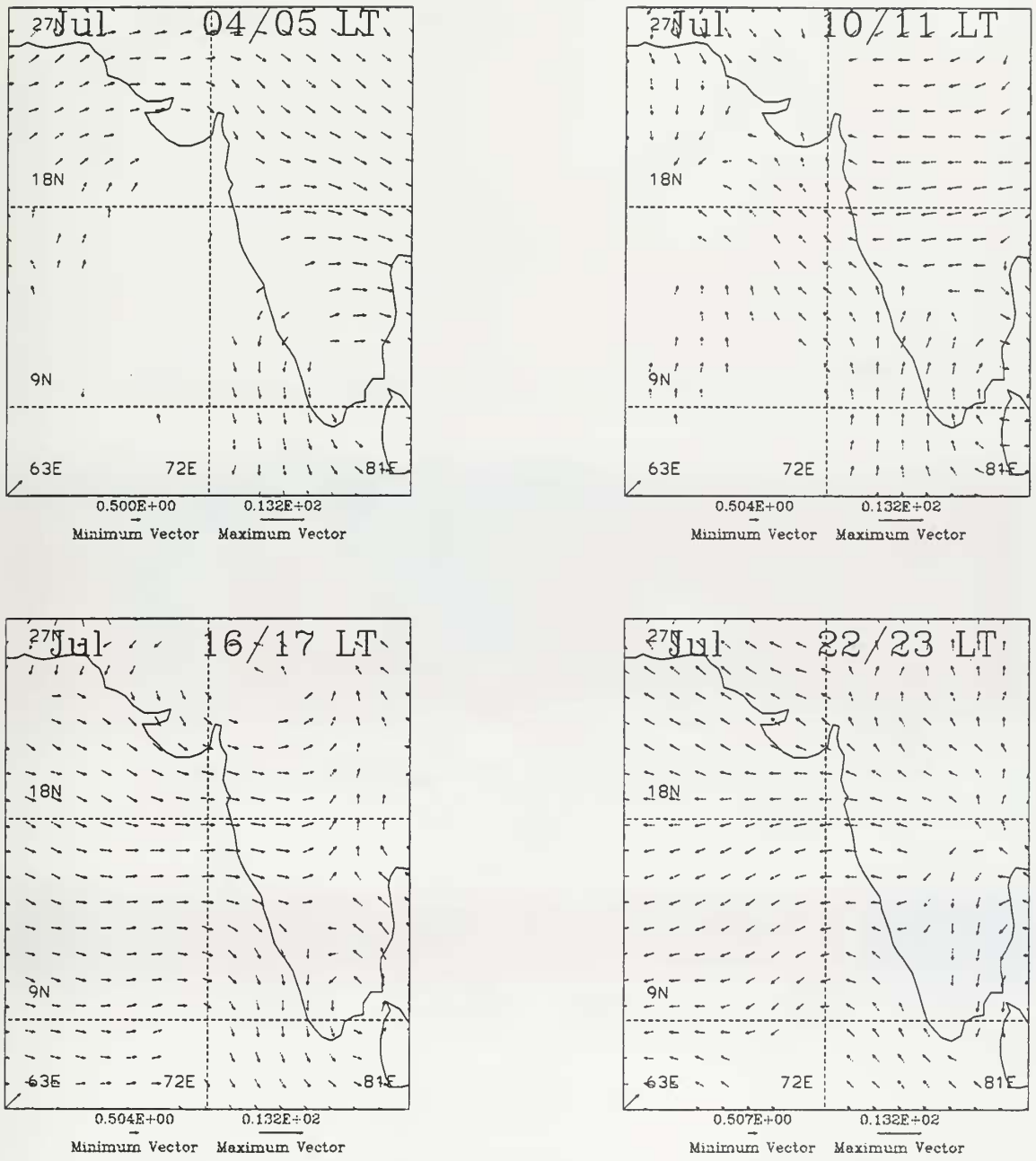

Figure 8c. As in Figure 8a except for July 1991.

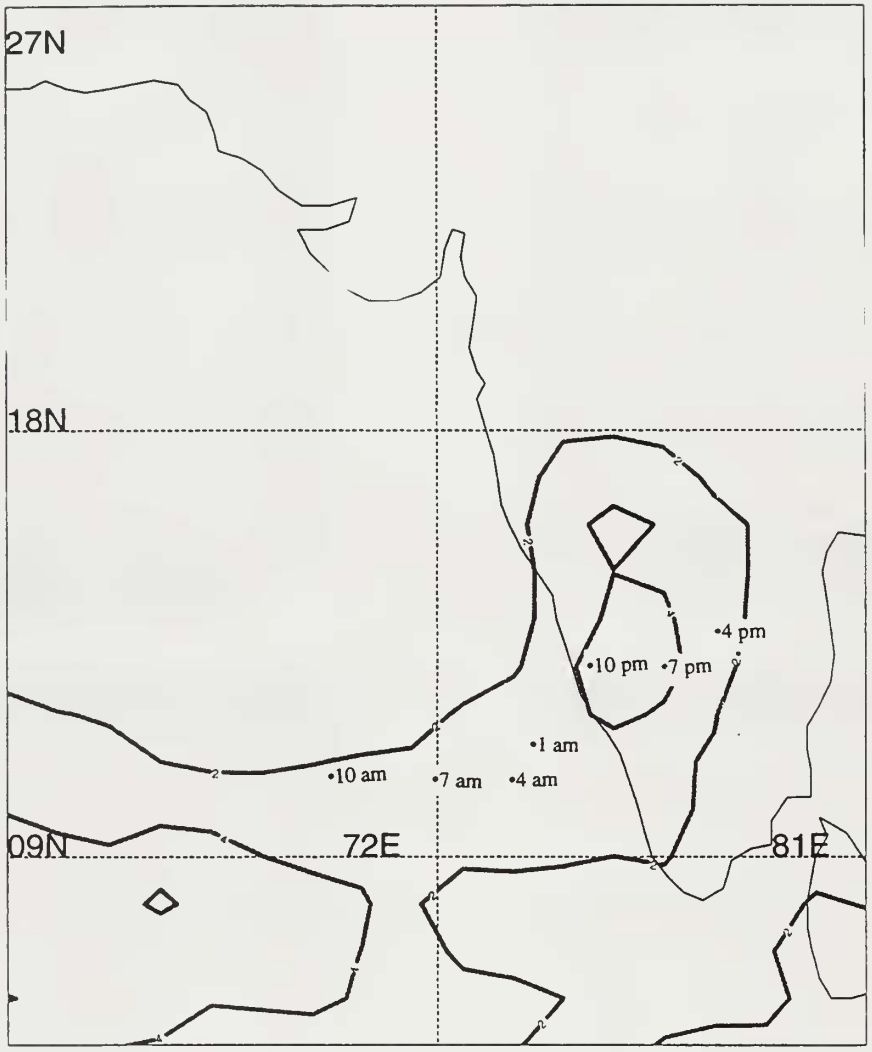

Figure 9. Monthly mean CI (°K) with three-hourly diurnal CI centers overlaid showing the propagation of convection during May 1991.

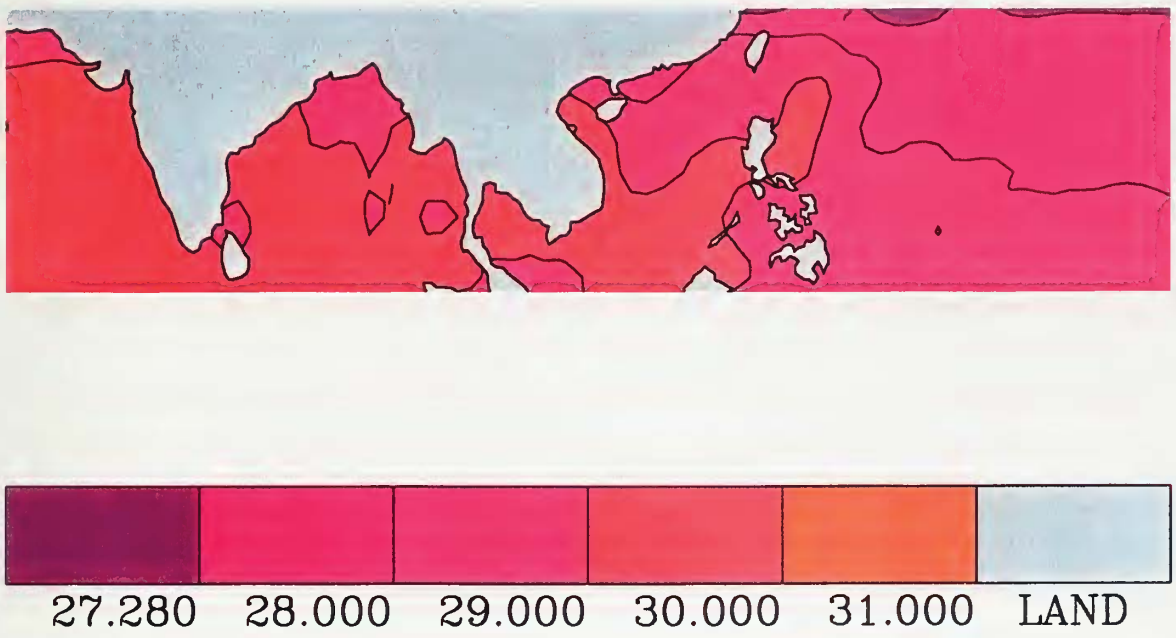

Figure 10. Monthly mean sea surface temperature (SST) for May 1991. Contour interval is 1 °C.

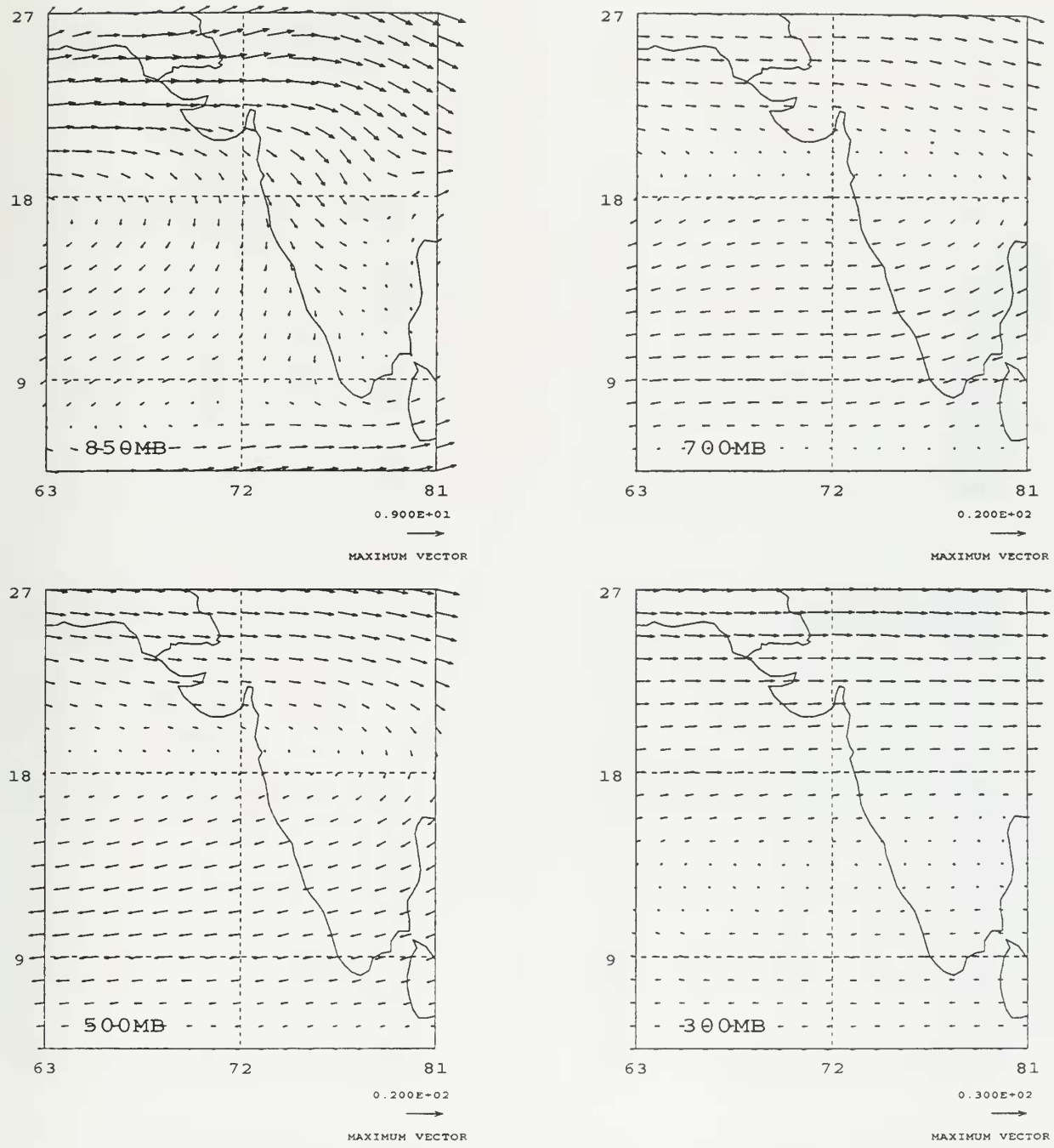

Figure 11. Monthly mean winds at 850, 700, 500 and 300 hPa for May 1991.

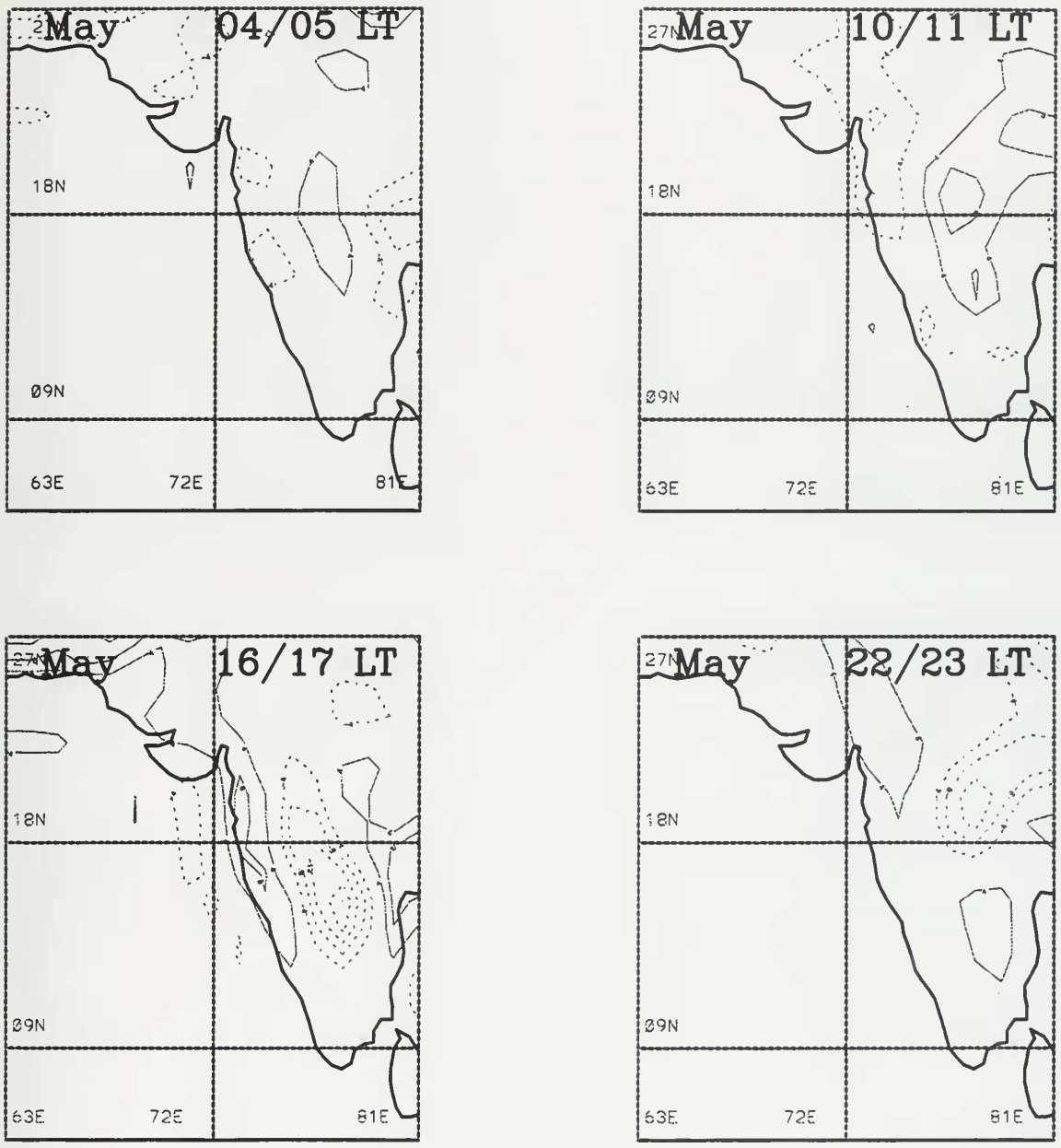

Figure 12a. West India 850 hPa divergence anomaly composite every 6 hours for May 1991. Contour interval is 4×10^{-6} s^{-1}. Solid (dashed) contours represent positive (negative) deviations from the mean.

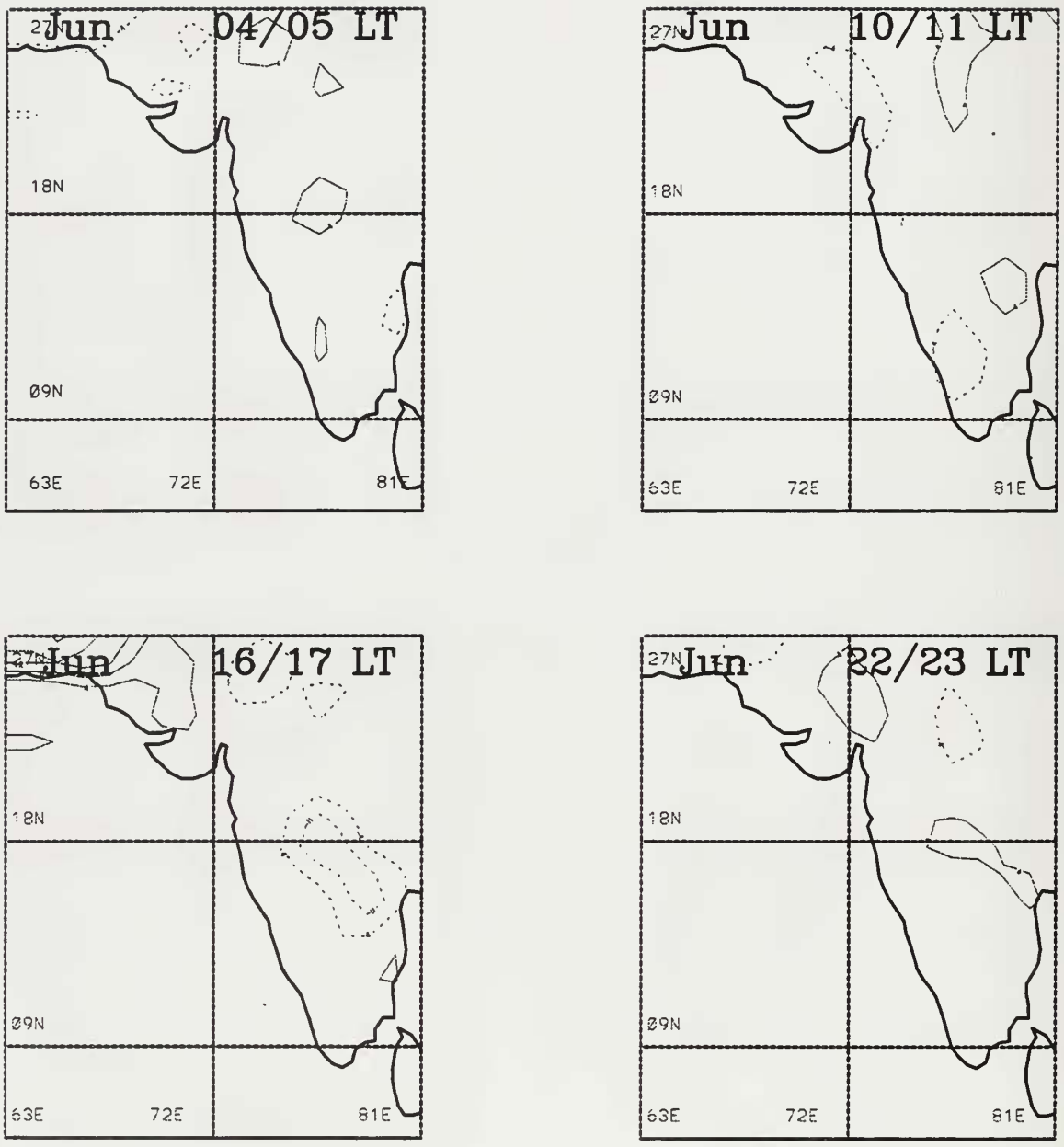

Figure 12b. As in Figure 12a except for June 1991.

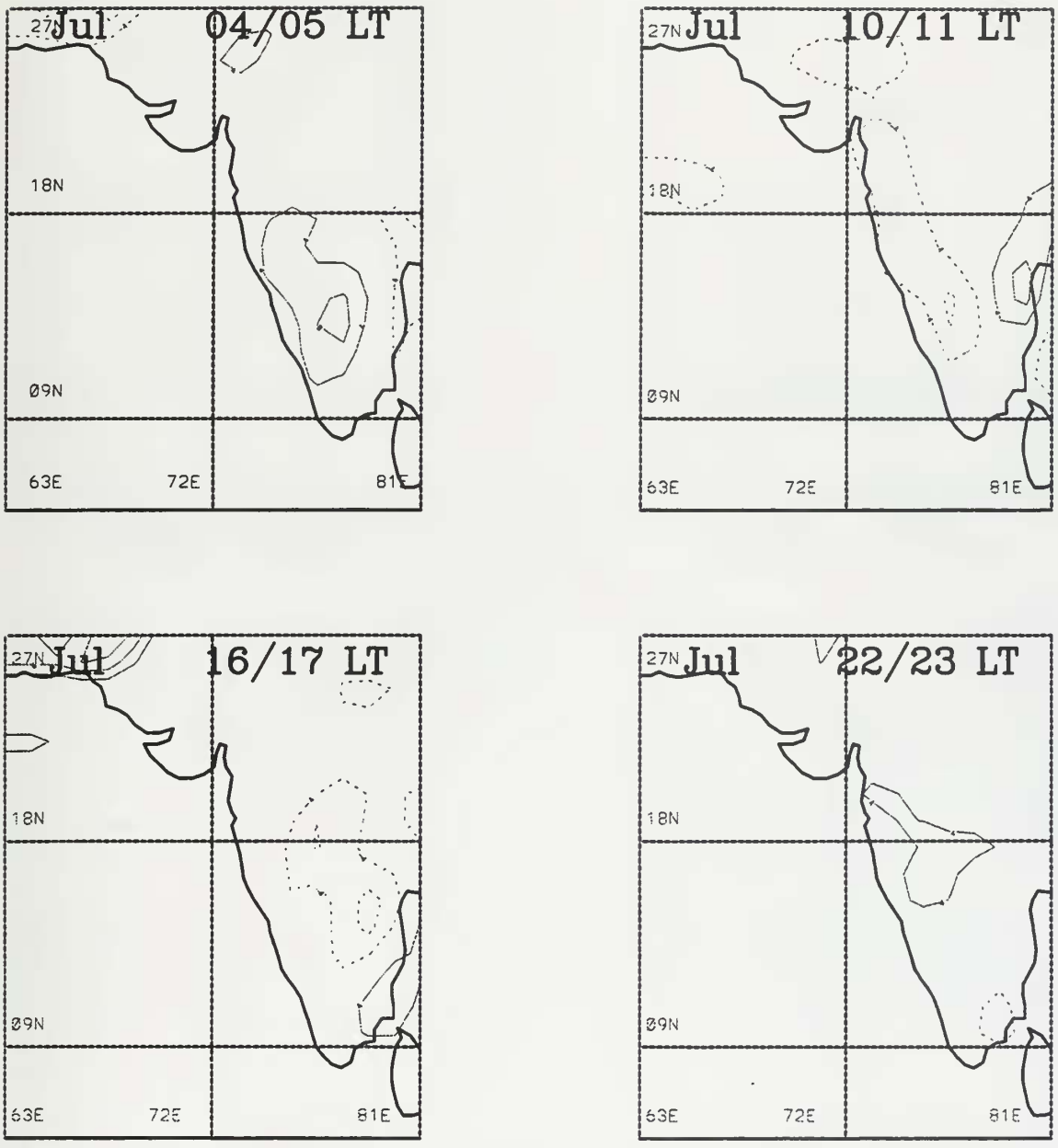

Figure 12c. As in Figure 12a except for July 1991.

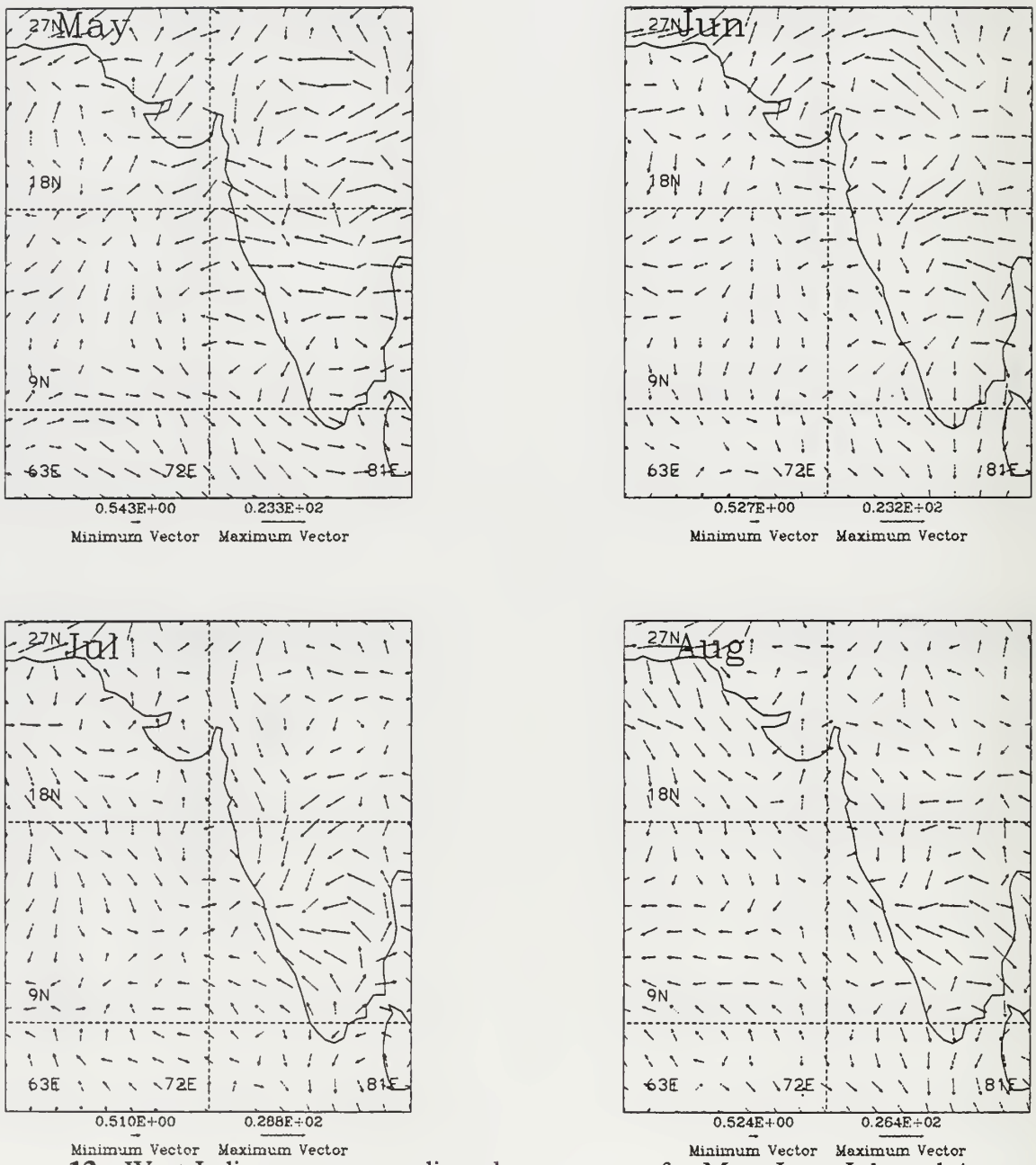

Figure 13. West India convergence diurnal components for May, June, July and August 1991. Phase and amplitude are represented in vector form based on a 24 hour clock with 12 midnight pointing north. All times are local time. Vector length indicates magnitude of convergence (-D850).

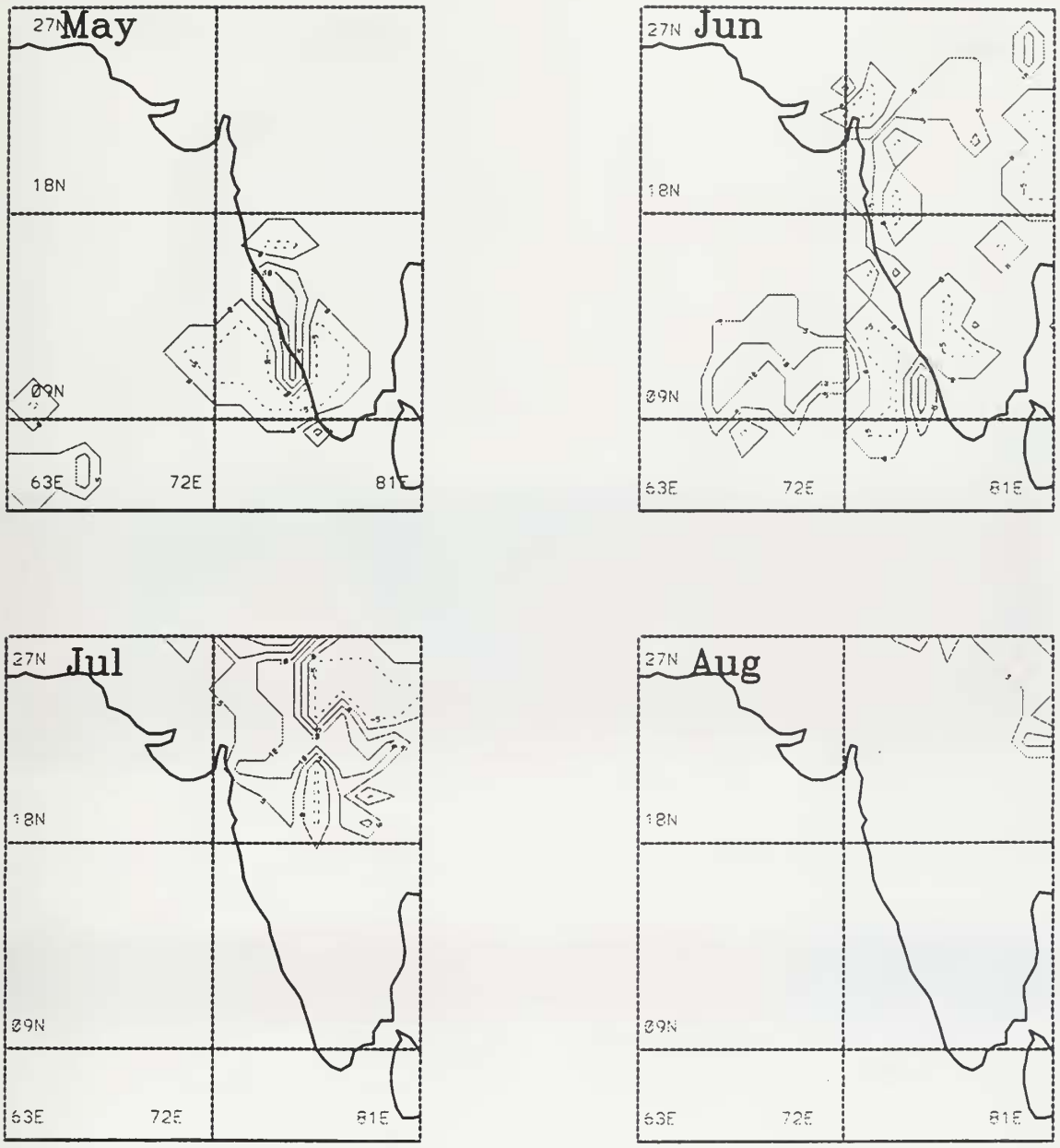

Figure 14. West India phase relationship between 850 hPa convergence and CI greater then 10 °K for May, June, July and August 1991. Contour interval is 5 hours. Positive (negative) values are solid (dashed). Values less (greater) than -5 (+5) indicate convergence leads (lags) convection. Values > +5 indicate convergence and convection are in phase. Values > 10 indicate convergence and convection are out of phase.

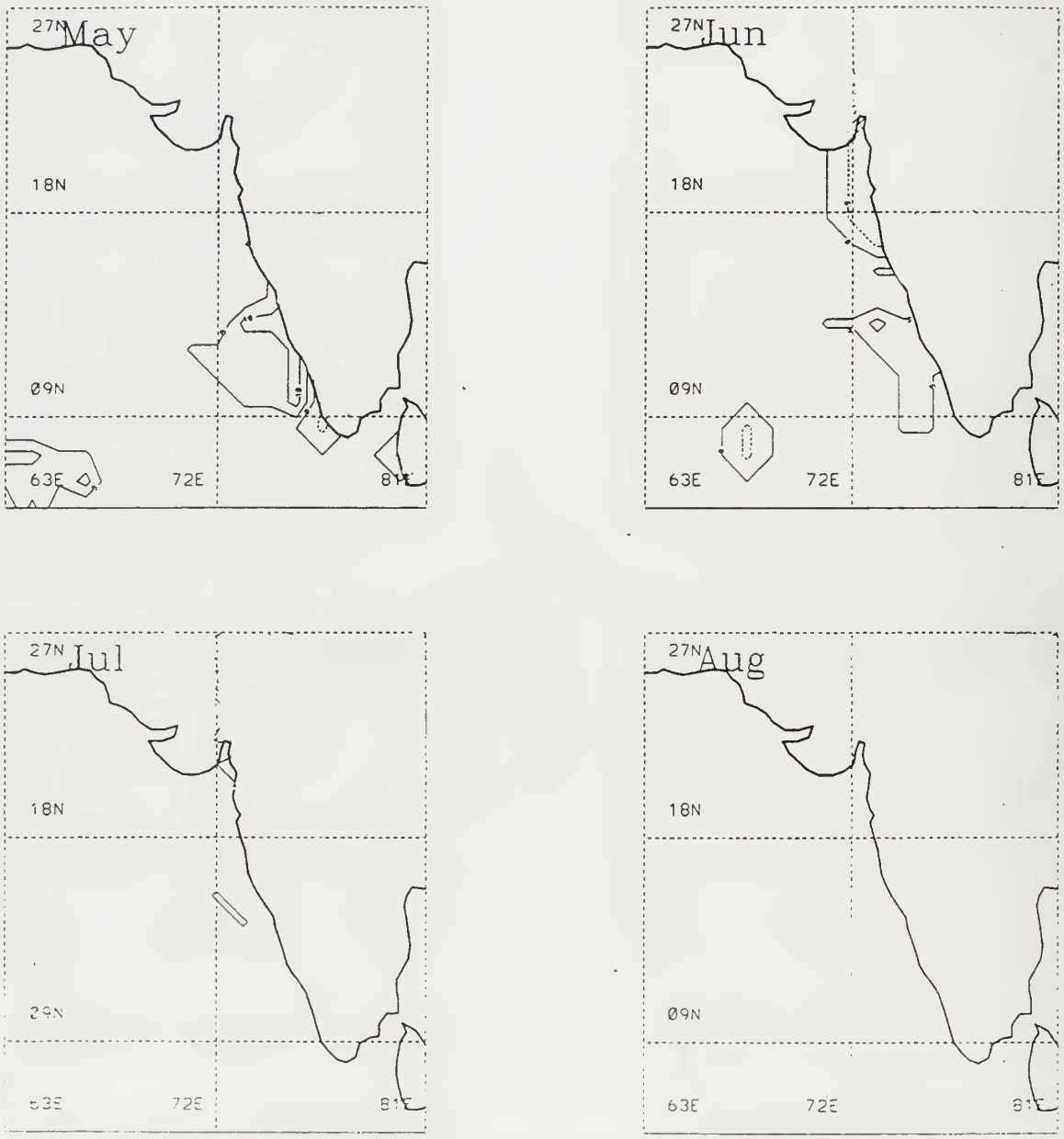

Figure 15. As in Figure 14 except the relationship is between latent heat flux and CI greater than 10 °K.

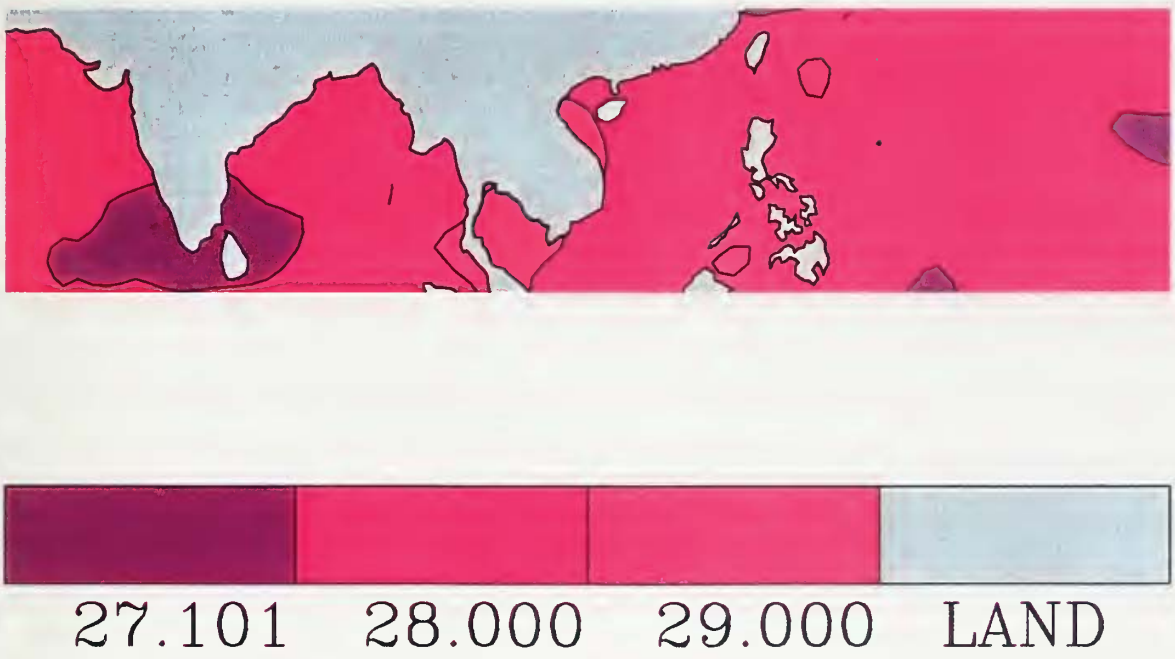

Figure 16. Monthly mean SST for June 1991. Contour interval is 1 °C.

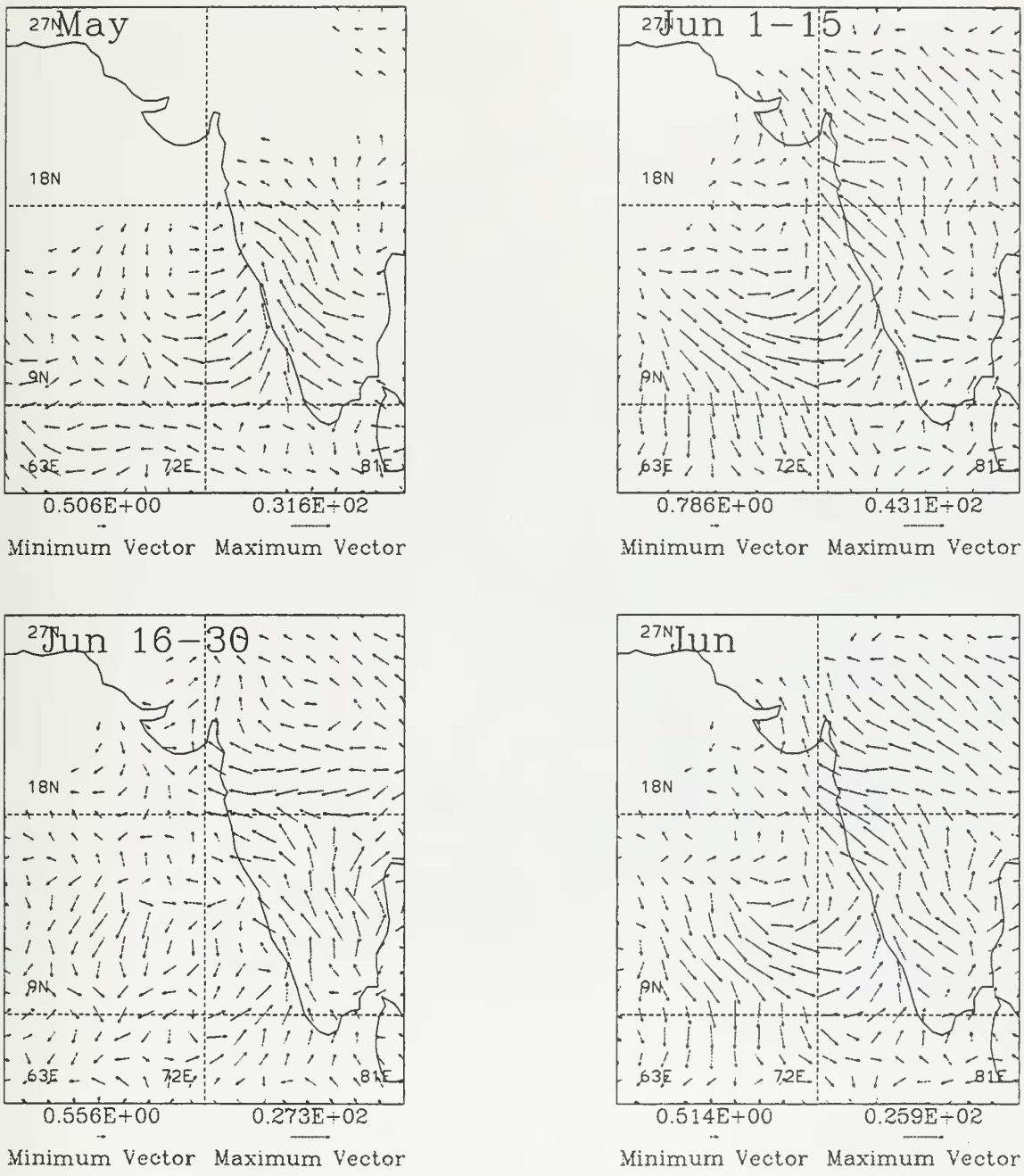

Figure 17. As in Figure 5 except a comparison between the first two weeks and last two weeks of June and the monthly means for May and June 1991.

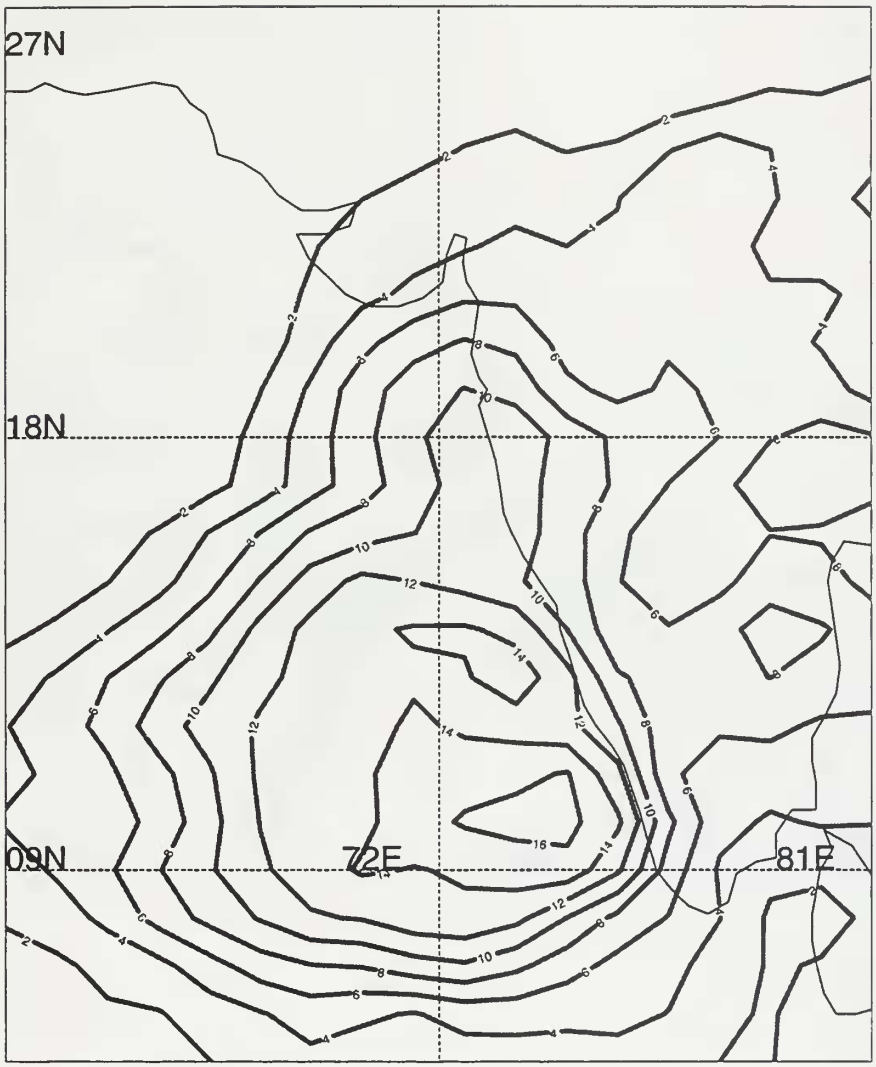

Figure 18. Mean CI for June 1-15. Contour interval is 2 °K.

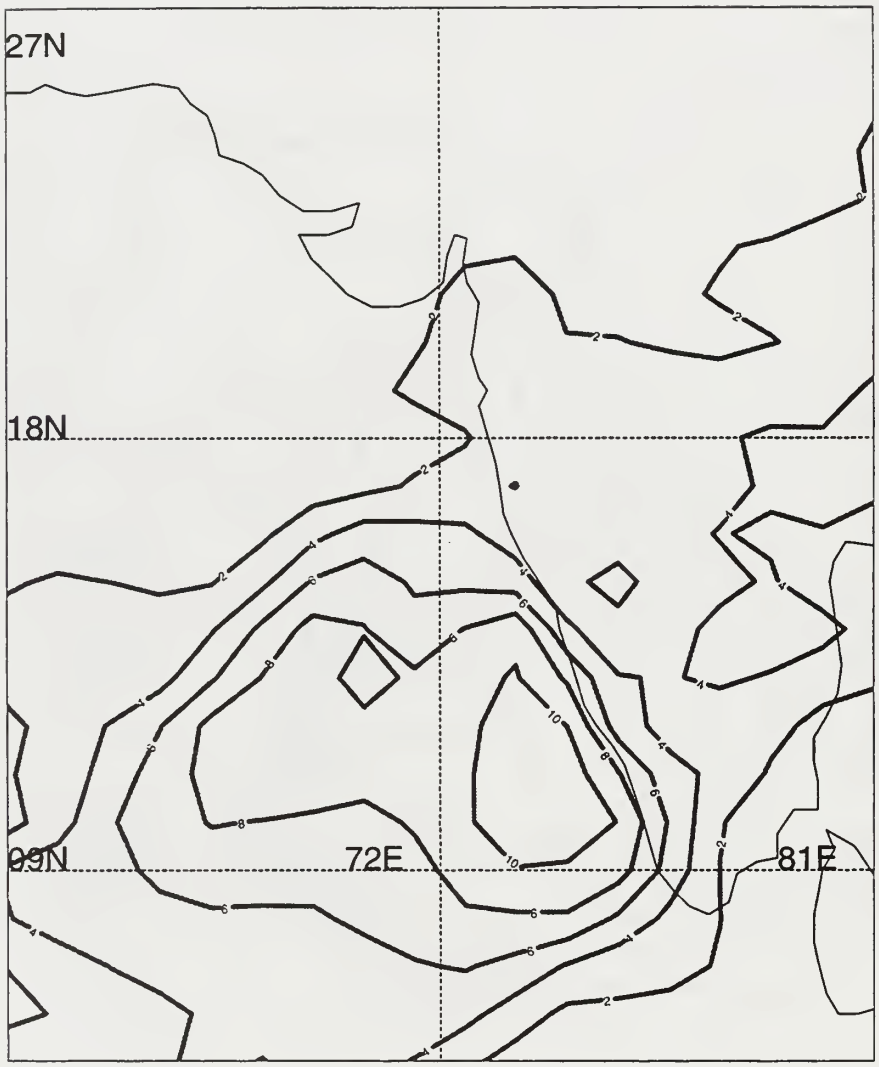

Figure 19. As in Figure 18 except for June 16-30.

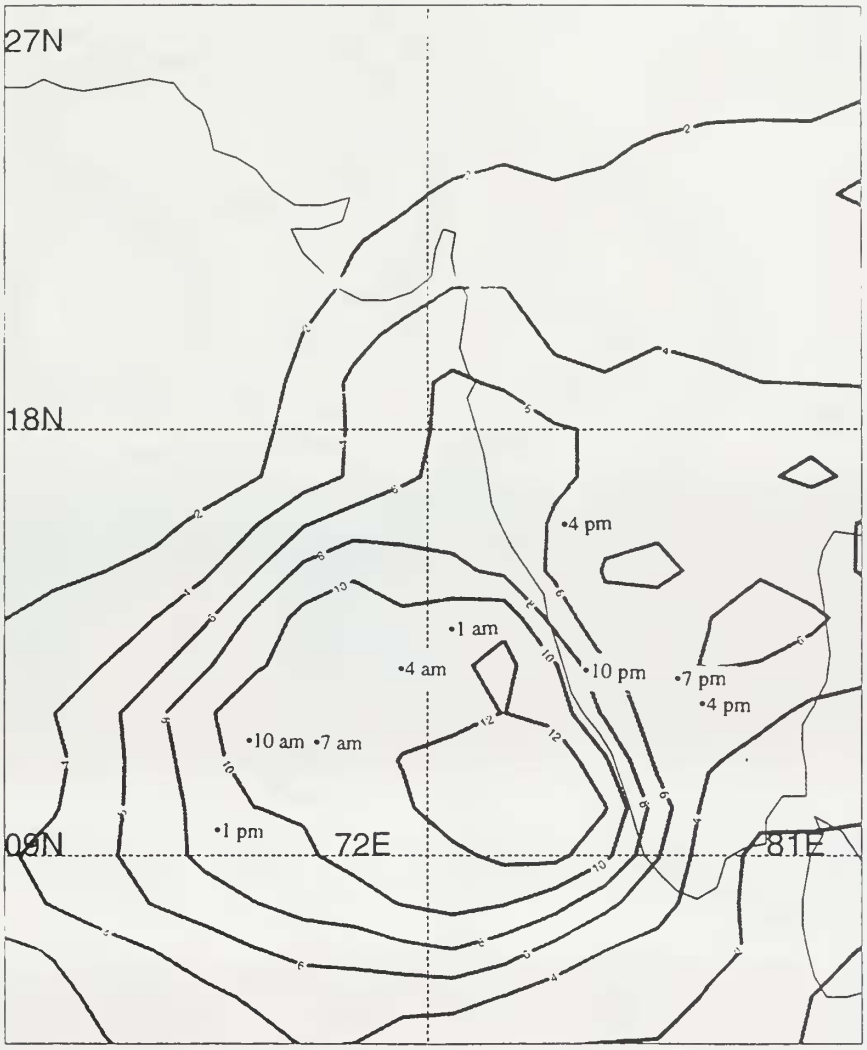

Figure 20. As in Figure 9 except for June 1991.

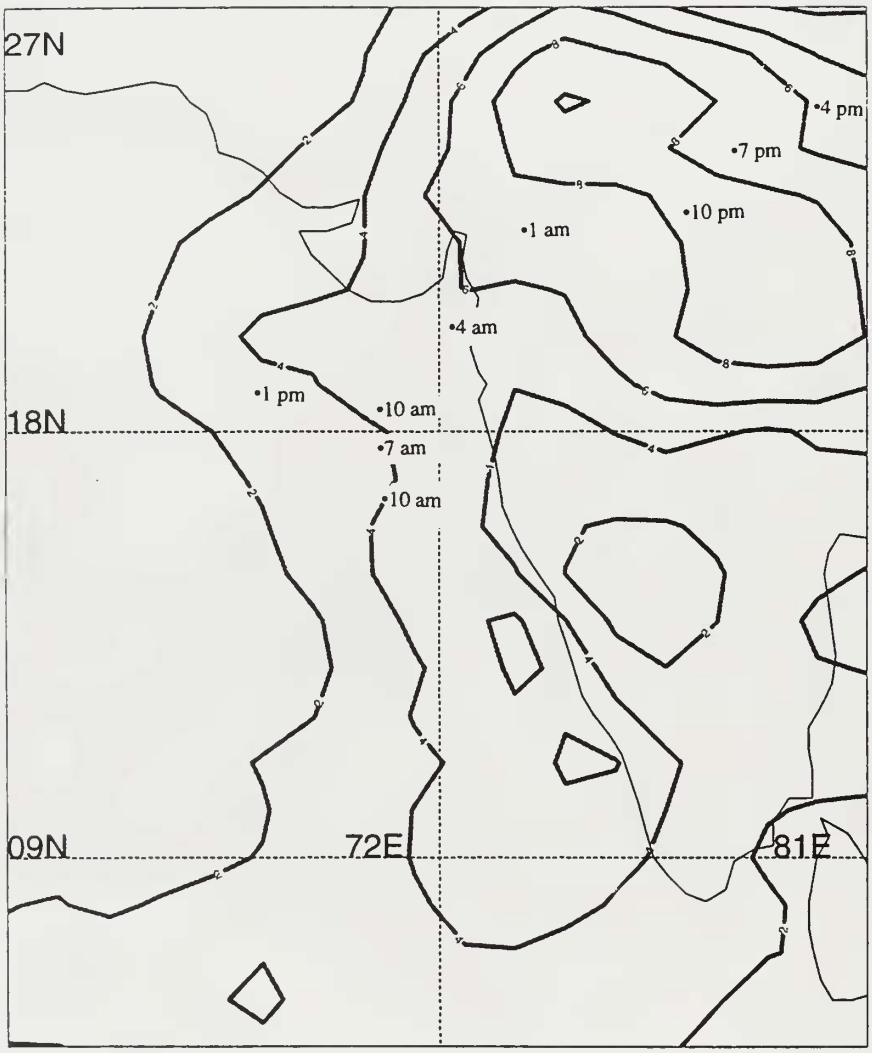

Figure 21. As in Figure 9 except for July 1991.

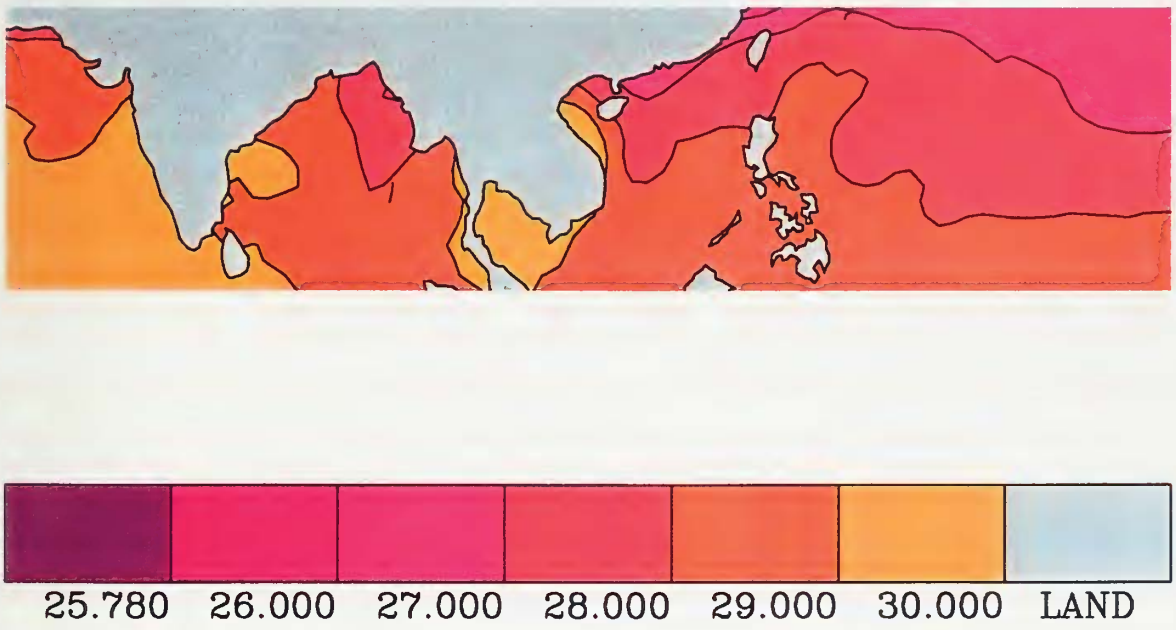

Figure 22. As in Figure 10 except for July 1991.

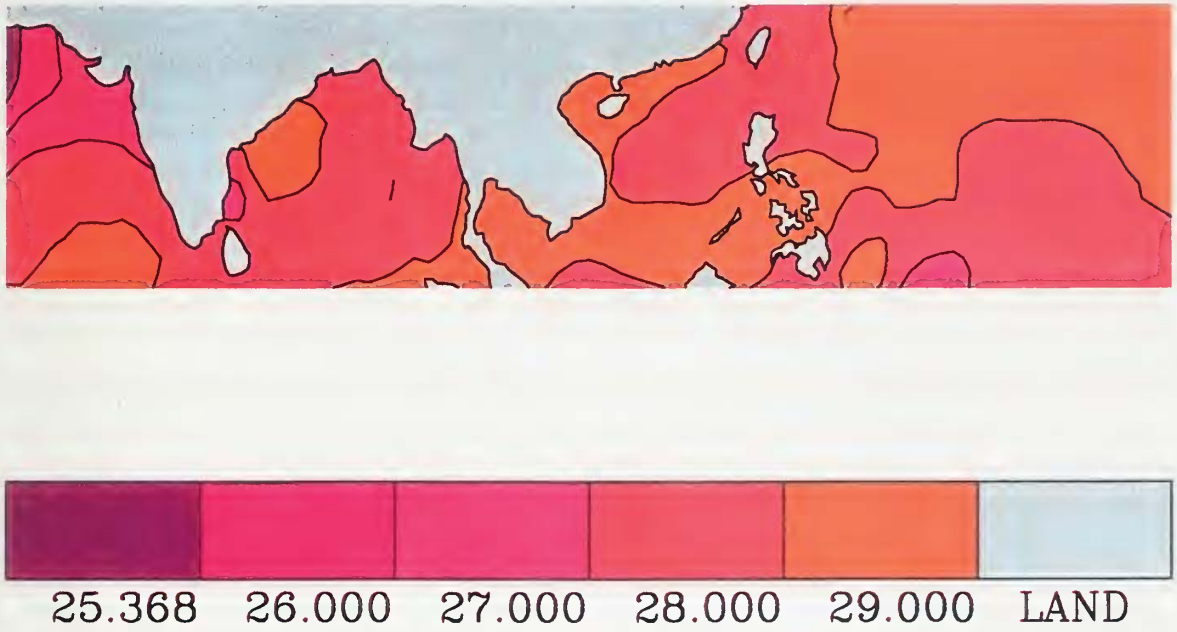

Figure 23. As in Figure 10 except for August 1991.

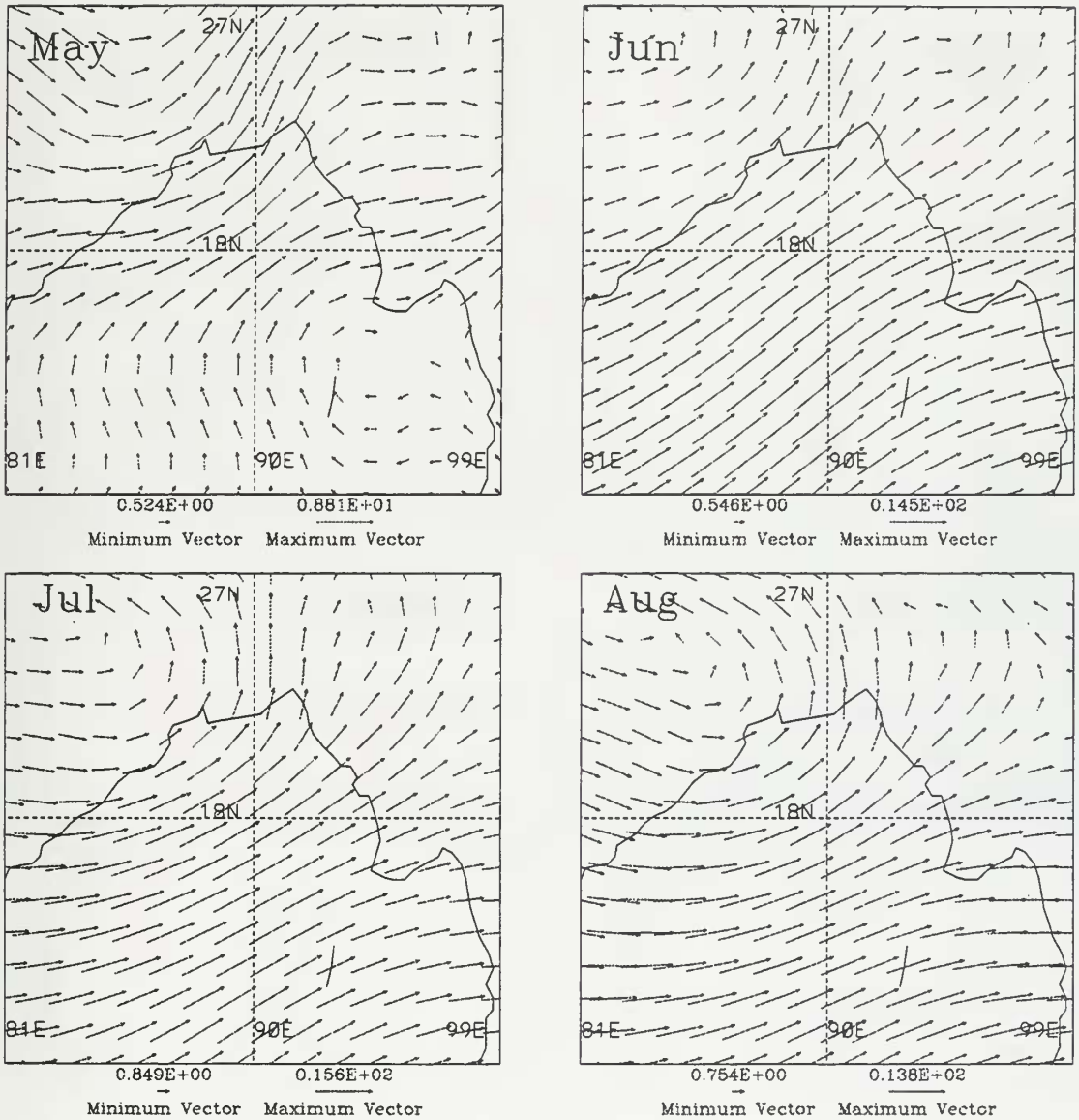

Figure 24. Bay of Bengal 850 hPa monthly mean winds (m/s) for May, June, July and August 1991.

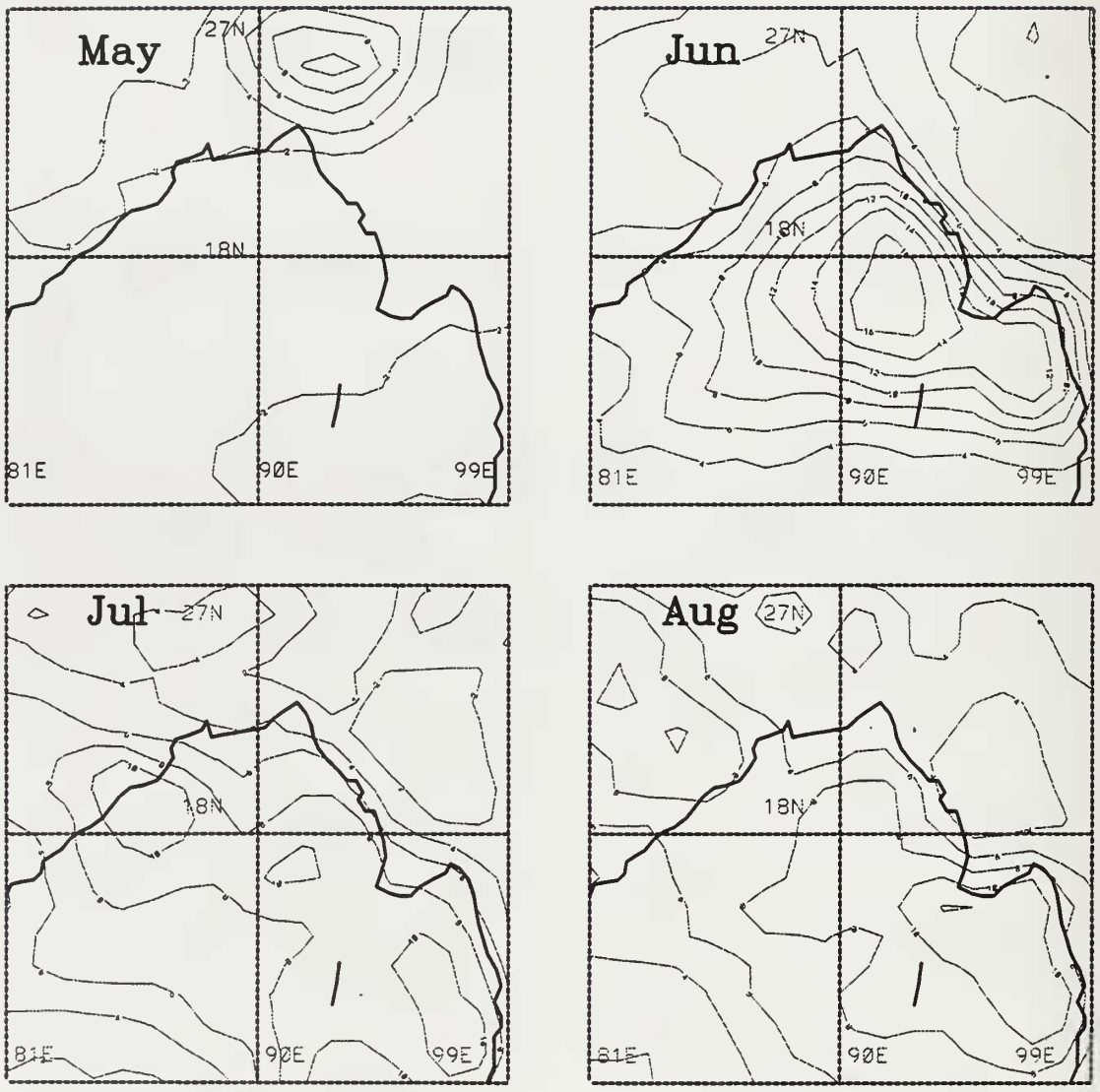

Figure 25. Bay of Bengal monthly mean convective Index (CI) for May, June, July and August 1991. Contour interval is 2 °K.

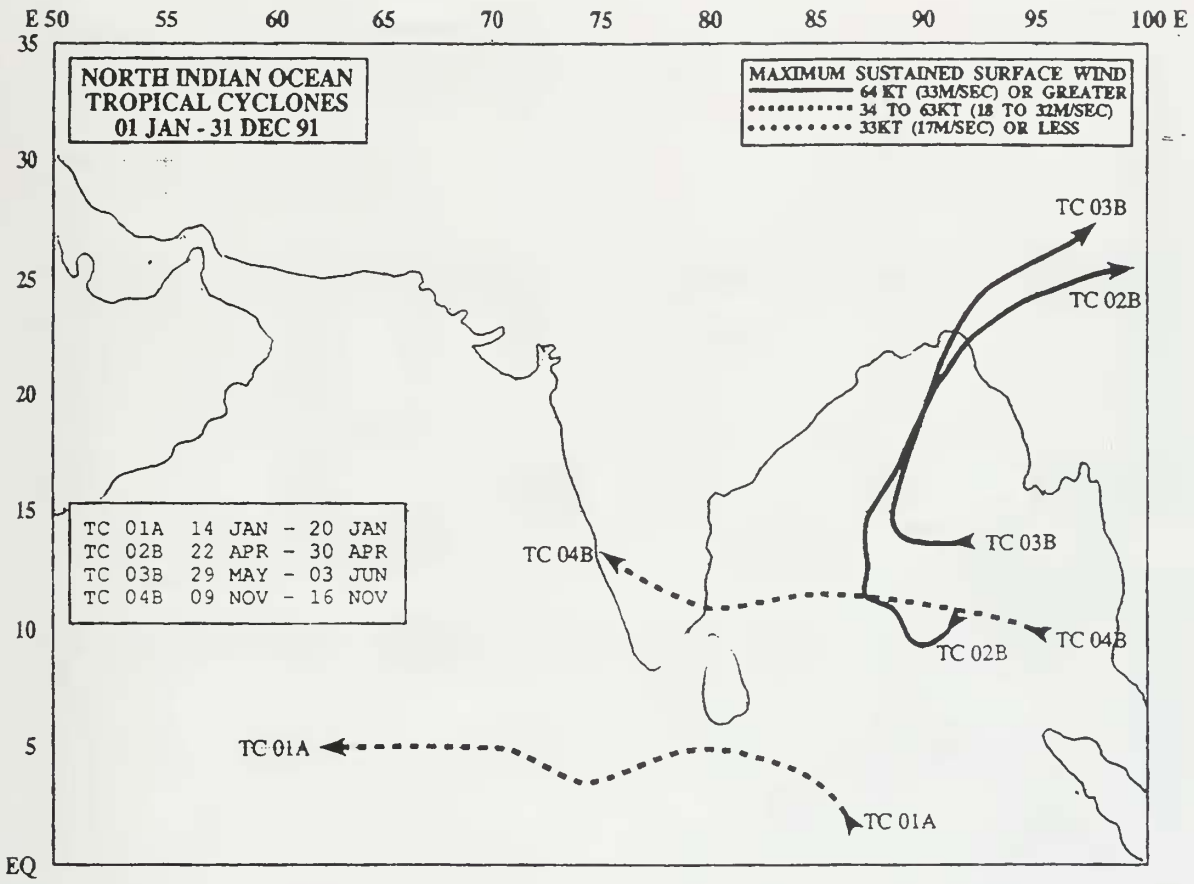

Figure 26. North Indian Ocean tropical cyclones during 1991. From Rudolph and Guard (1991).

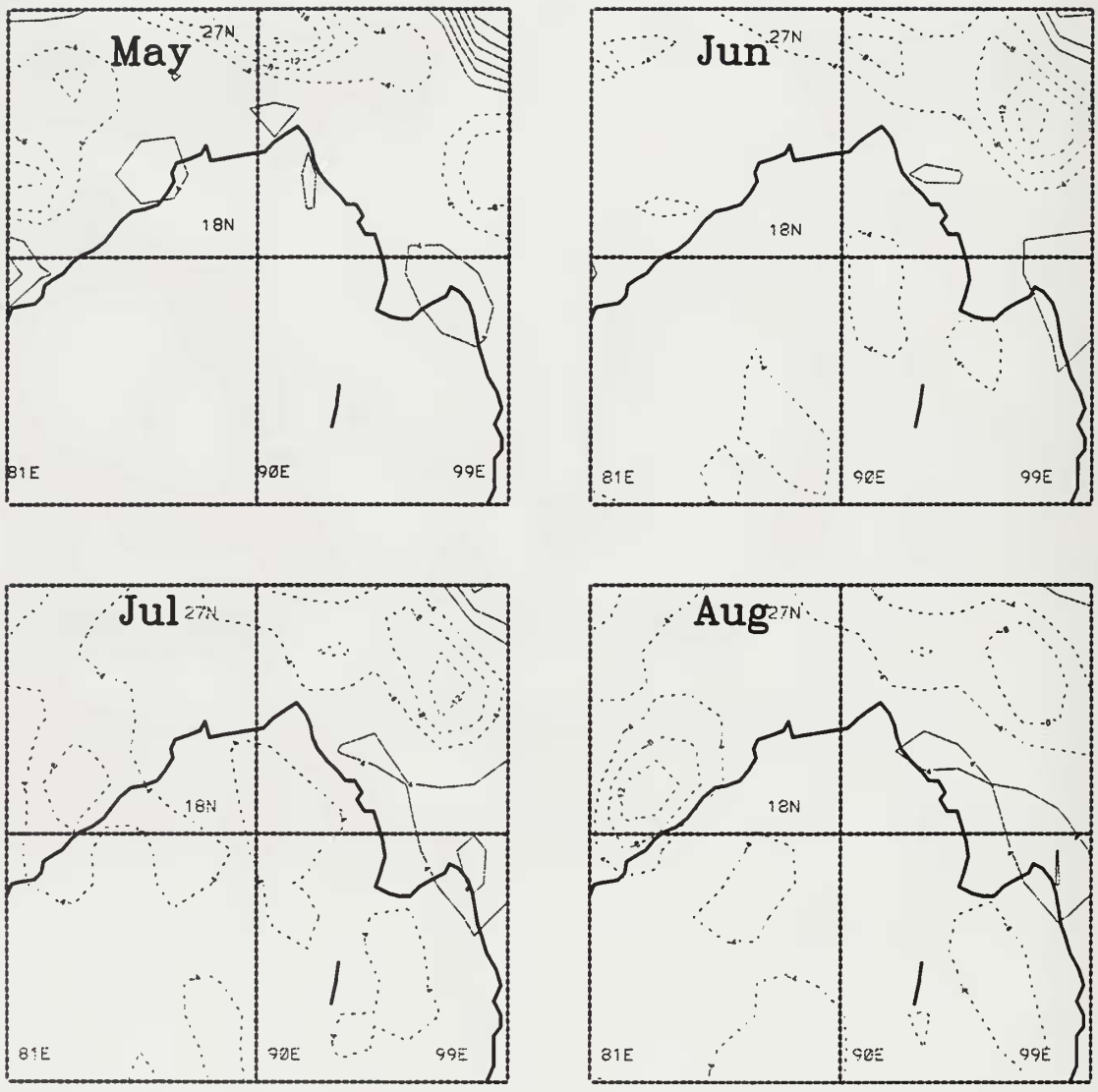

Figure 27. Bay of Bengal monthly mean 850 hPa divergence (10^{-6} s^{-1}) for May, June, July and August 1991. Contour interval is 4x 10^{-6} s^{-1}.

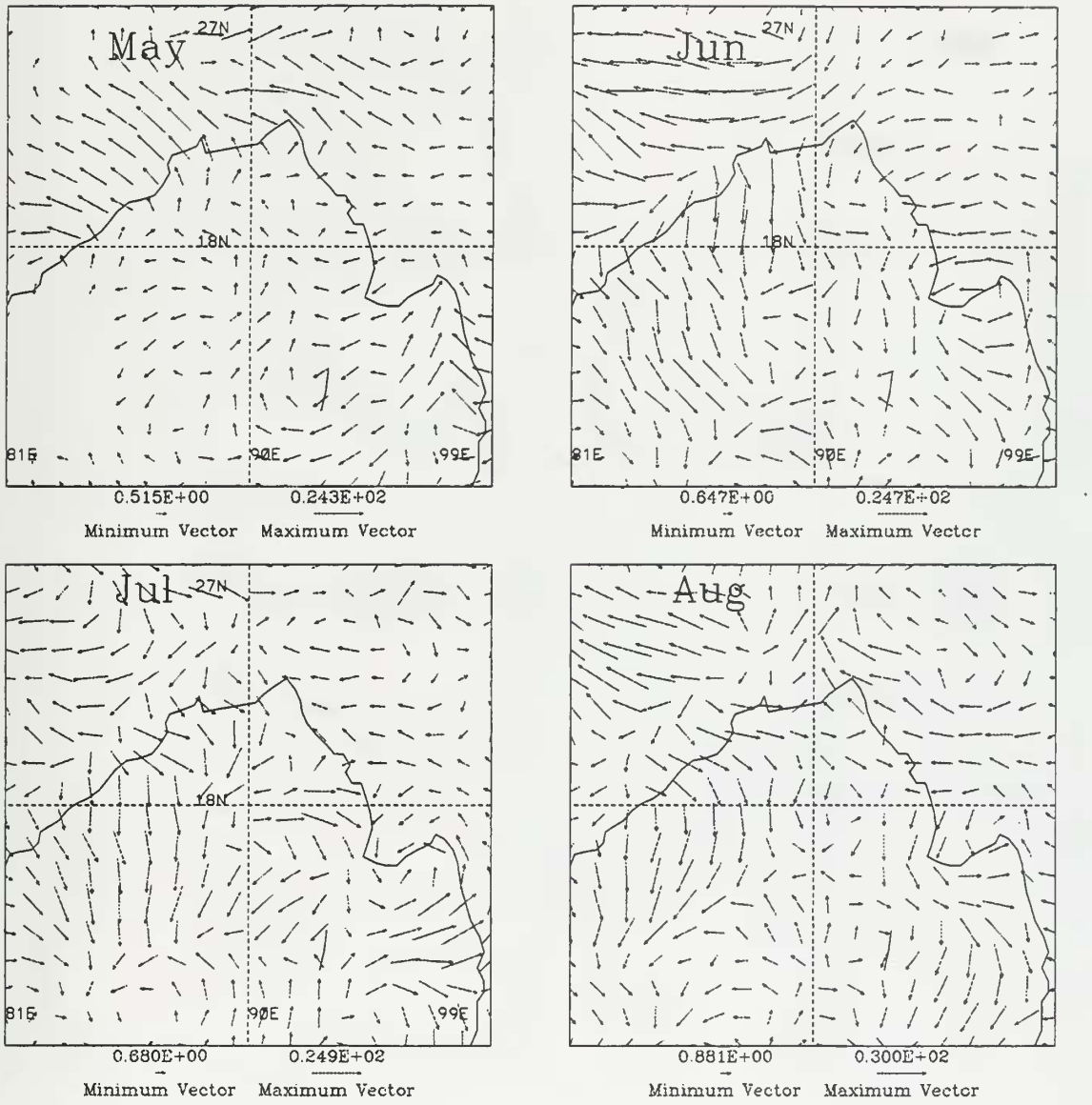

Figure 28. Bay of Bengal CI diurnal components for May, June, July and August 1991. Phase and amplitude are represented in vector form based on a 24 hour clock with 12 midnight pointing north. All times are local time. Vector length indicates magnitude of CI.

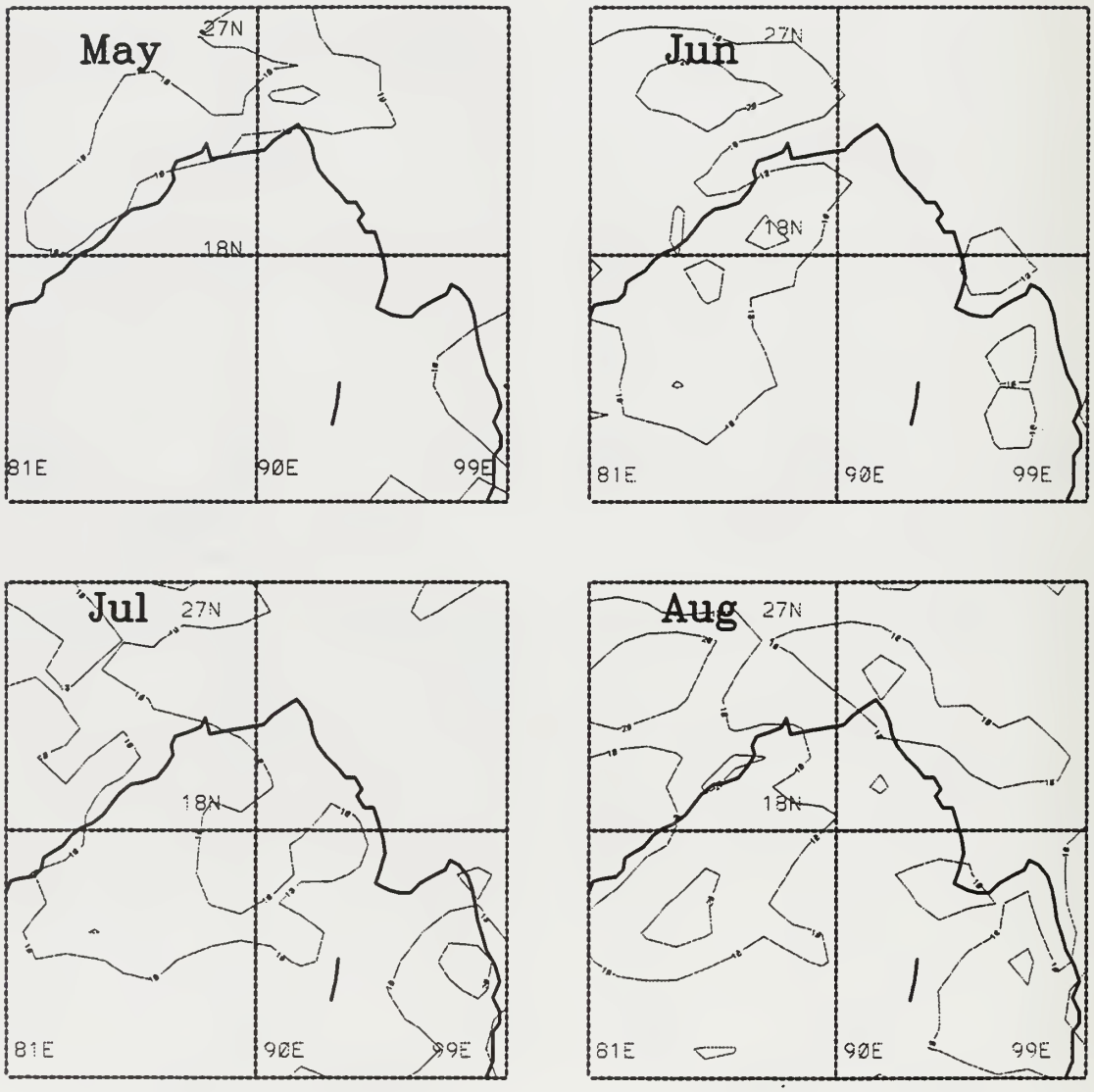

Figure 29. Bay of Bengal horizontal distribution of CI diurnal amplitude for May, June, July and August 1991. Contour interval is 10 °K.

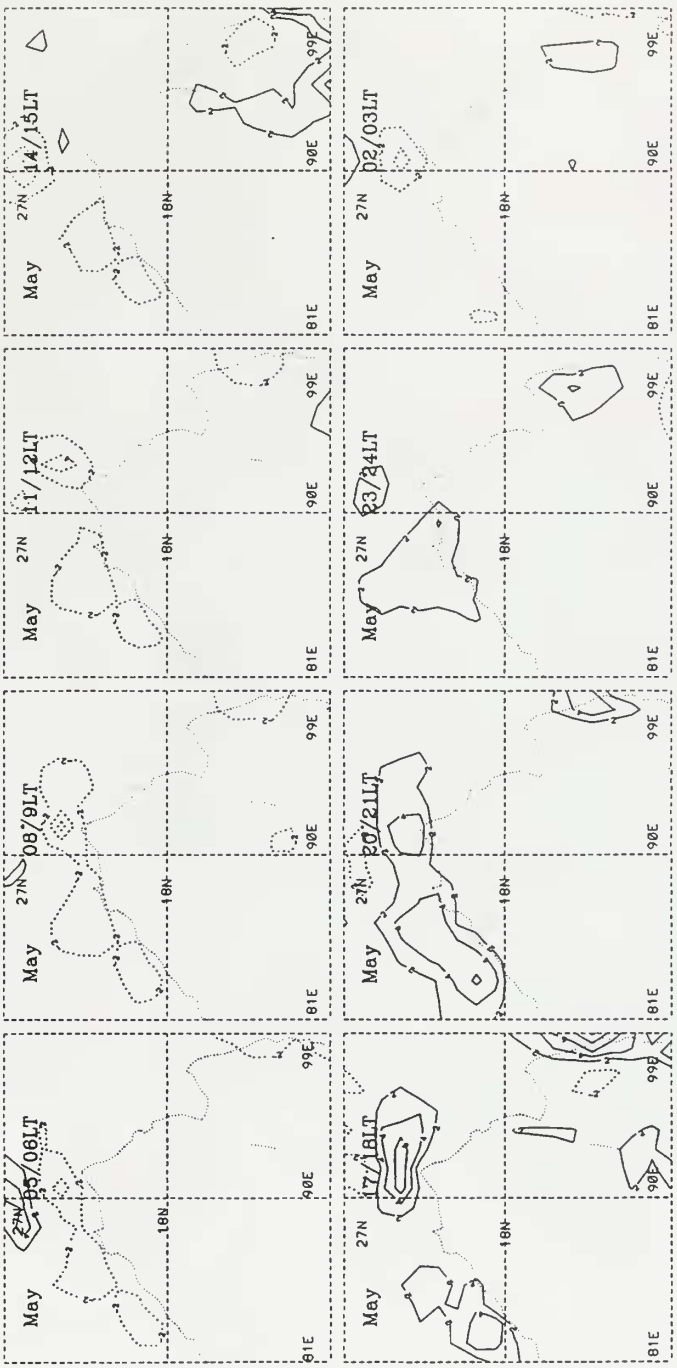

Figure 30a. Bay of Bengal Diurnal CI anomaly composite every 3 hours for May 1991. Contour interval is 2 °K. Solid (dashed) contours represent positive (negative) deviations from the monthly mean.

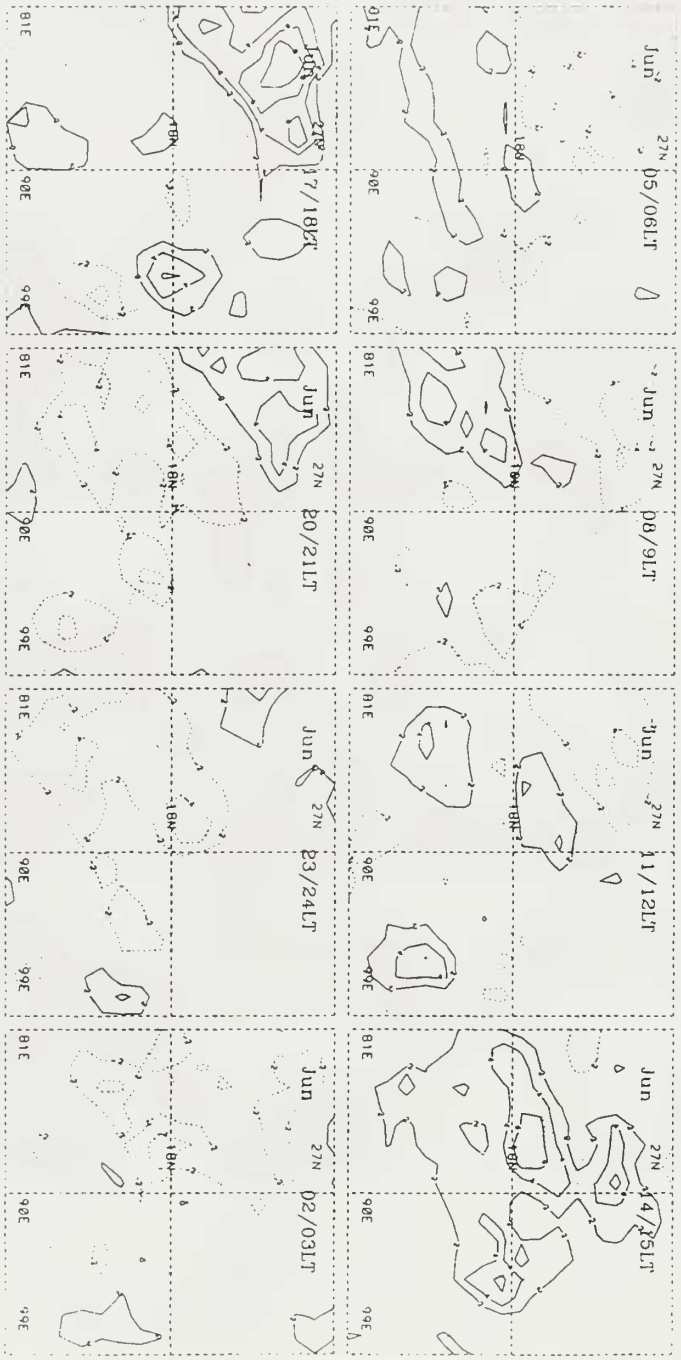

Figure 30b. As in Figure 30a except for June 1991.

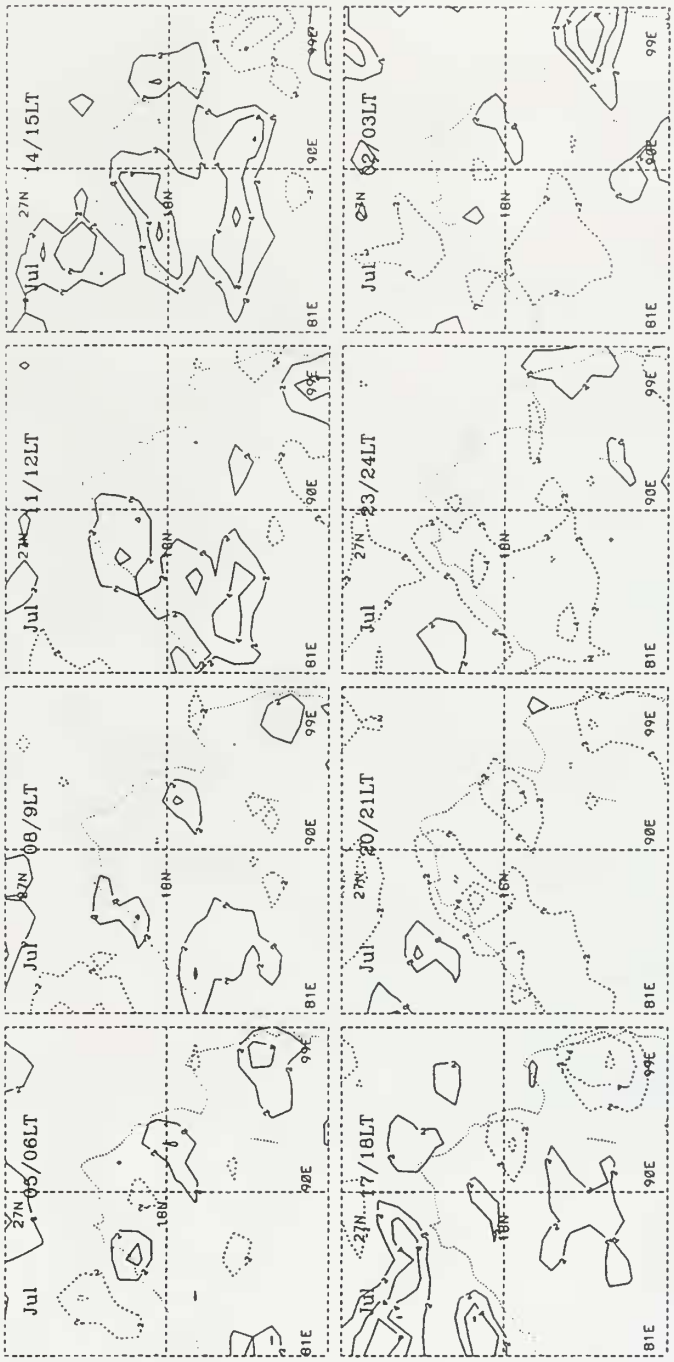

Figure 30c. As in Figure 30a except for July 1991.

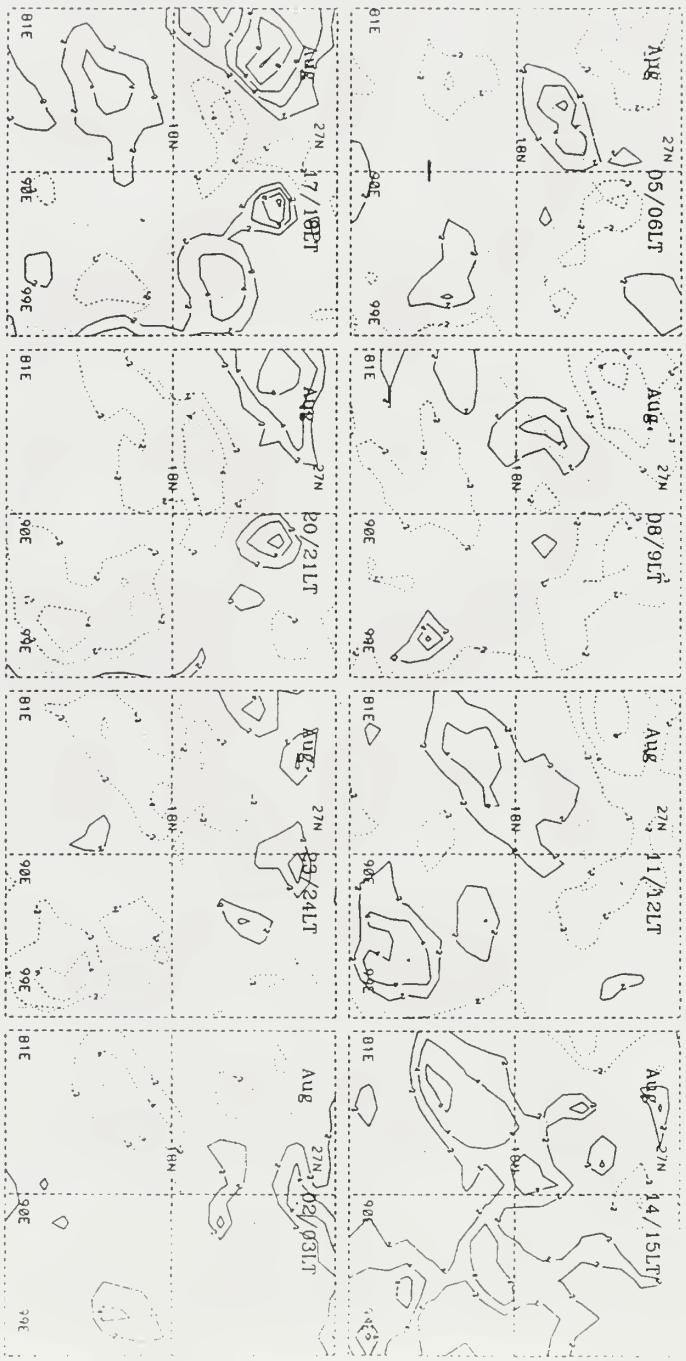

Figure 30d. As in Figure 30a except for August 1991.

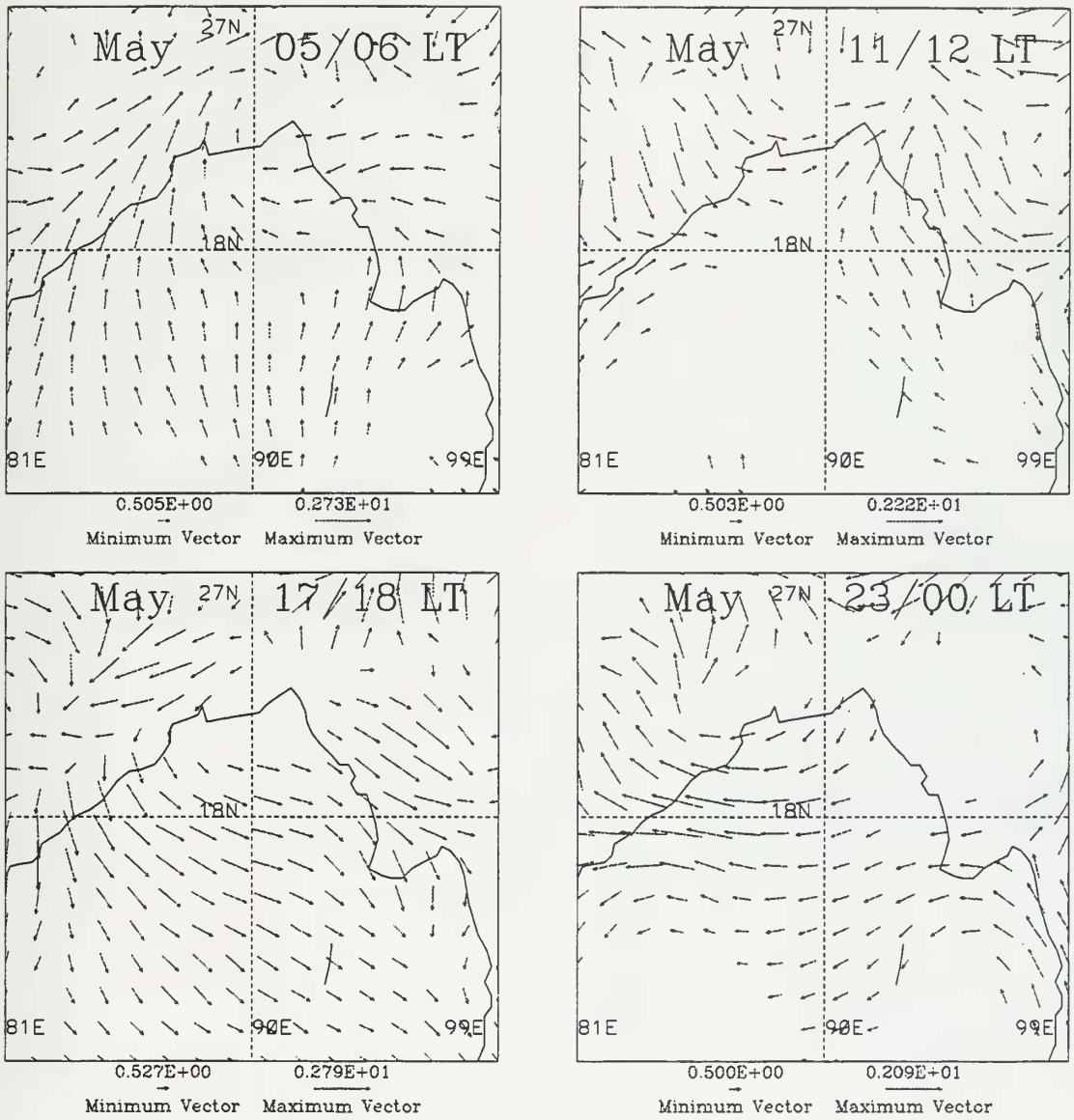

Figure 31a. Bay of Bengal 850 hPa wind anomaly composite every 6 hours for May 1991. Vector direction and size represents direction and magnitude of the deviation from the mean.

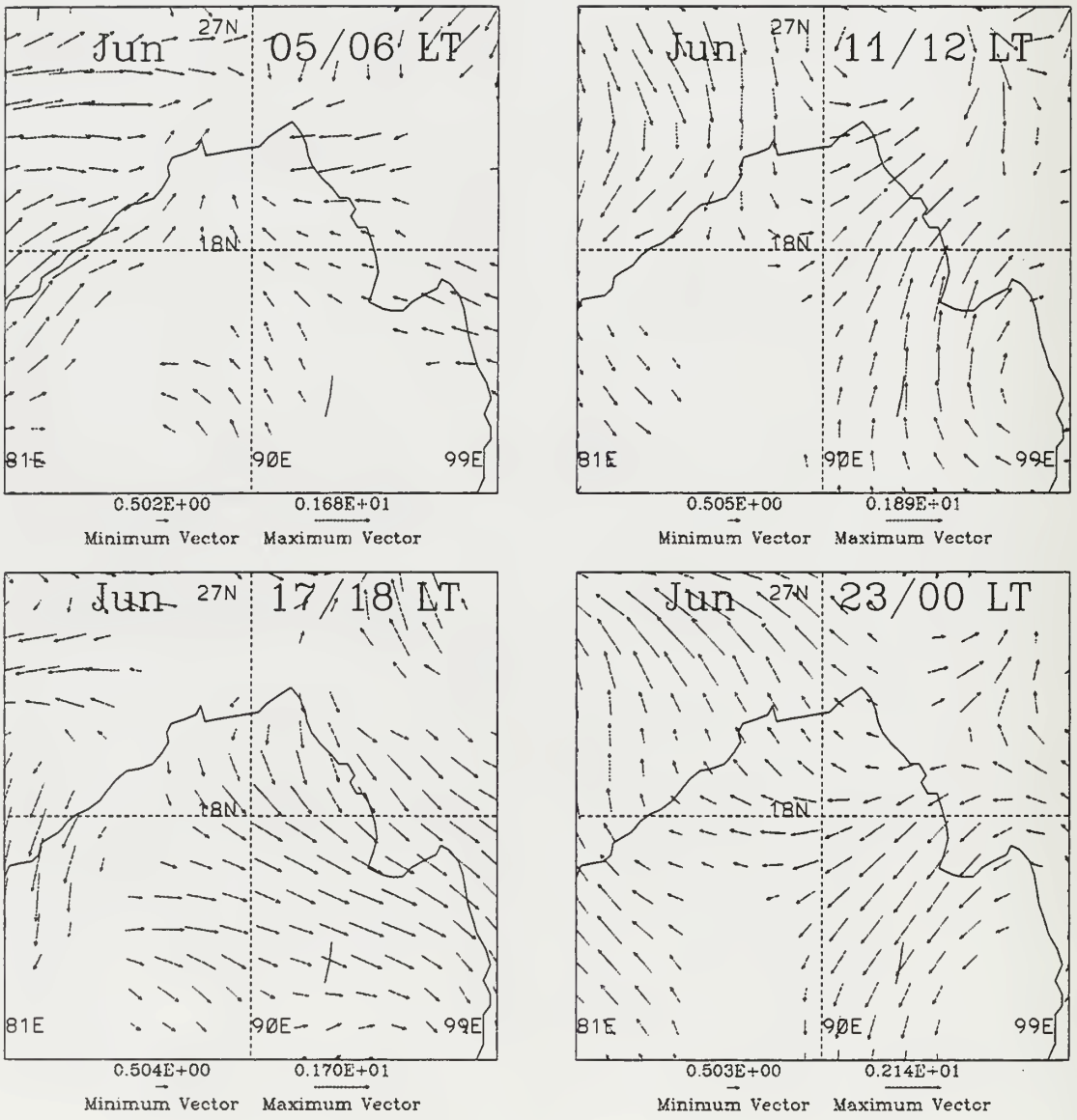

Figure 31b. As in Figure 31a except for June 1991.

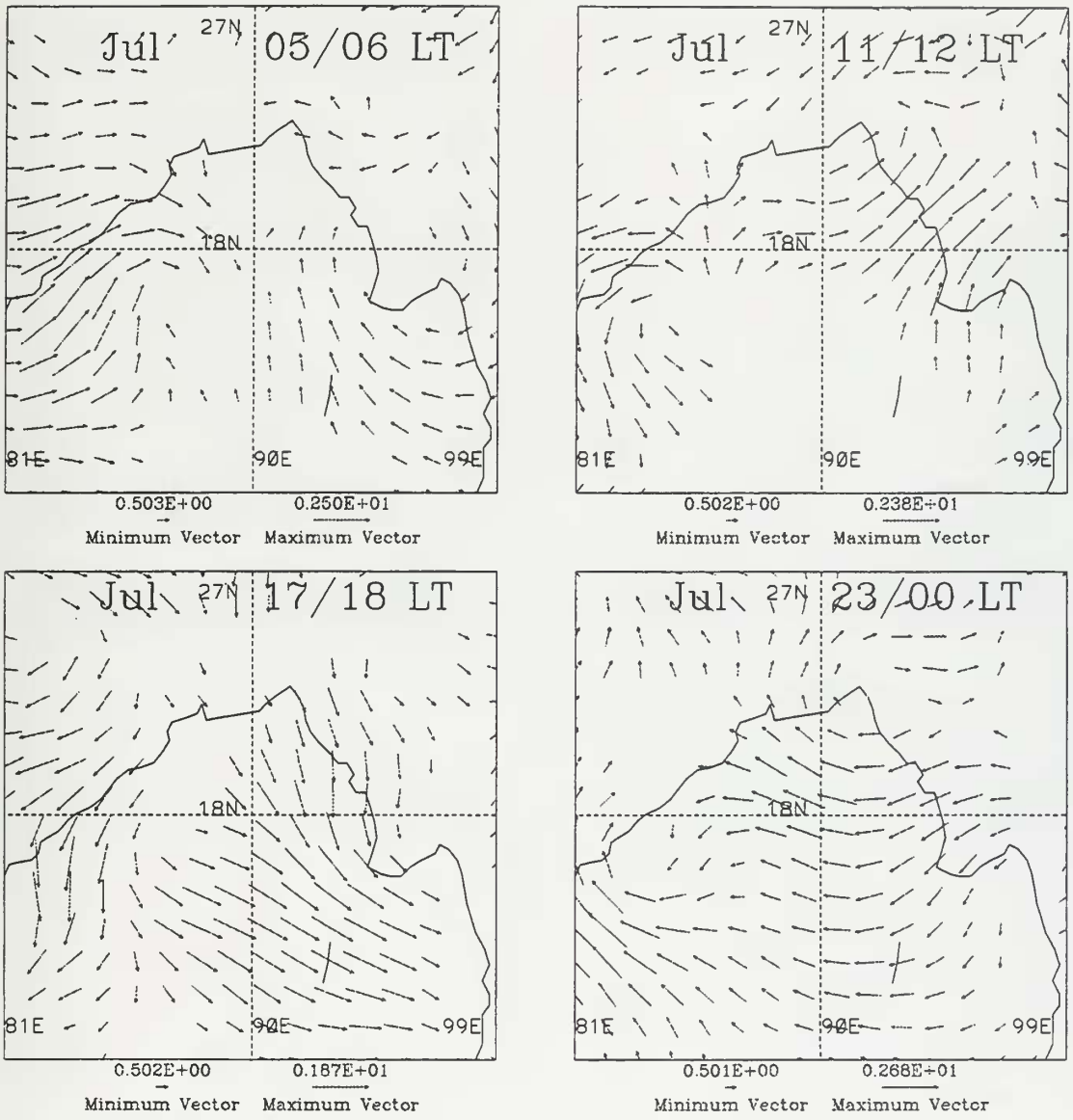

Figure 31c. As in Figure 31a except for July 1991.

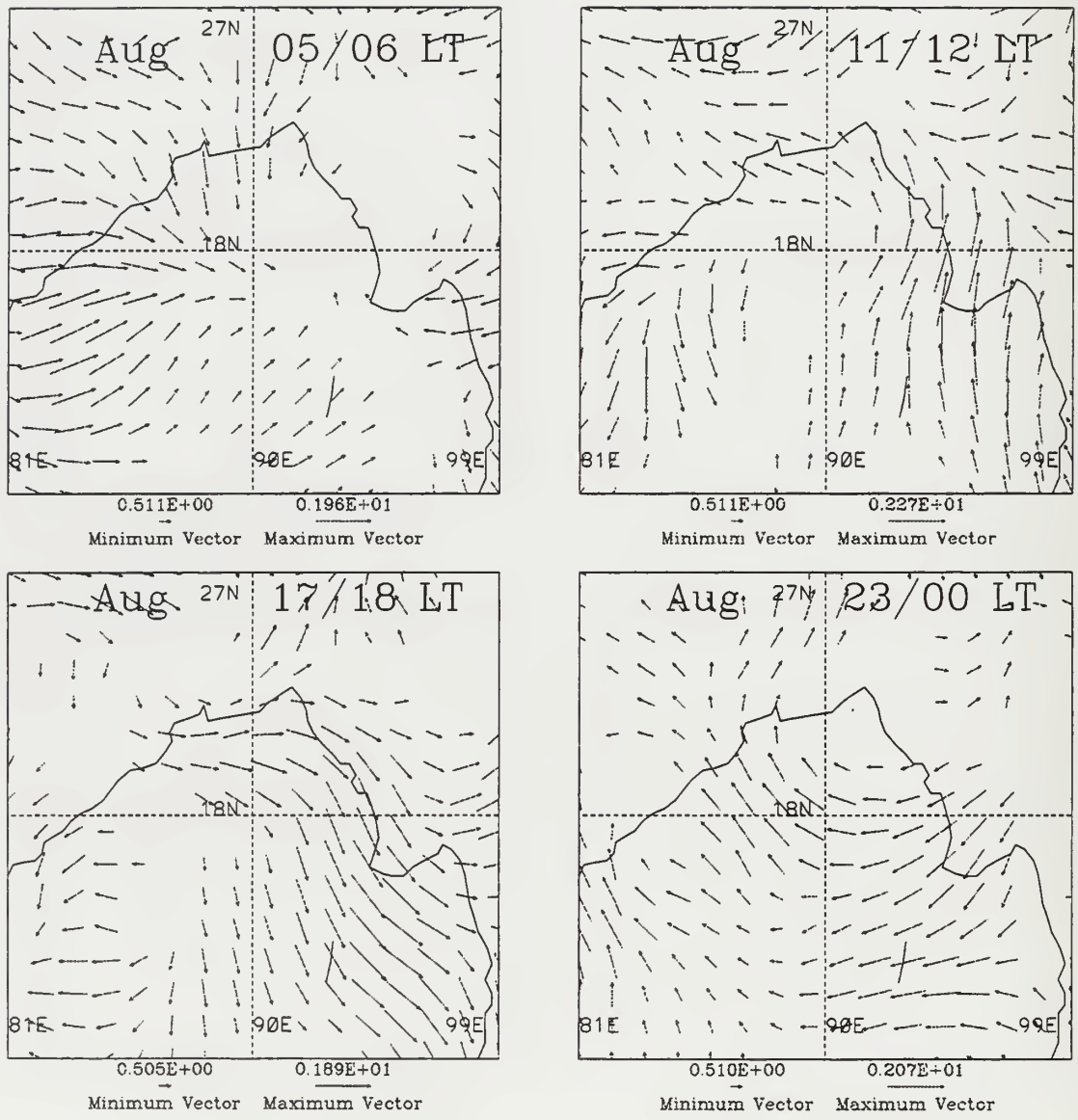

Figure 31d. As in Figure 31a except for August 1991.

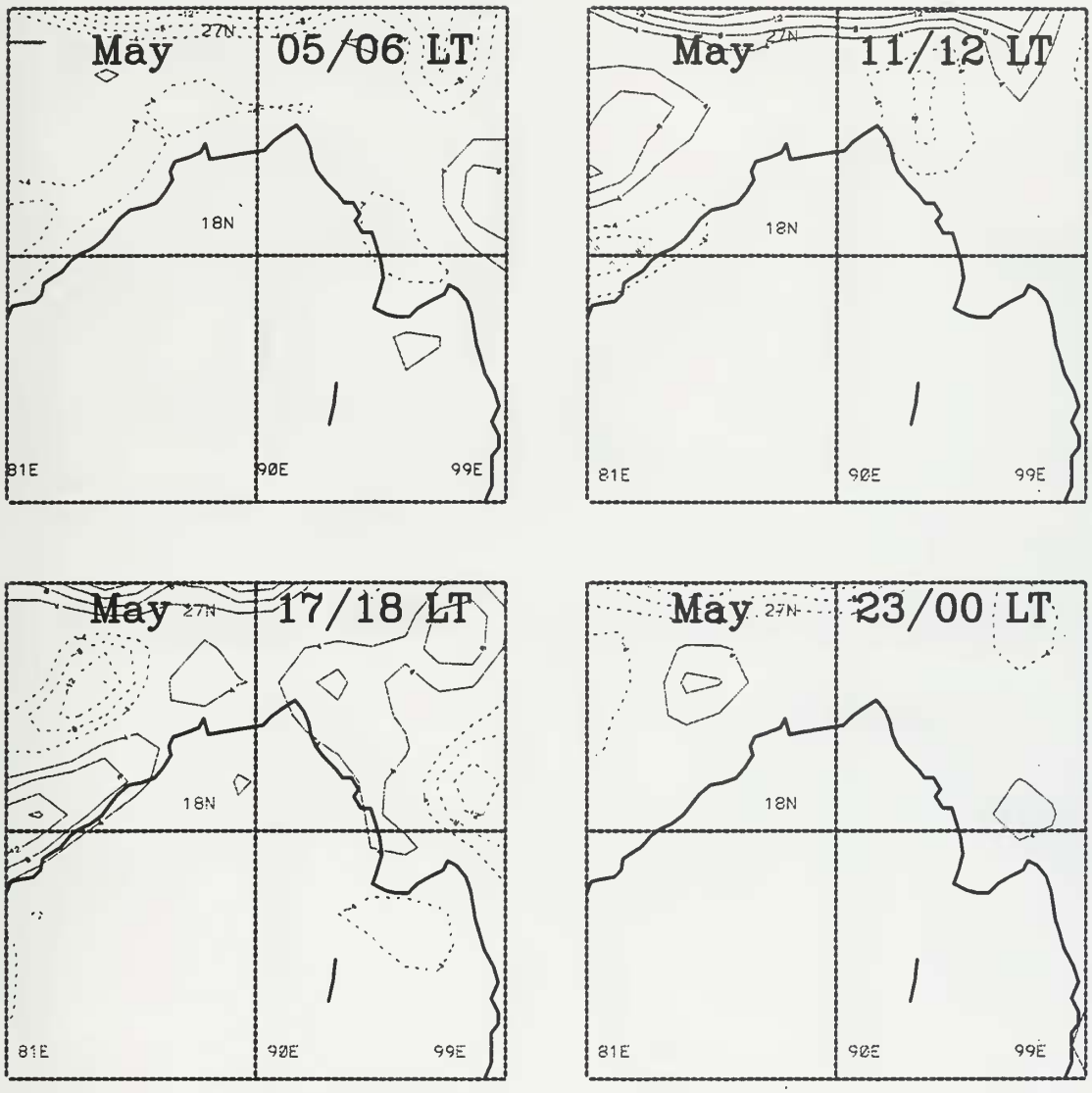

Figure 32a. Bay of Bengal 850 hPa divergence anomaly composite every 6 hours for May 1991. Contour interval is 4×10^{-6} s^{-1}. Solid (dashed) contours represent positive (negative) deviations from the mean.

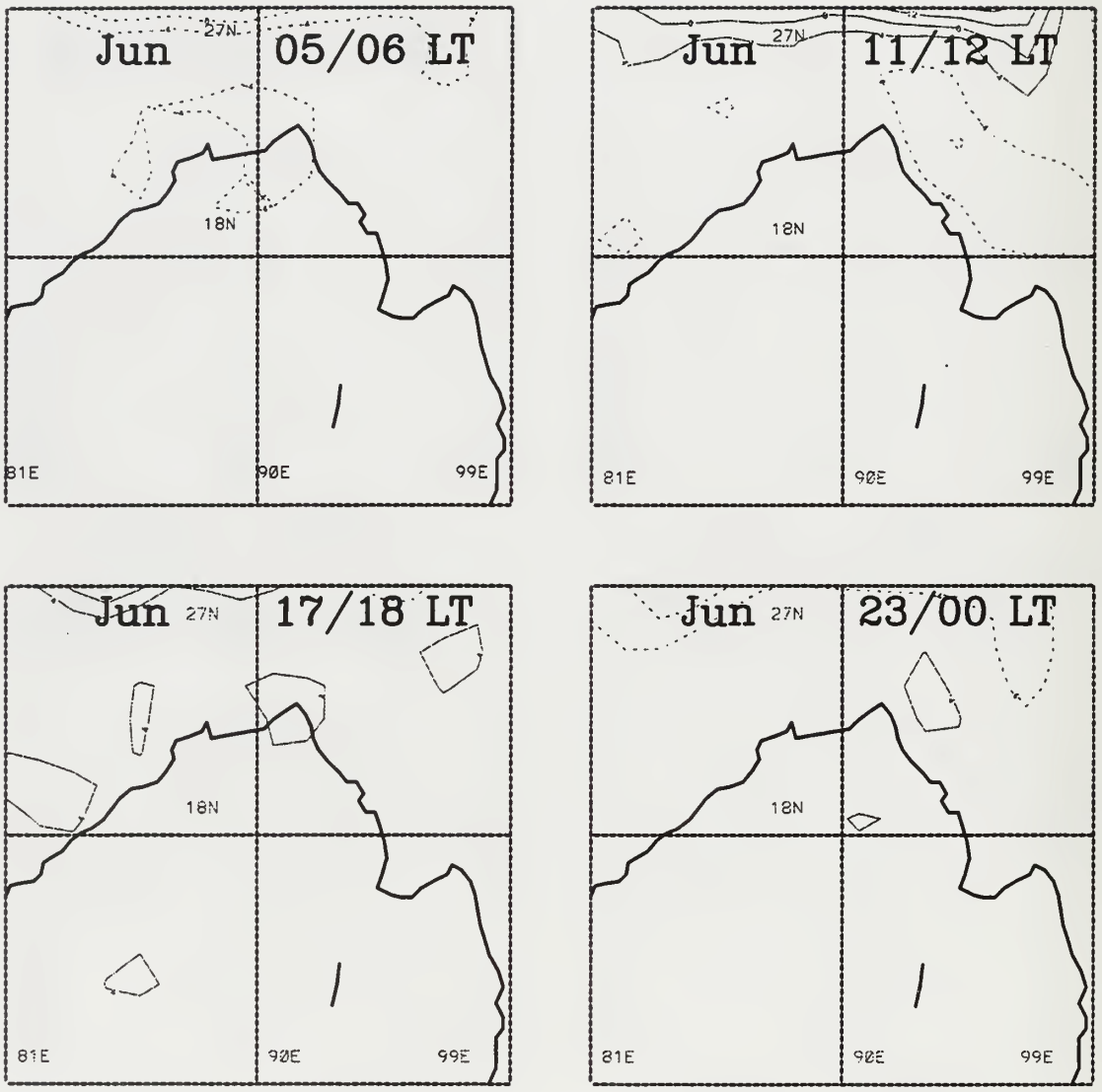

Figure 32b. As in Figure 32a except for June 1991.

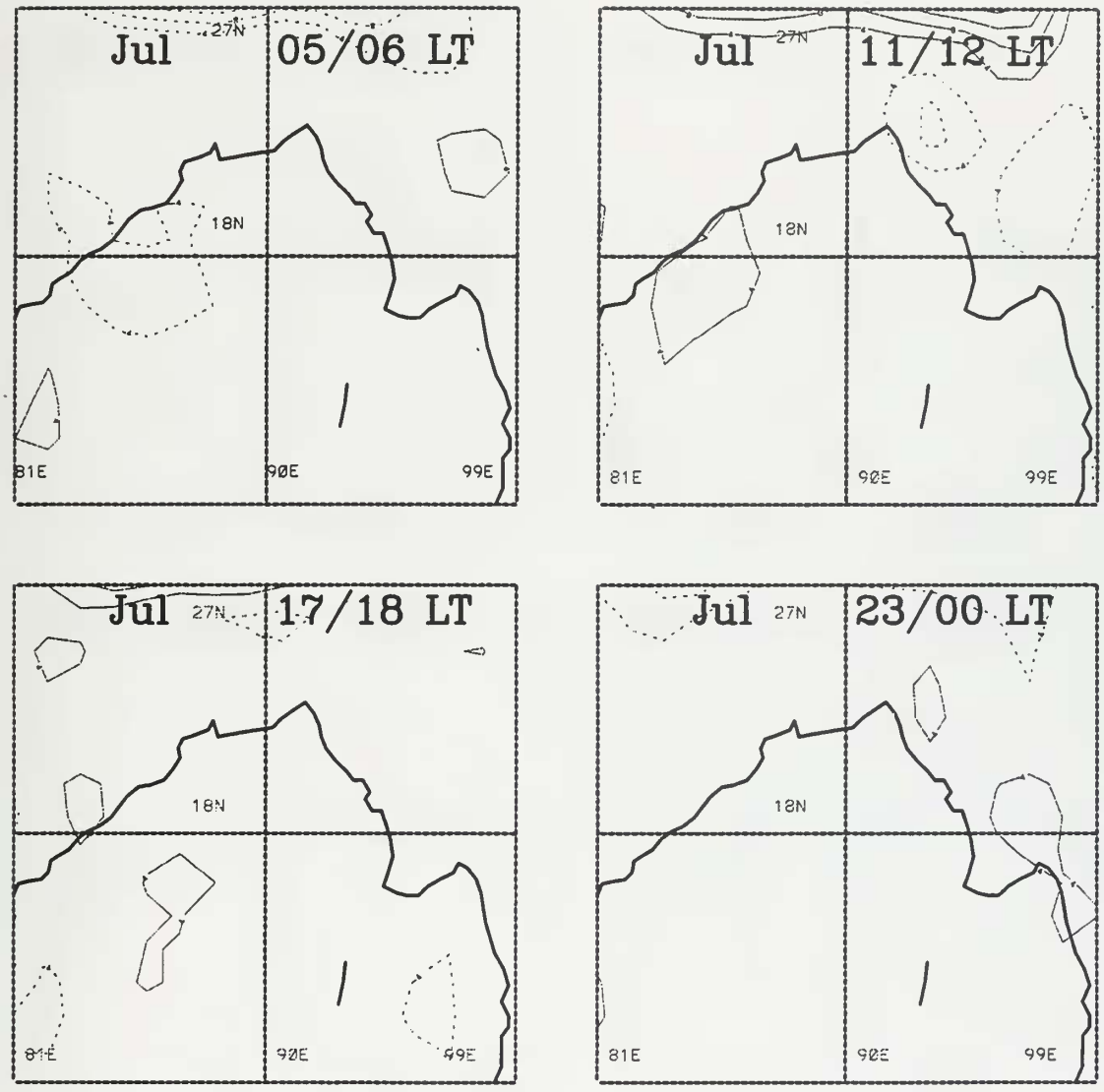

Figure 32c. As in Figure 32a except for July 1991.

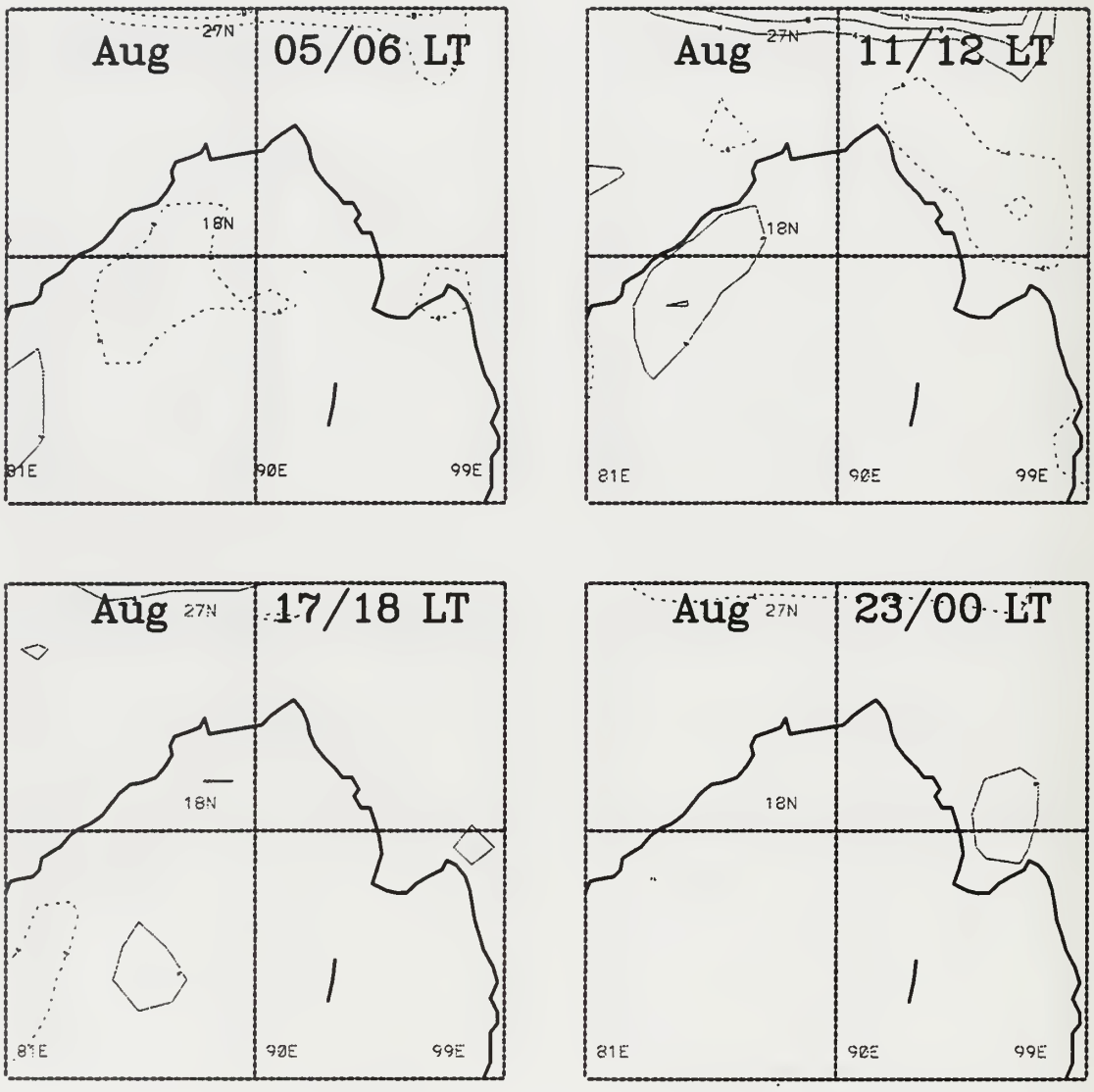

Figure 32d. As in Figure 32a except for August 1991.

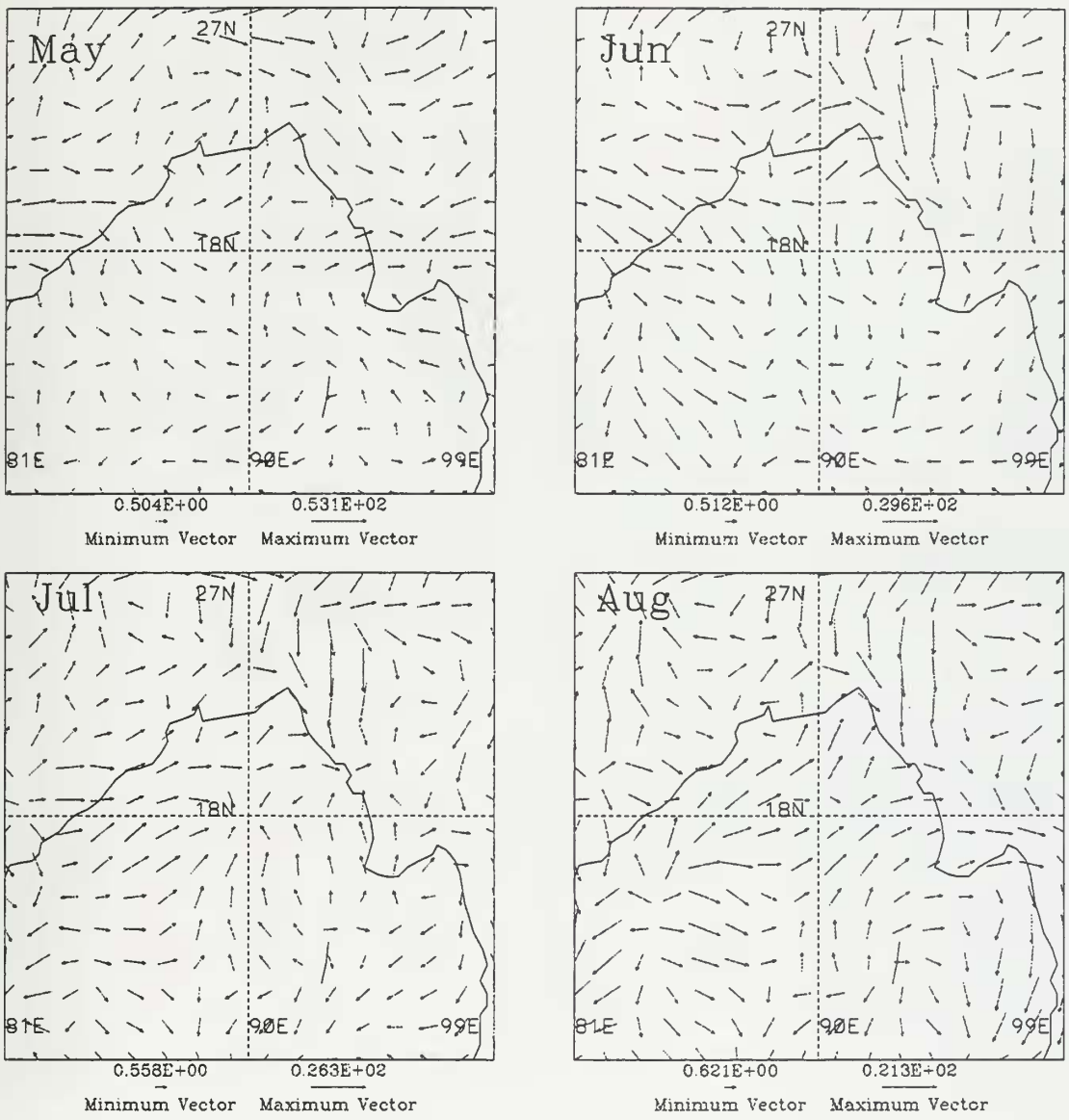

Figure 33. Bay of Bengal convergence diurnal components for May, June, July and August 1991. Phase and amplitude are represented in vector form based on a 24 hour clock with 12 midnight pointing north. All times are local time. Vector length indicates magnitude of convergence (-D850).

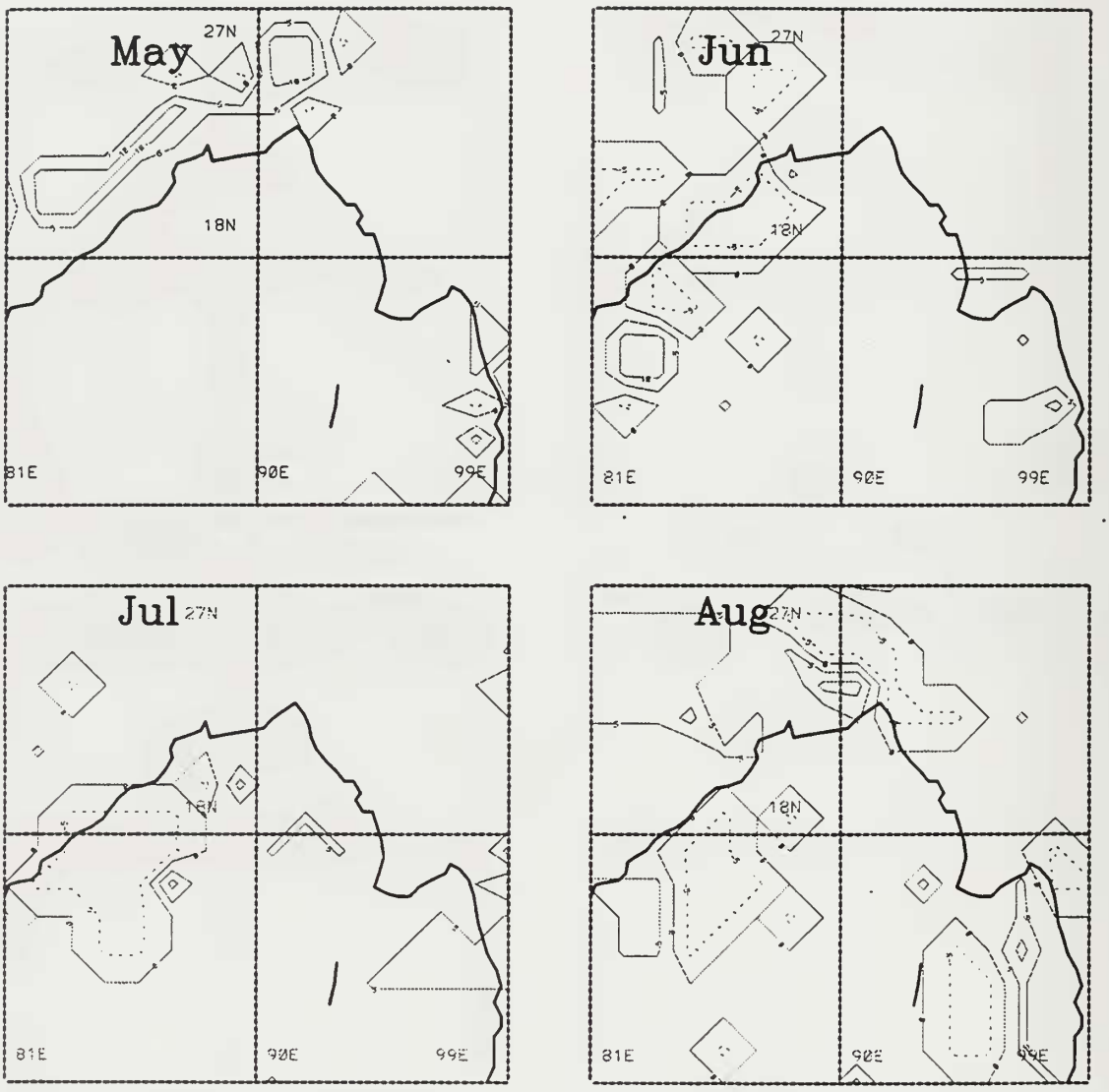

Figure 34. Bay of Bengal phase relationship between 850 hPa convergence and CI greater then 10 °K for May, June, July and August 1991. Contour interval is 5 hours. Positive (negative) values are solid (dashed). Values less (greater) than -5 (+5) indicate convergence leads (lags) convection. Values >5 indicate convergence and convection are in phase. Values >10 indicate convergence and convection are out of phase.

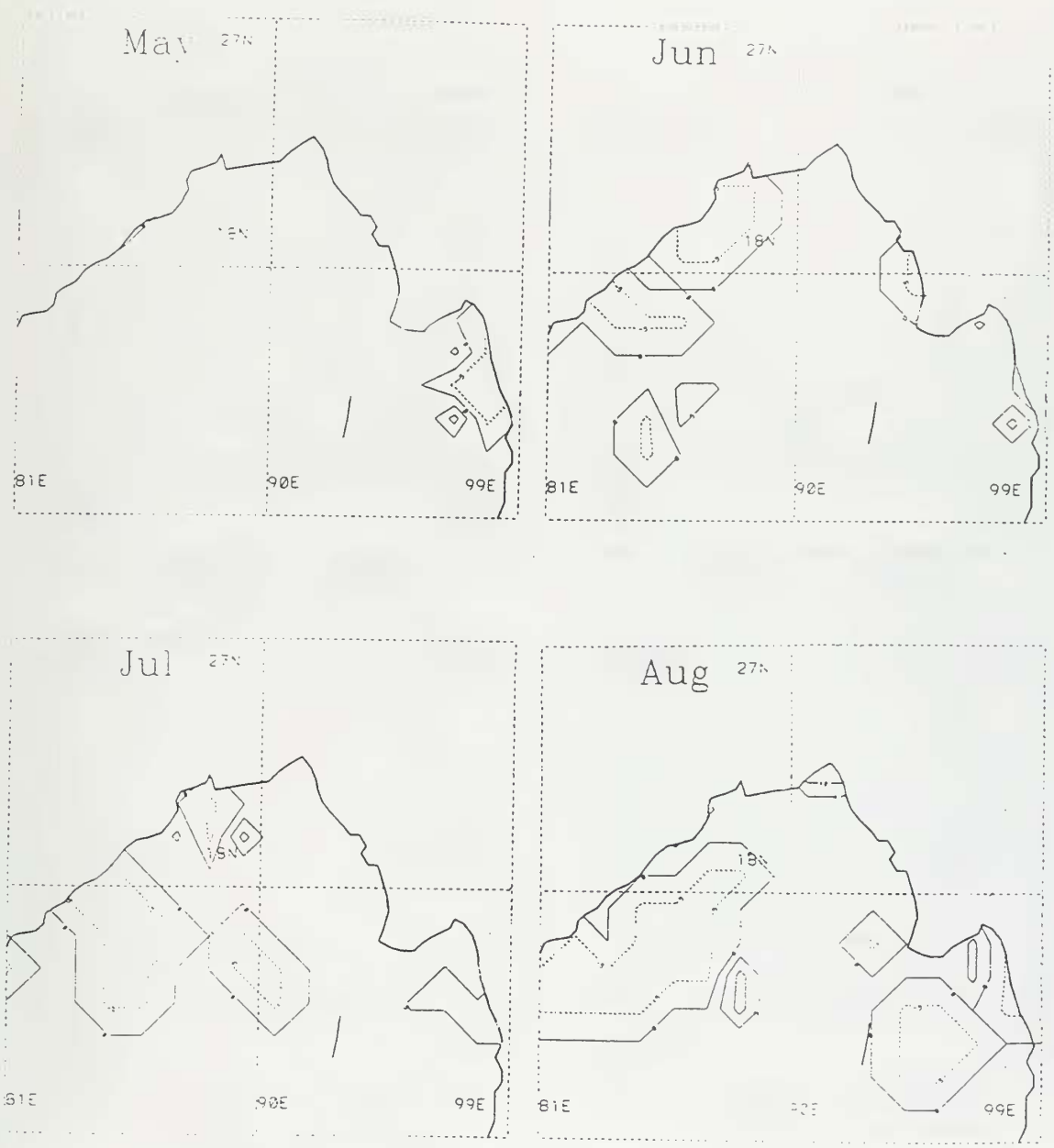

Figure 35. As in Figure 34 except the relationship is between latent heat flux and CI greater than 10 °K.

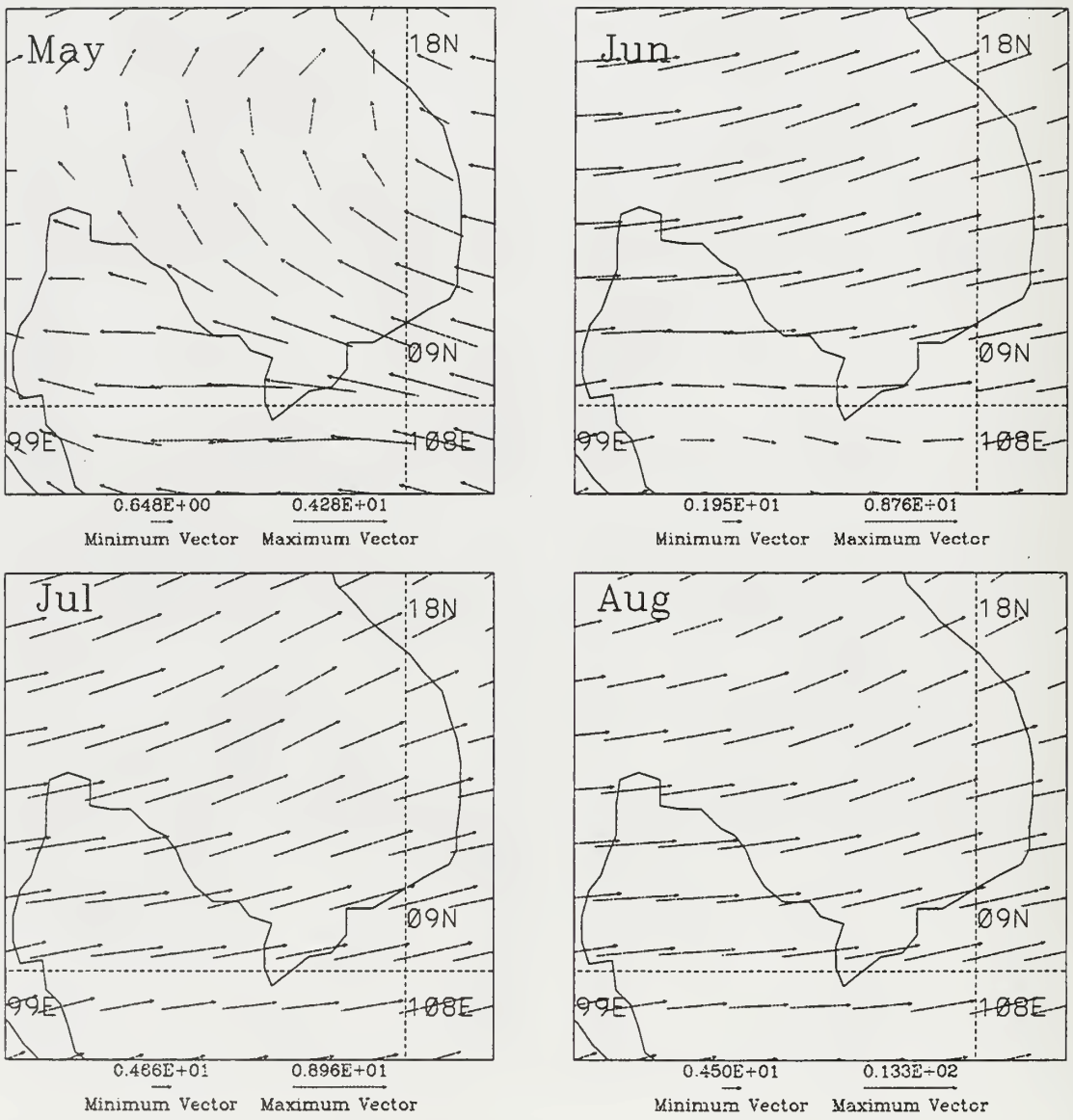

Figure 36. Indochina 850 hPa monthly mean winds (m/s) for May, June, July and August 1991.

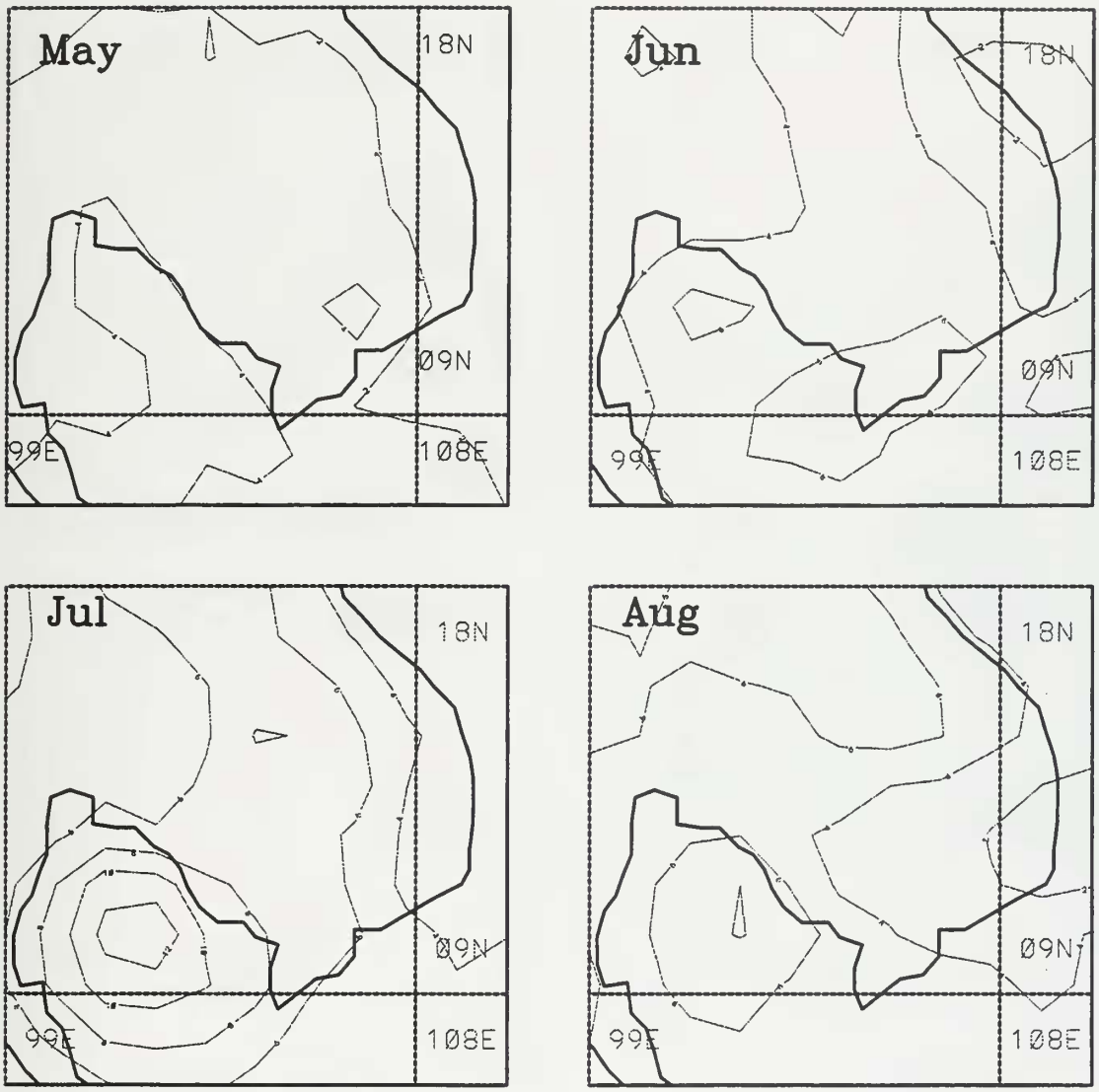

Figure 37. Indochina monthly mean convective Index (CI) for May, June, July and August 1991. Contour interval is 2 °K.

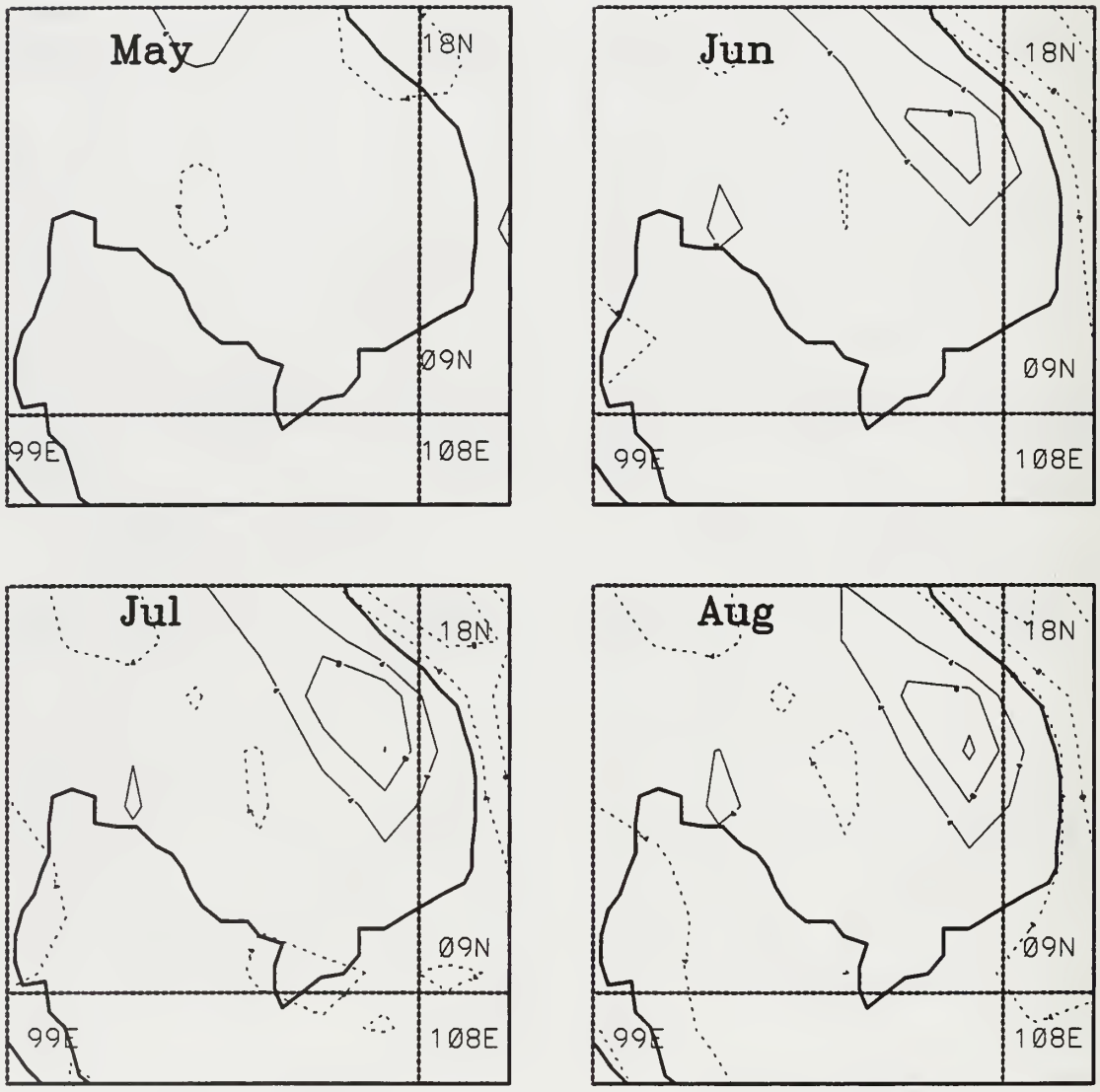

Figure 38. Indochina monthly mean 850 hPa divergence (10^{-6} s^{-1}) for May, June, July and August 1991. Contour interval is 4x 10^{-6} s^{-1}.

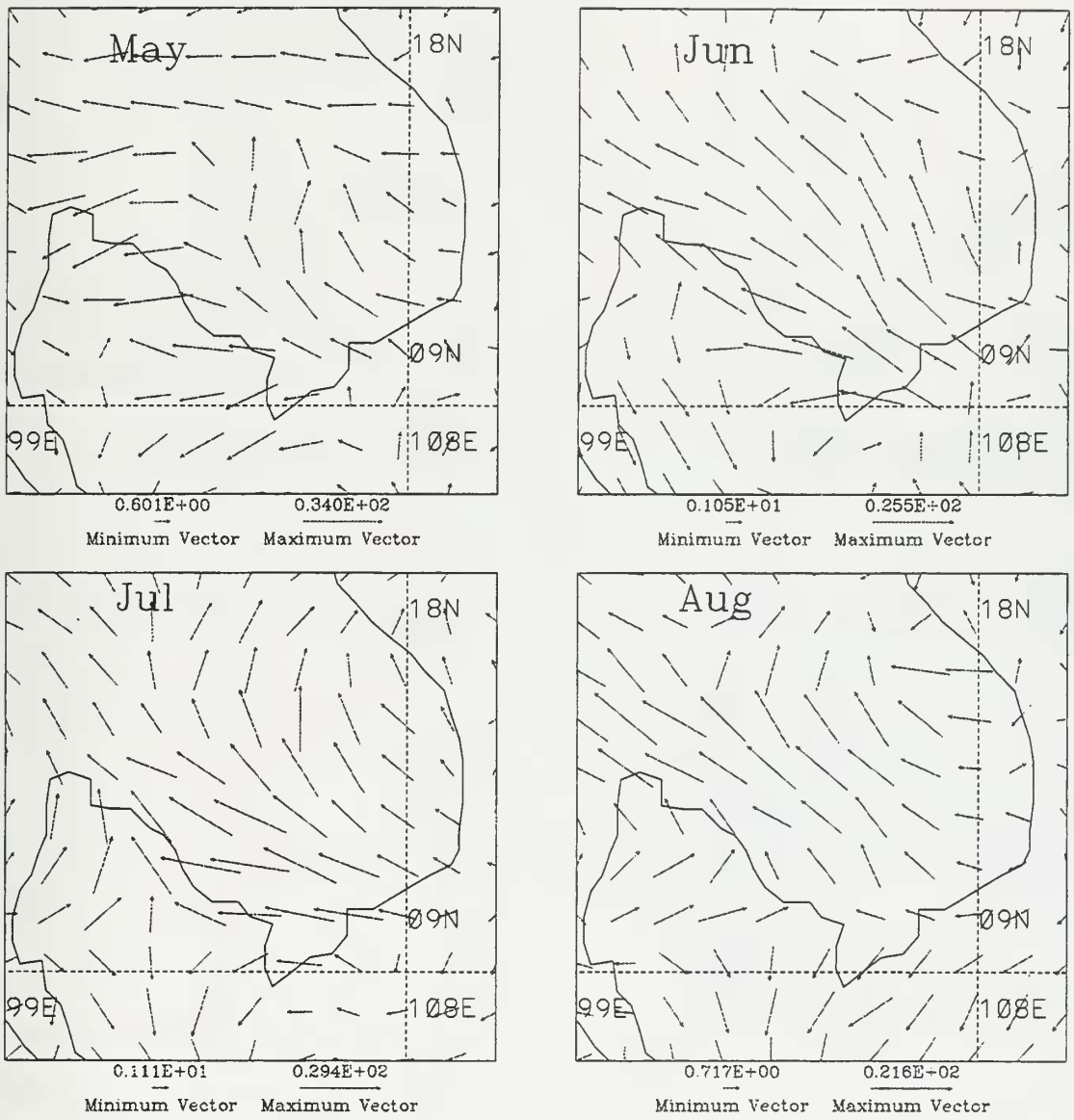

Figure 39. Indochina CI diurnal components for May, June, July and August 1991. Phase and amplitude are represented in vector form based on a 24 hour clock with 12 midnight pointing north. All times are local time. Vector length indicates magnitude of CI.

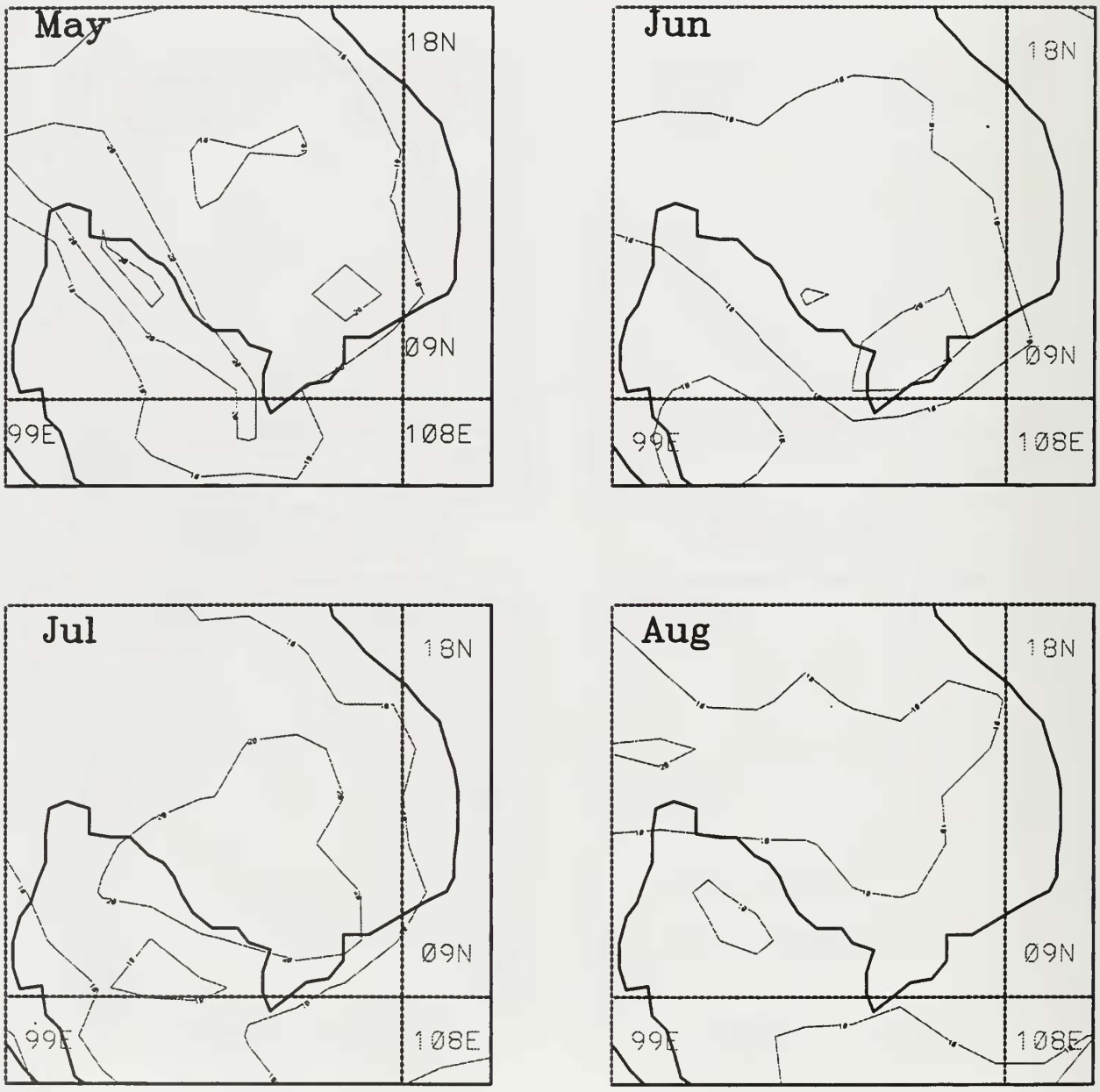

Figure 40. Indochina horizontal distribution of CI diurnal amplitude for May, June, July and August 1991. Contour interval is 10 °K.

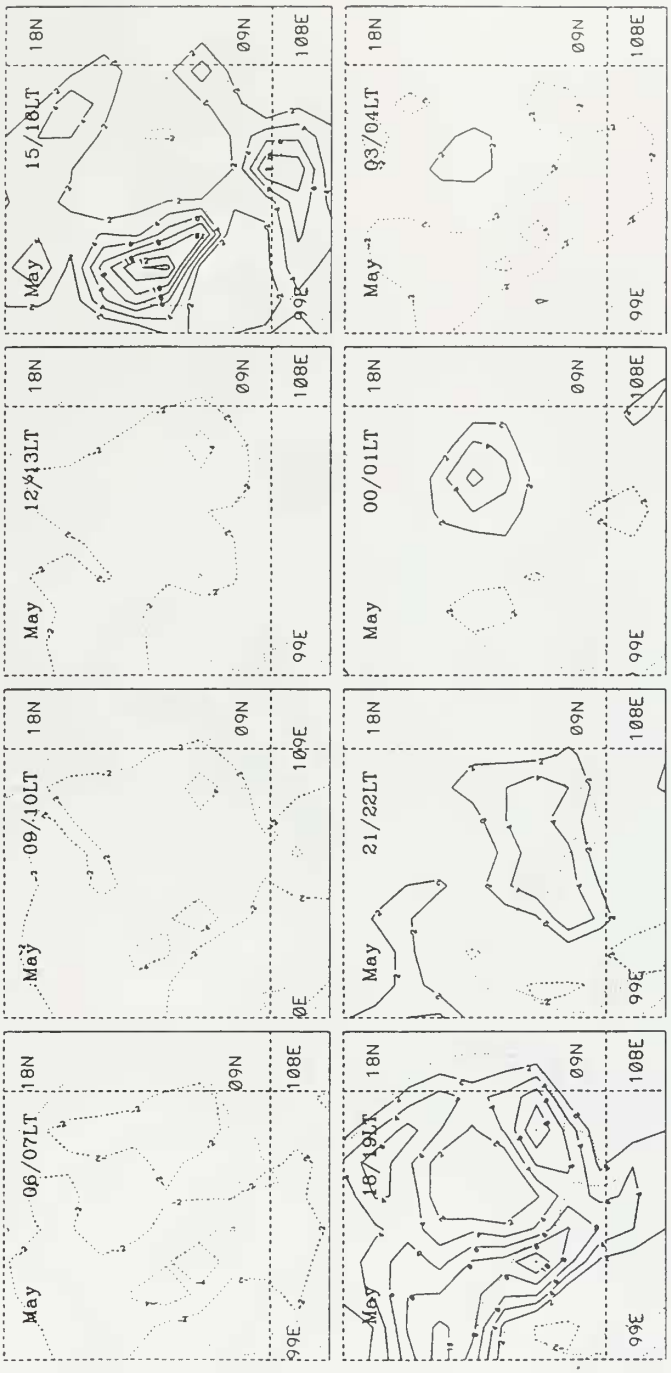

Figure 41a. Indochina diurnal CI anomaly composite every 3 hours for May 1991. Contour interval is 2 °K. Solid (dashed) contours represent positive (negative) deviations from the monthly mean.

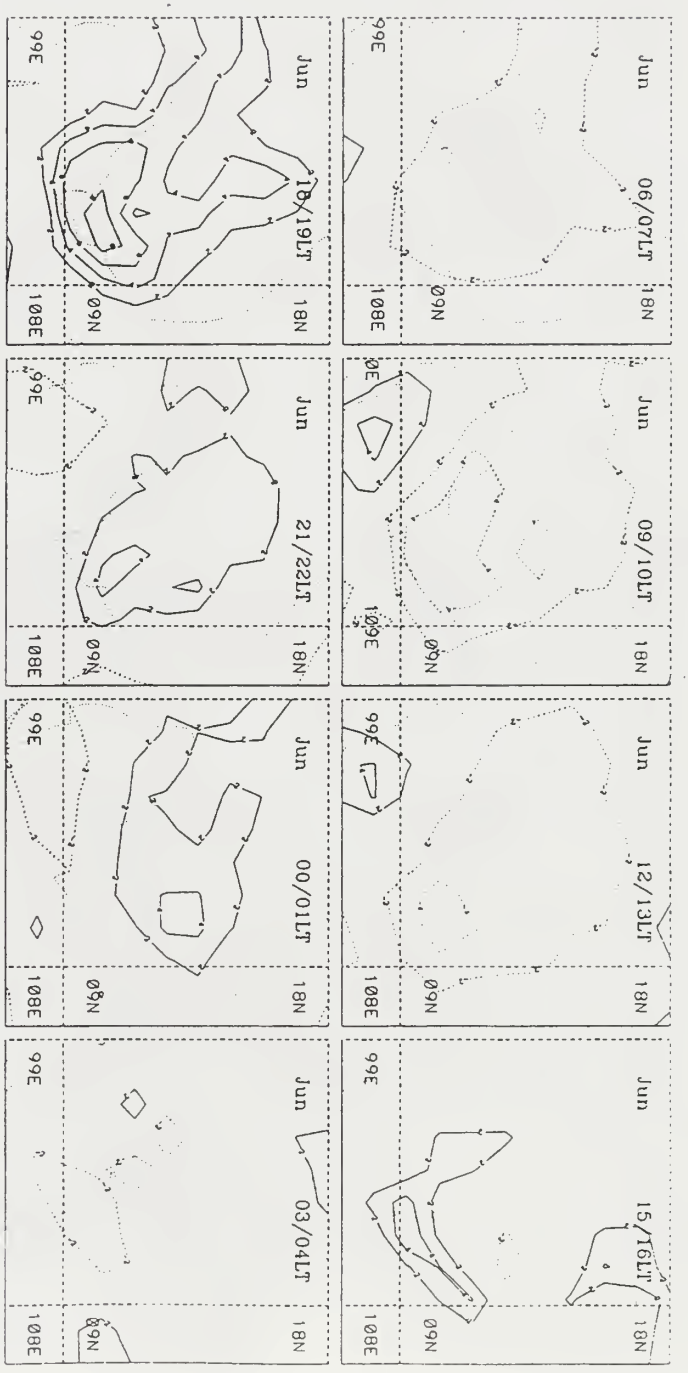

Figure 41b. As in Figure 41a except for June 1991.

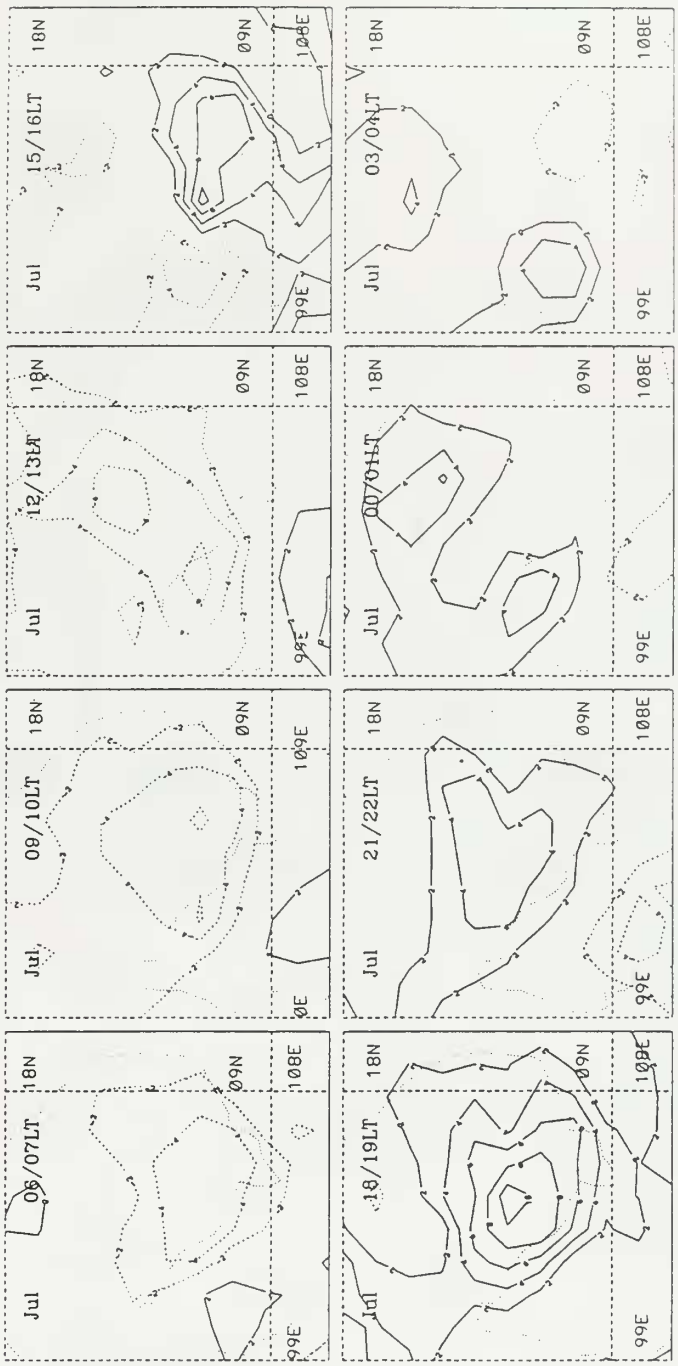

Figure 41c. As in Figure 41a except for July 1991.

Figure 41d. As in Figure 41a except for August 1991.

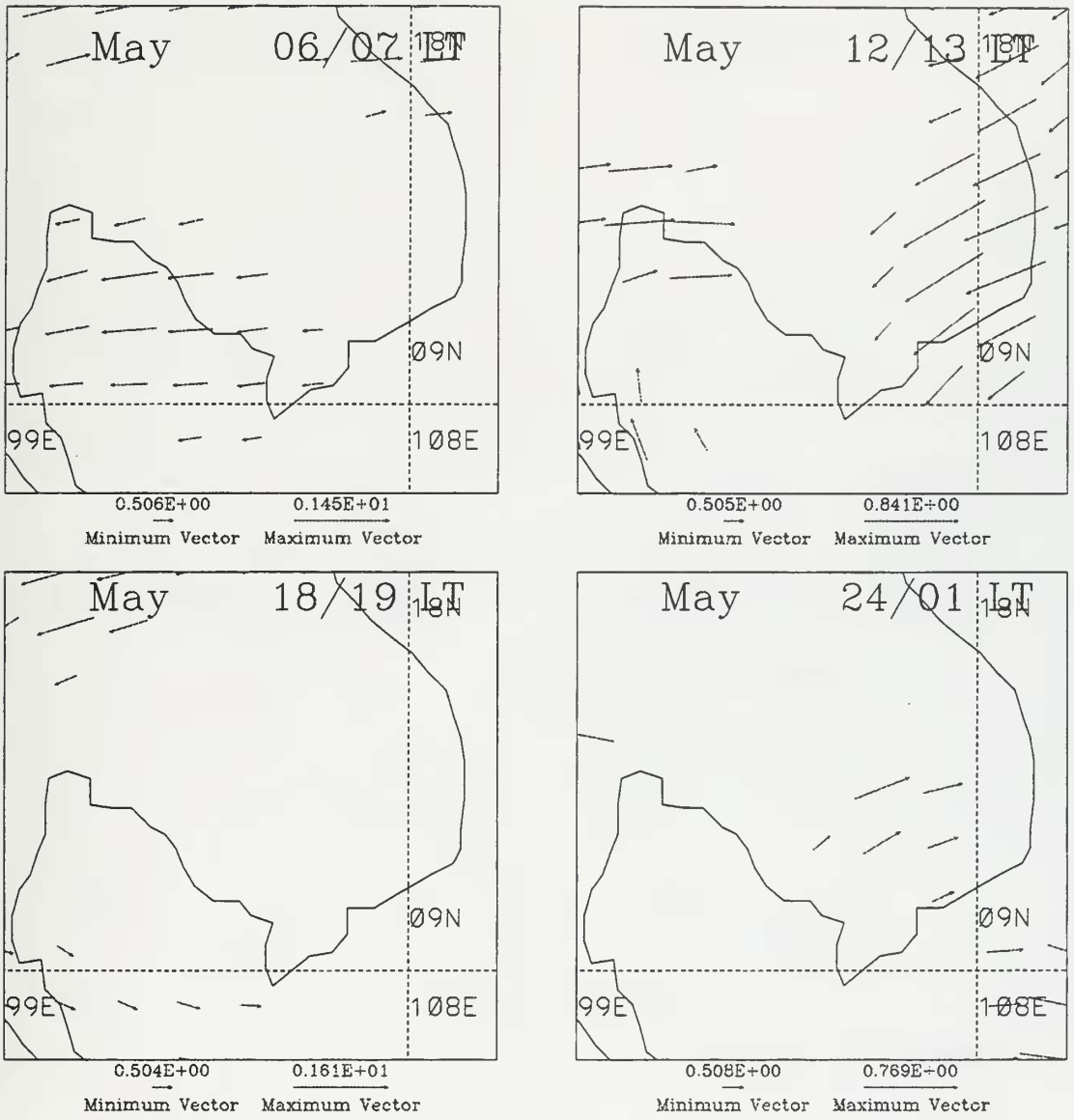

Figure 42a. Indochina 850 hPa wind anomaly composite every 6 hours for May 1991. Vector direction and size represents direction and magnitude of the deviation from the mean.

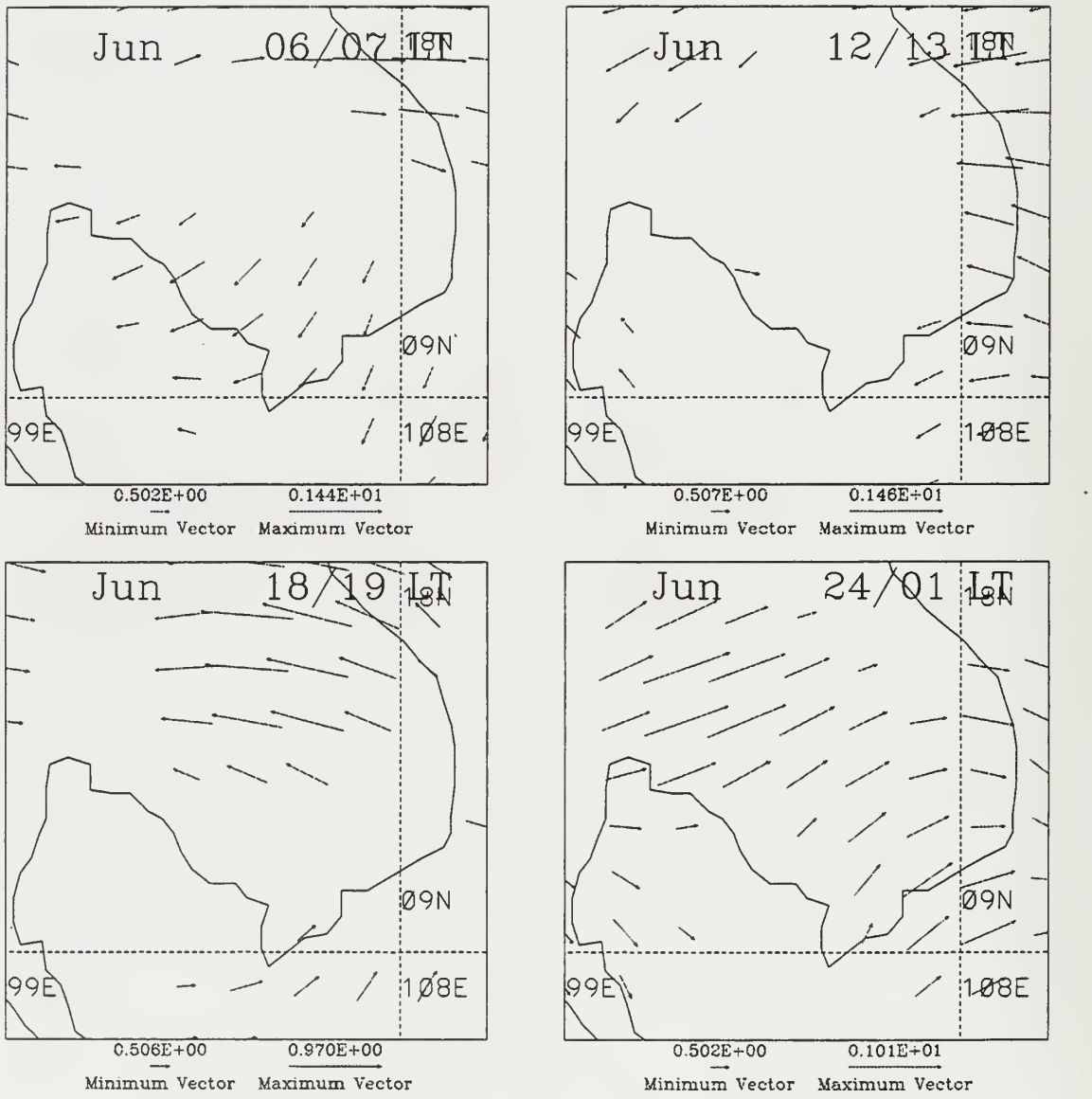

Figure 42b. As in Figure 42a except for June 1991.

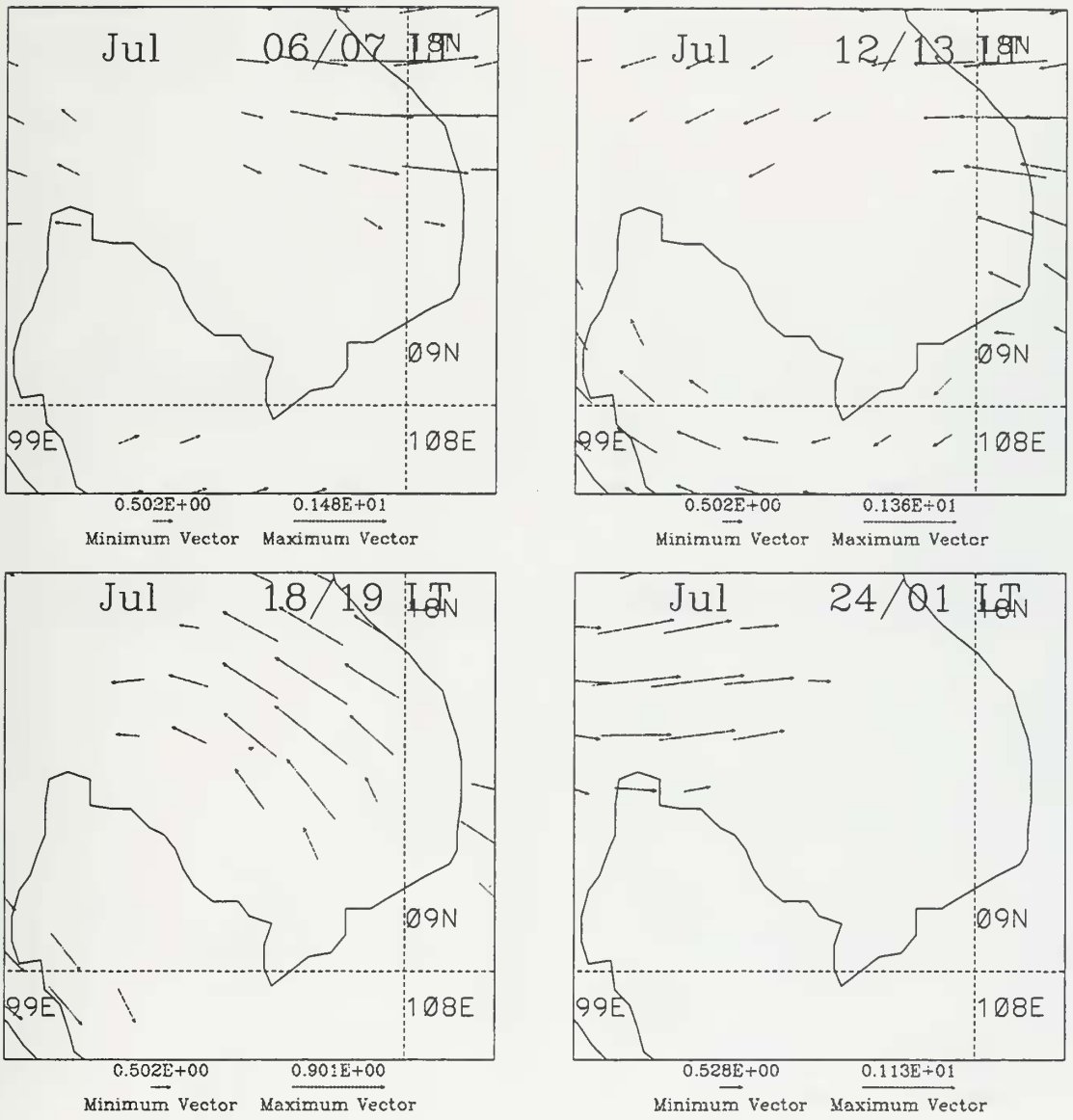

Figure 42c. As in Figure 42a except for July 1991.

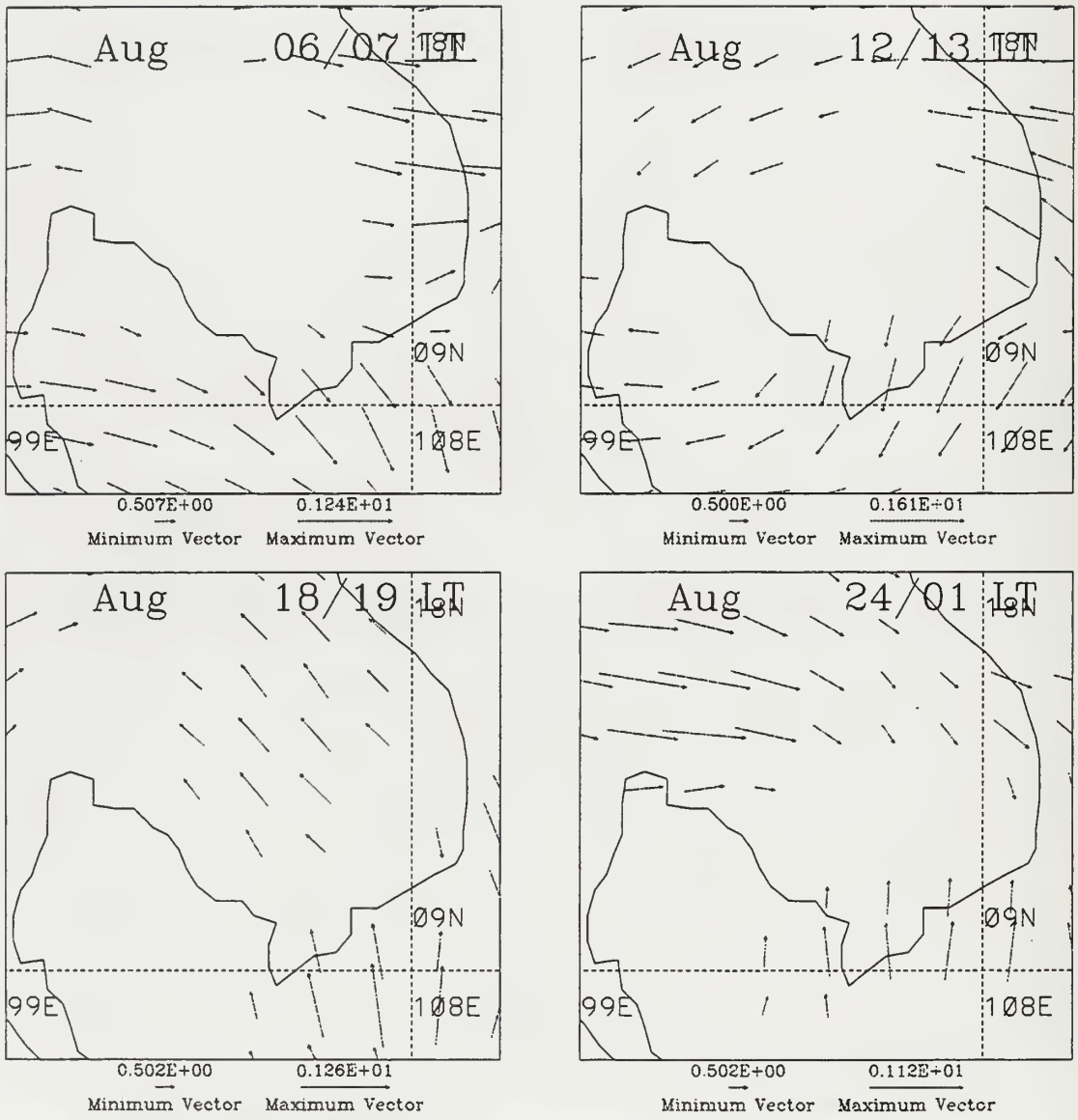

Figure 42d. As in Figure 42a except for August 1991.

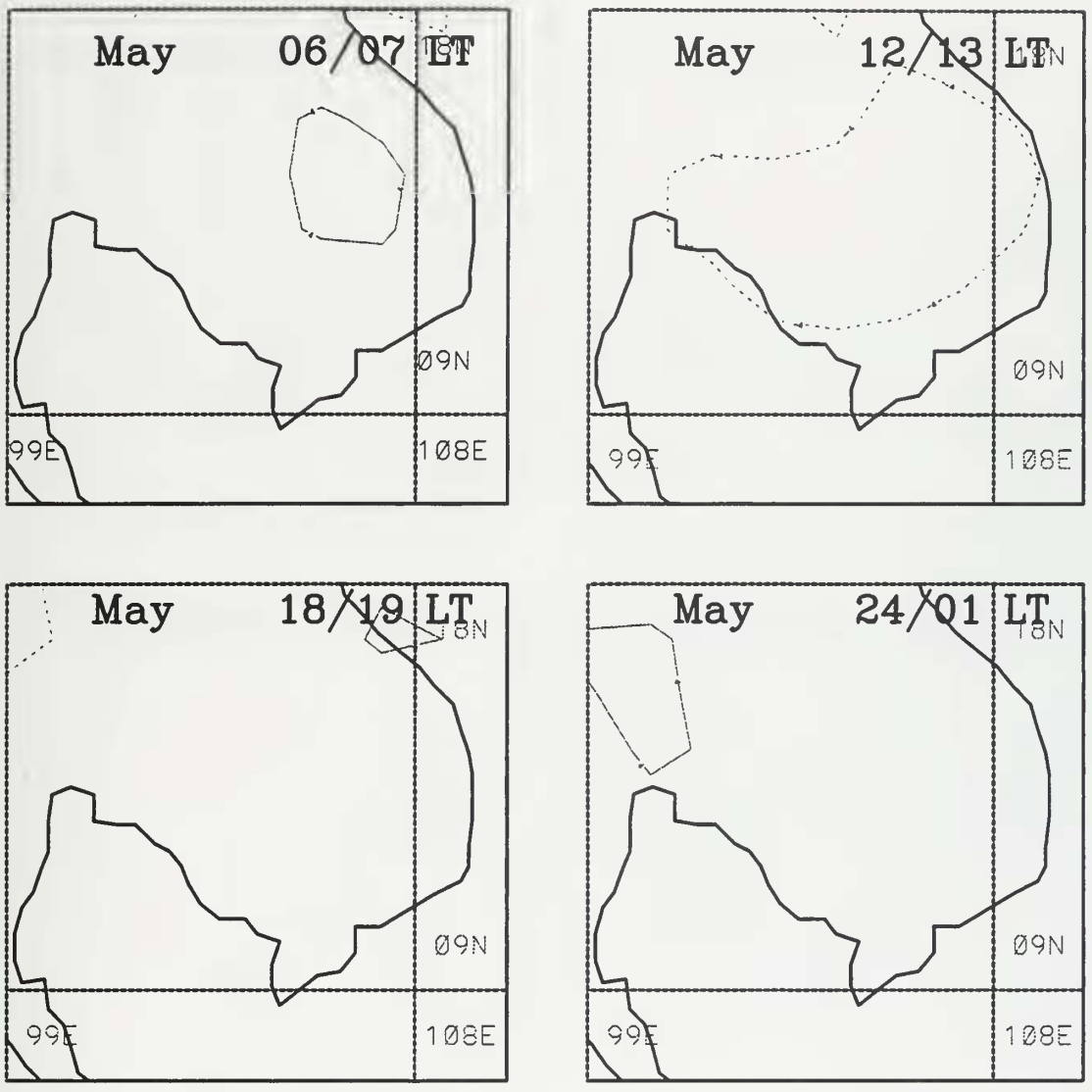

Figure 43a. Indochina 850 hPa divergence anomaly composite every 6 hours for May 1991. Contour interval is 4×10^{-6} s^{-1}. Solid (dashed) contours represent positive (negative) deviations from the mean.

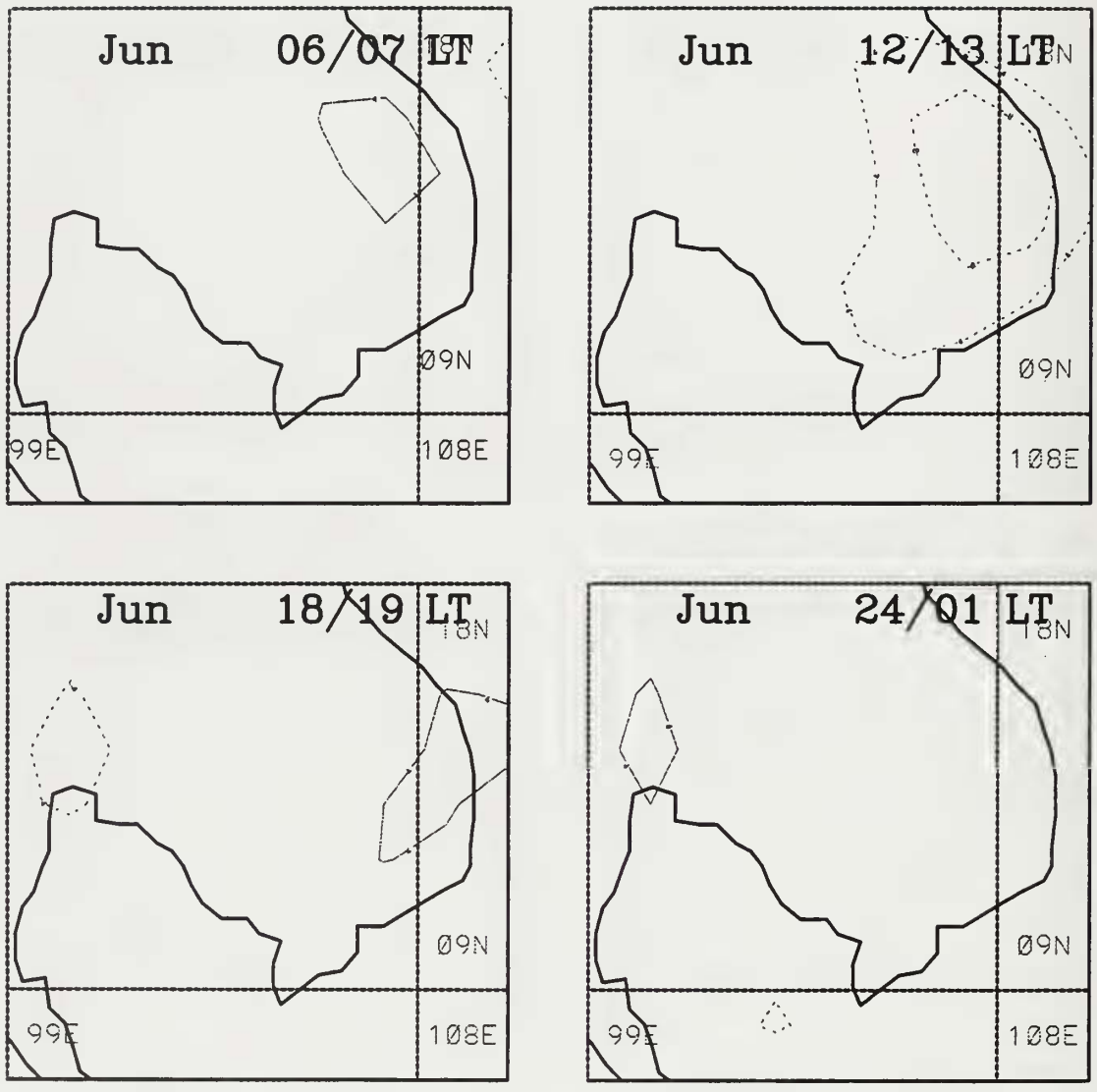

Figure 43b. As in Figure 43a except for June 1991.

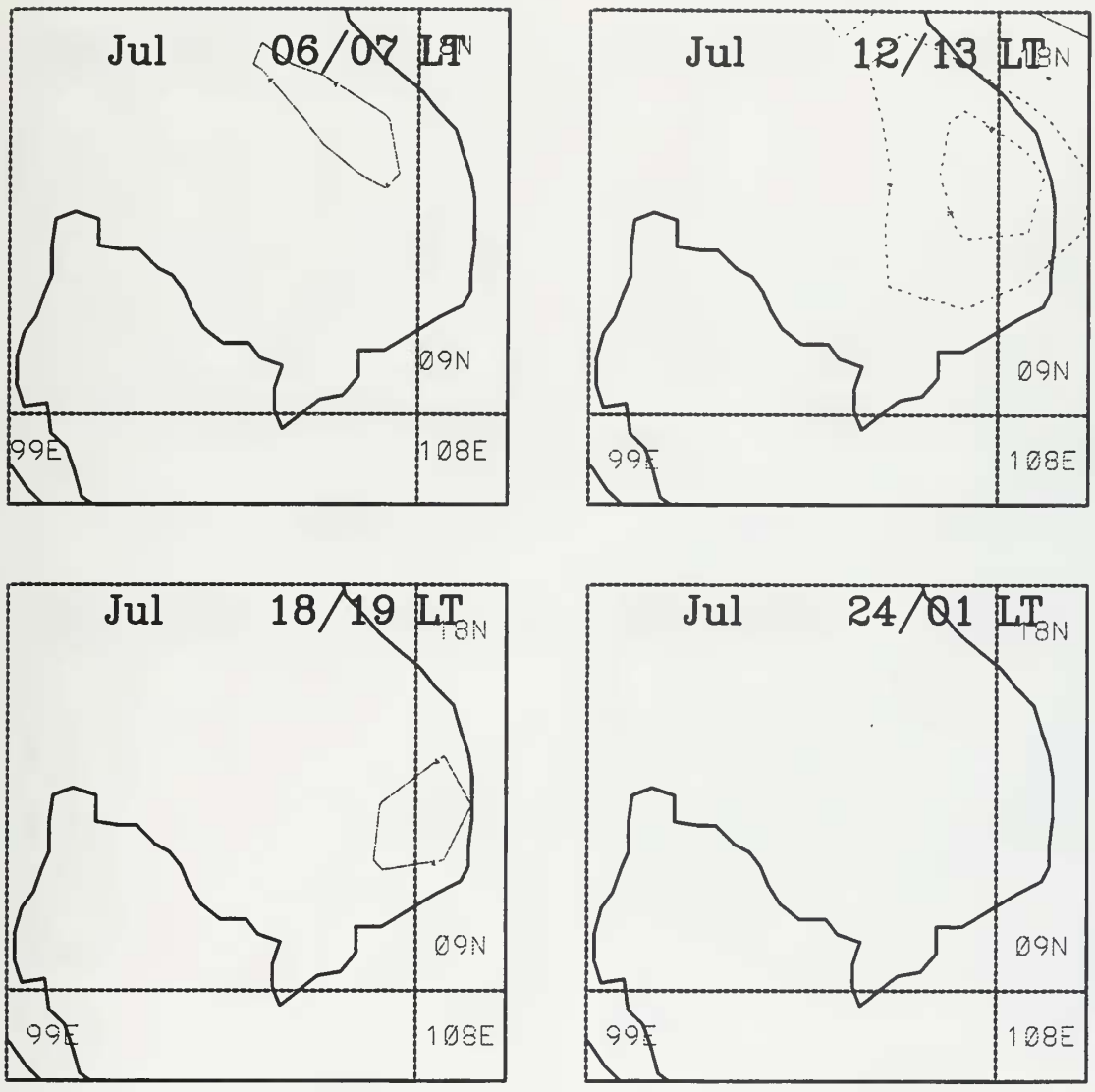

Figure 43c. As in Figure 43a except for July 1991.

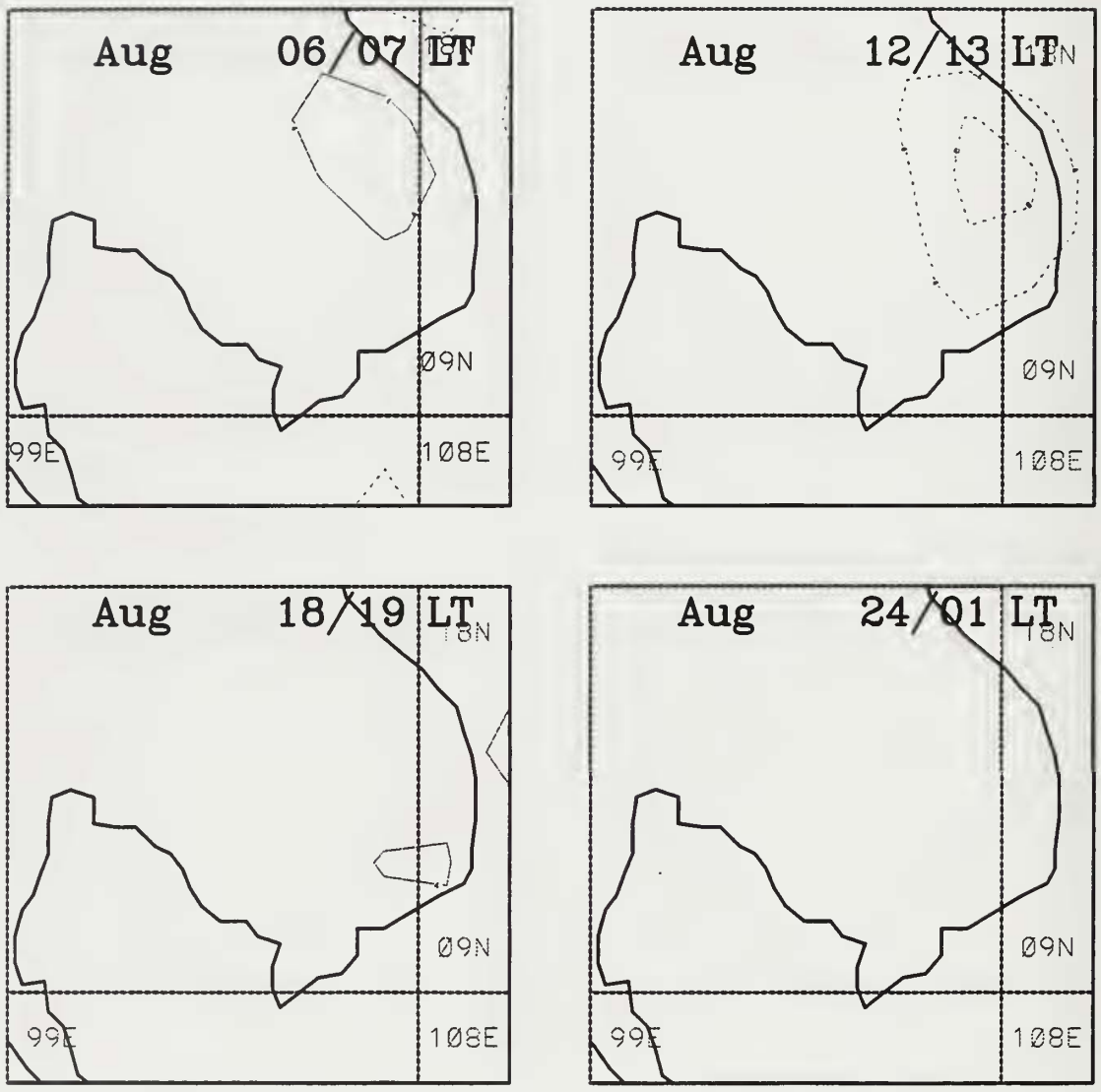

Figure 43d. As in Figure 43a except for August 1991.

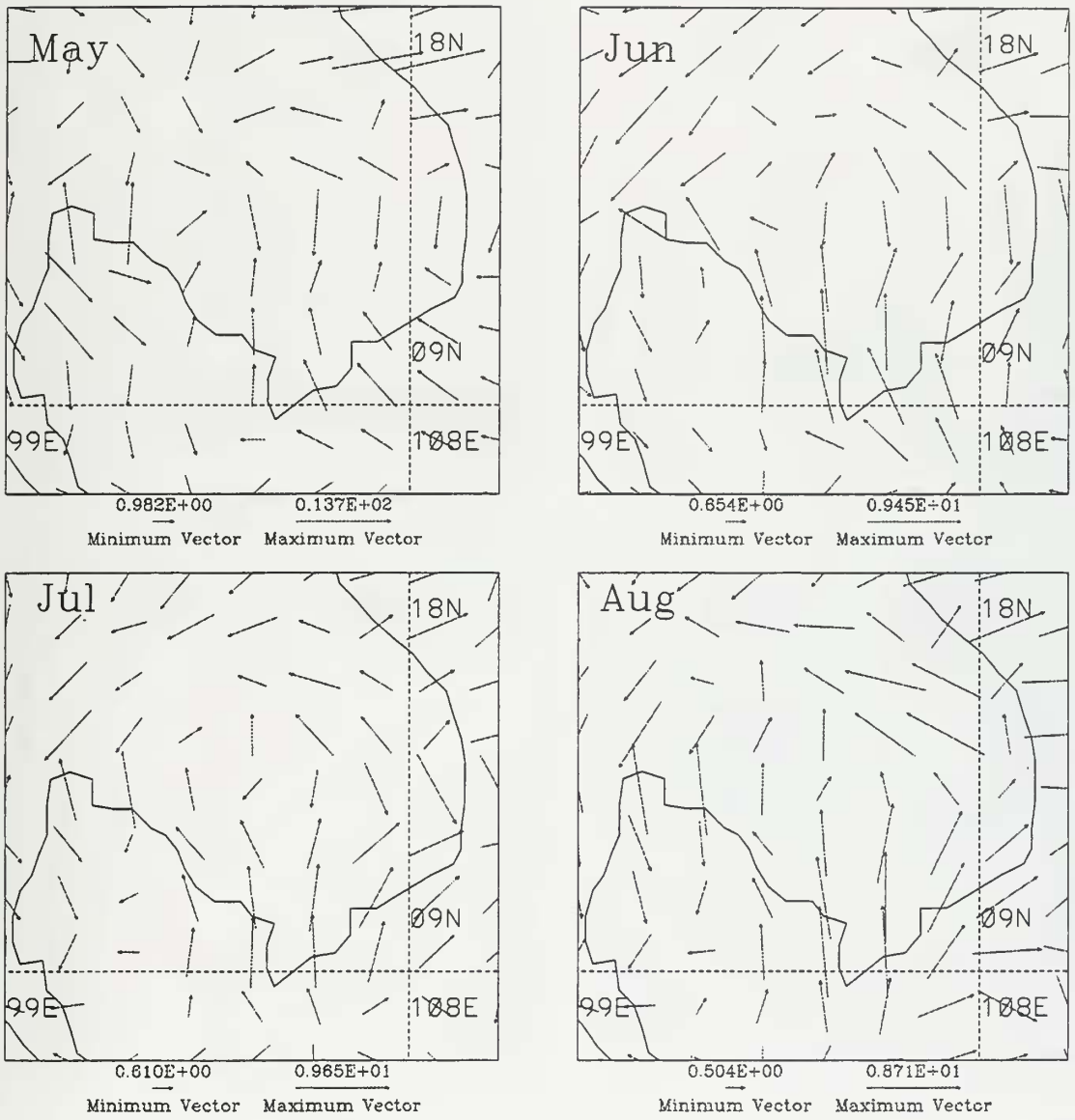

Figure 44. Indochina convergence diurnal components for May, June, July and August 1991. Phase and amplitude are represented in vector form based on a 24 hour clock with 12 midnight pointing north. All times are local time. Vector length indicates magnitude of convergence (-D850).

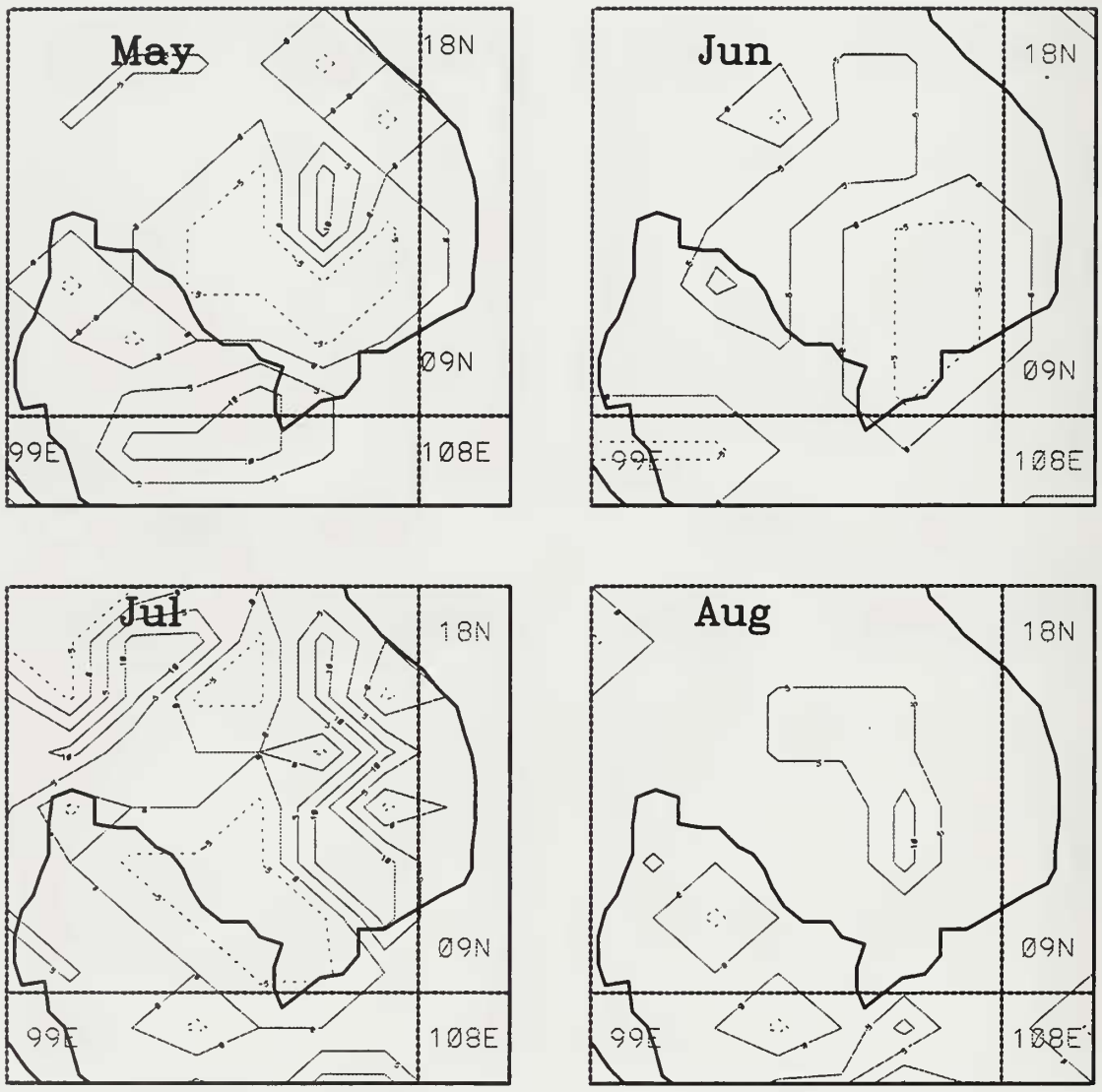

Figure 45. Indochina Phase relationship between 850 hPa convergence and CI greater then 10 °K for May, June, July and August 1991. Contour interval is 5 hours. Positive (negative) values are solid (dashed). Values less (greater) than -5 (+5) indicate convergence leads (lags) convection. Values >5 indicate convergence and convection are in phase. Values >10 indicate convergence and convection are out of phase.

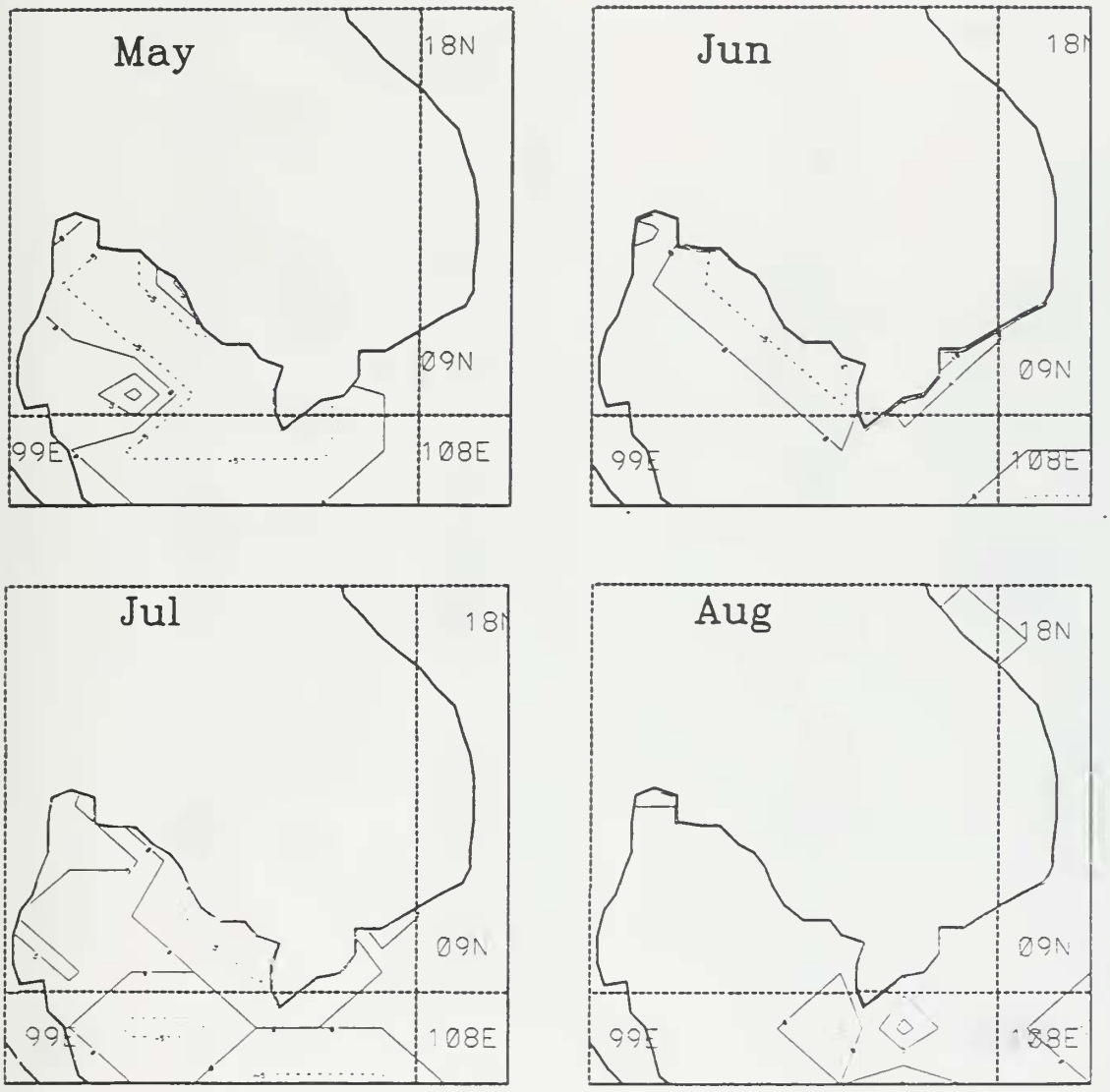

Figure 46. As in Figure 34 except the relationship is between latent heat flux and CI greater than 10 °K.

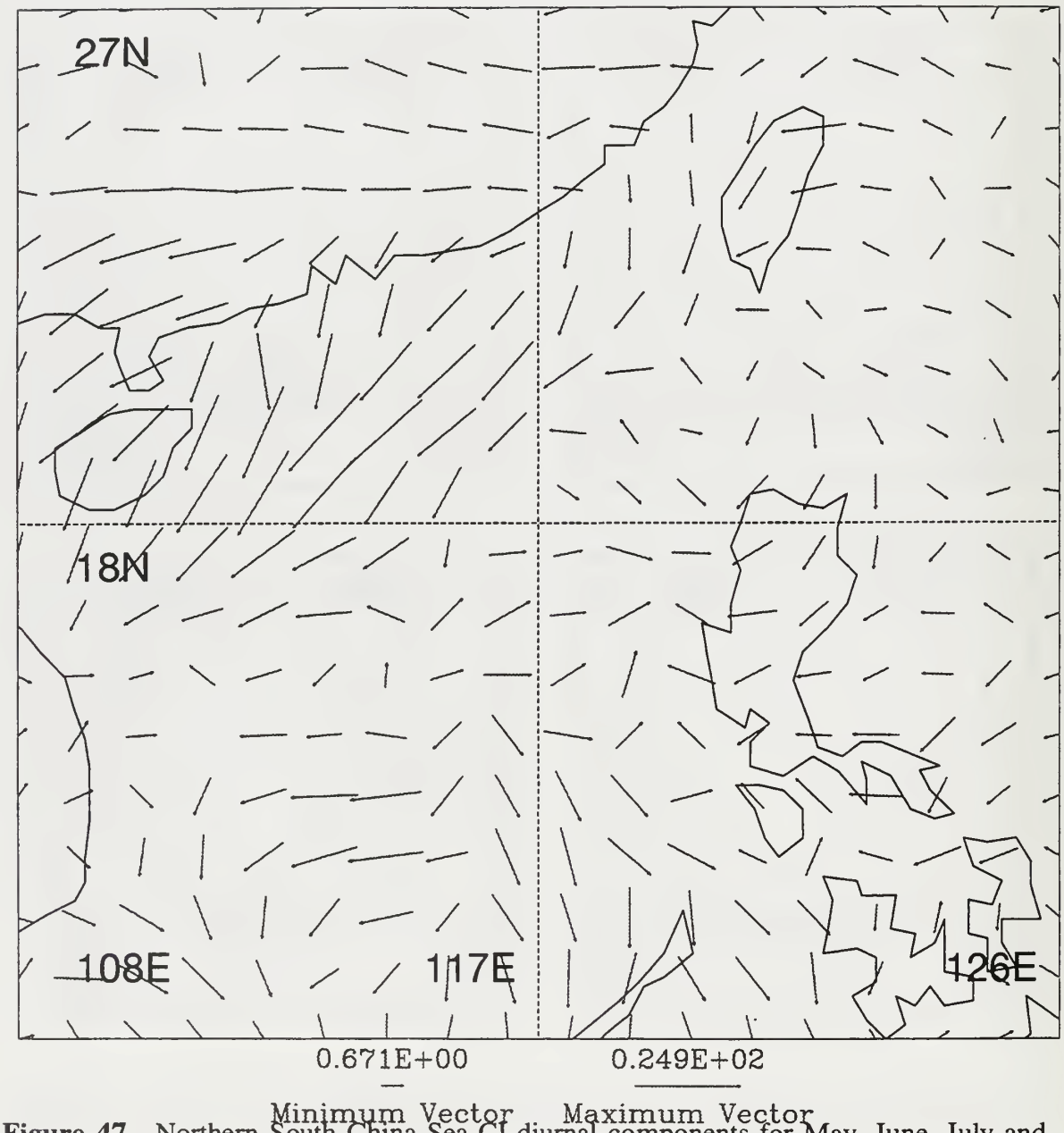

Figure 47. Northern South China Sea CI diurnal components for May, June, July and August 1991. Phase and amplitude are represented in vector form based on a 24 hour clock with 12 midnight pointing north. All times are local time. Vector length indicates magnitude of CI.

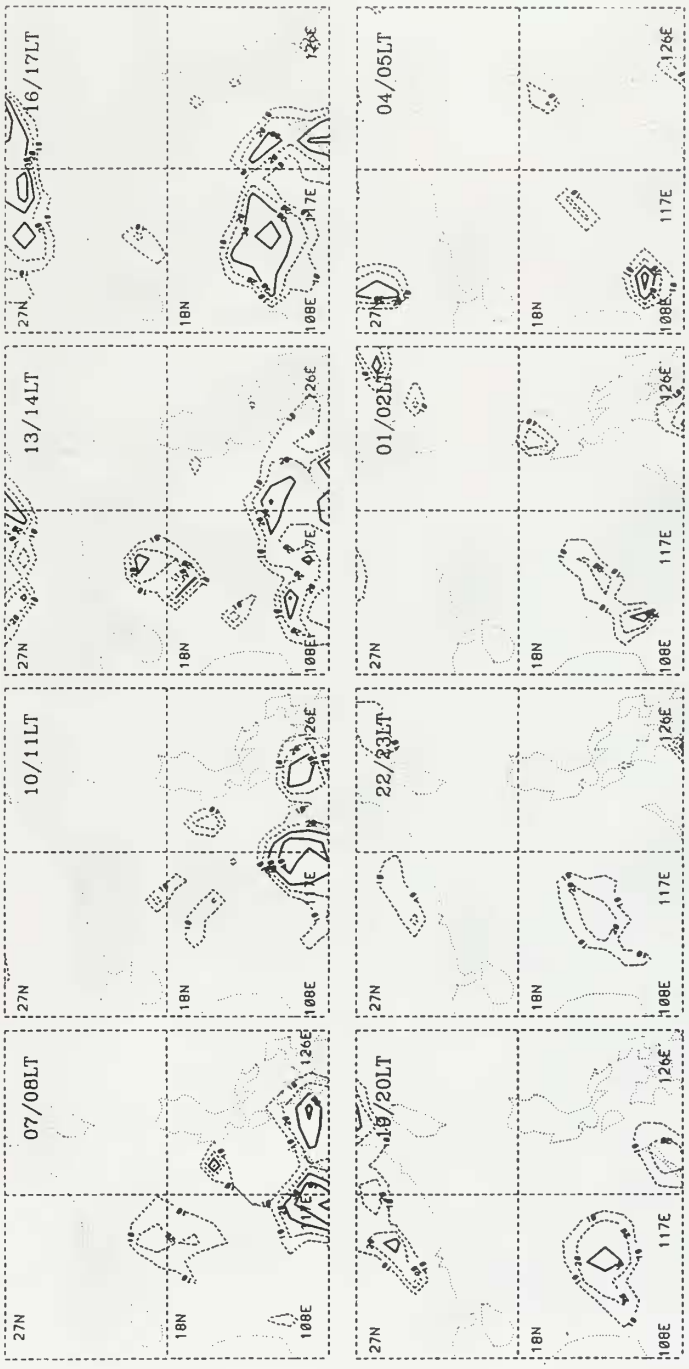

Figure 48a. Northern South China Sea three-hourly CI for June 6,1991. Contour interval is 10 °K. Contours greater (less) than 25 °K are solid (dashed).

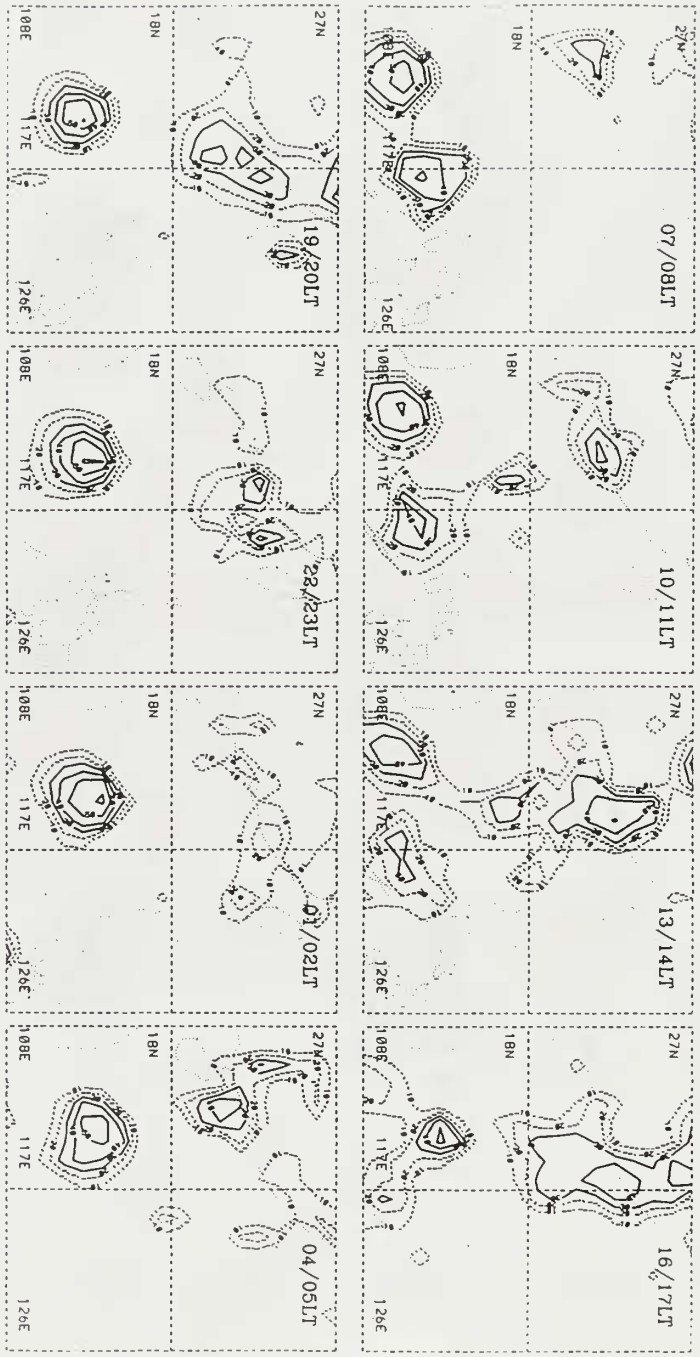

Figure 48b. As in Figure 48a except for June 8 .

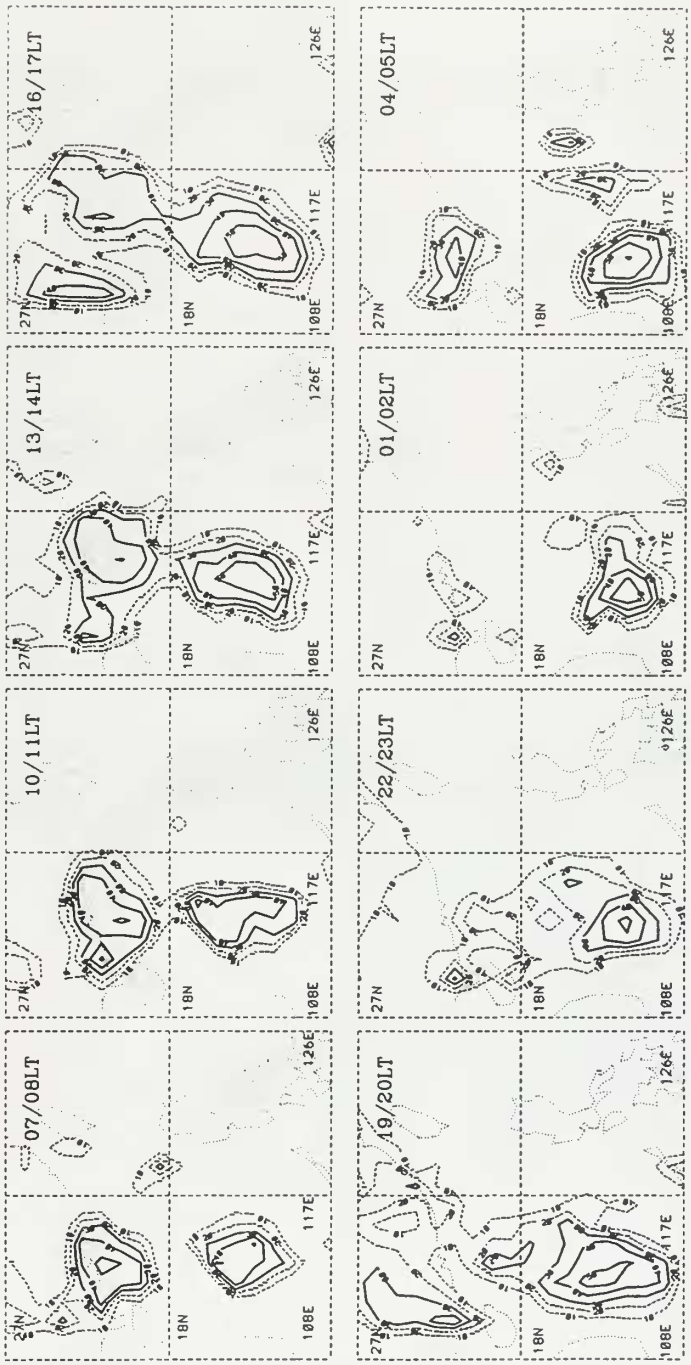

Figure 48c. As in Figure 48a except for June 9 .

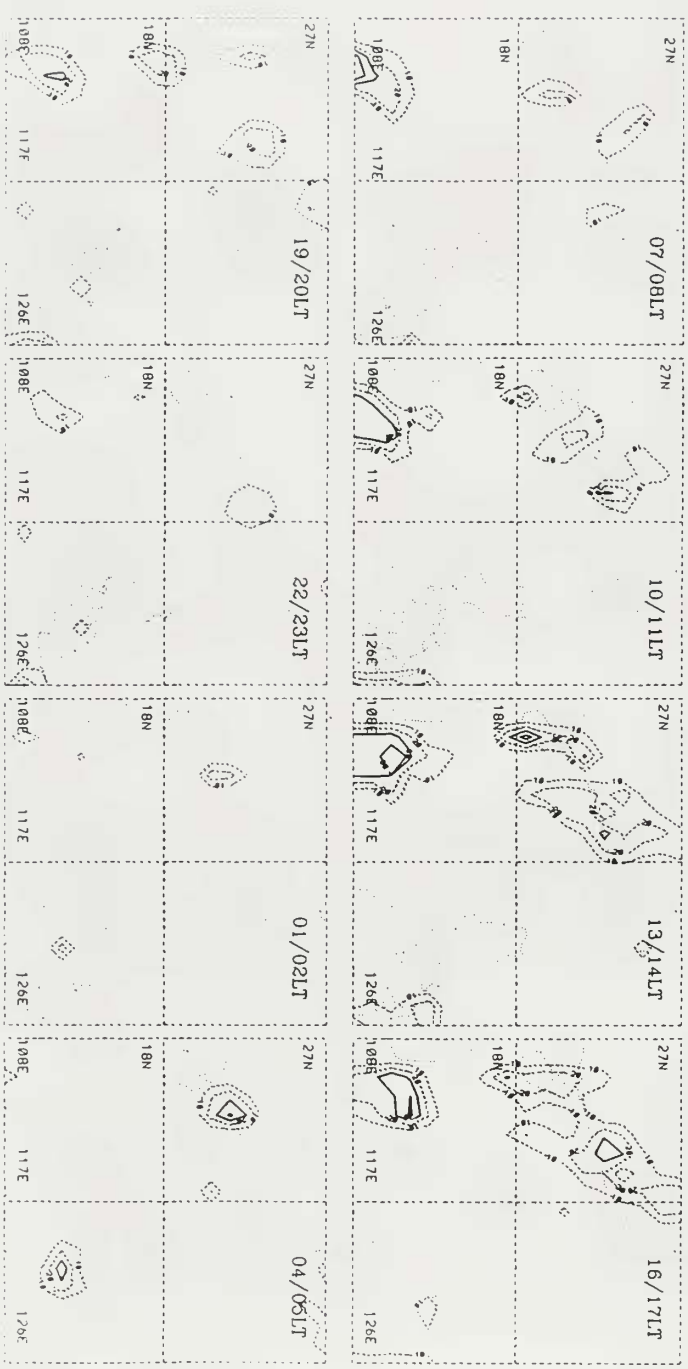

Figure 48d. As in Figure 48a except for June 11 .

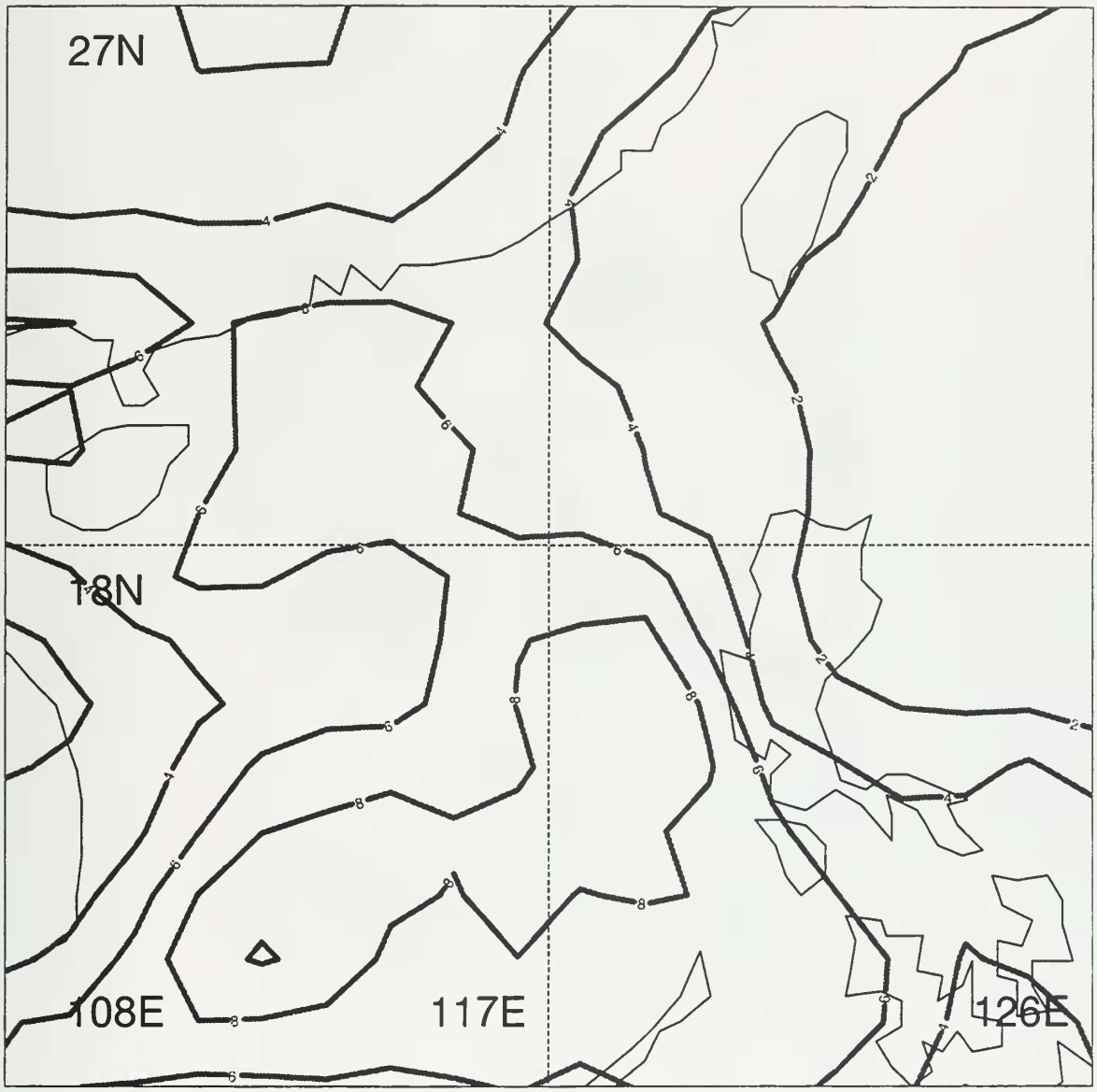

Figure 49. Northern South China Sea monthly mean convective Index (CI) for June 1991. Contour interval is 2 °K.

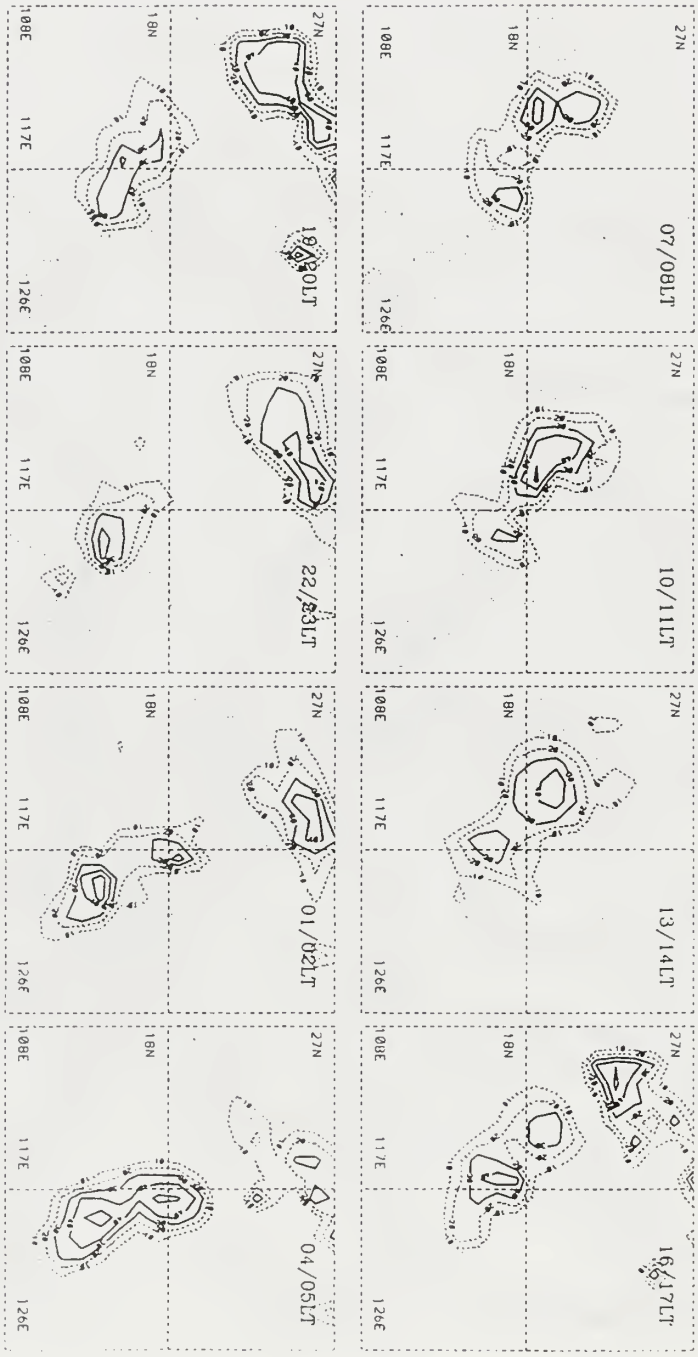

Figure 50a. Case II. Same as Figure 48a except for June 19, 1991.

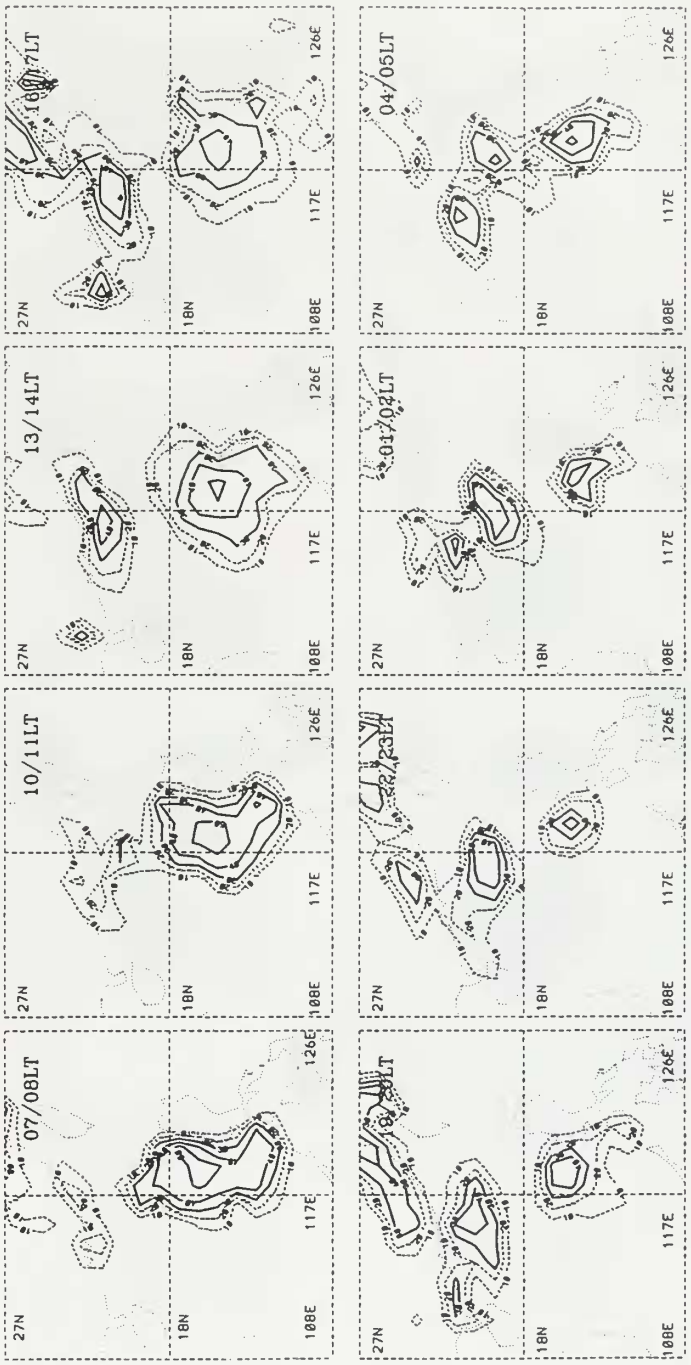

Figure 50b. As in Figure 50a except for June 20.

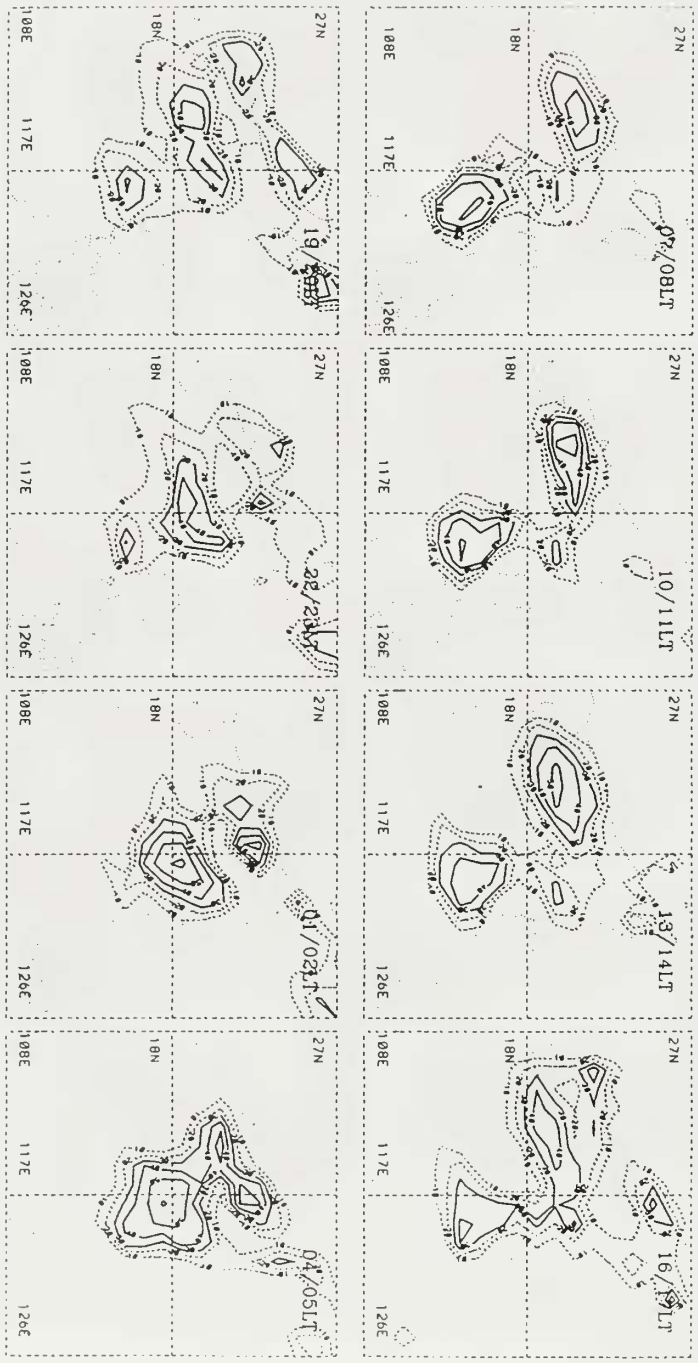

Figure 50c. As in Figure 50a except for June 21.

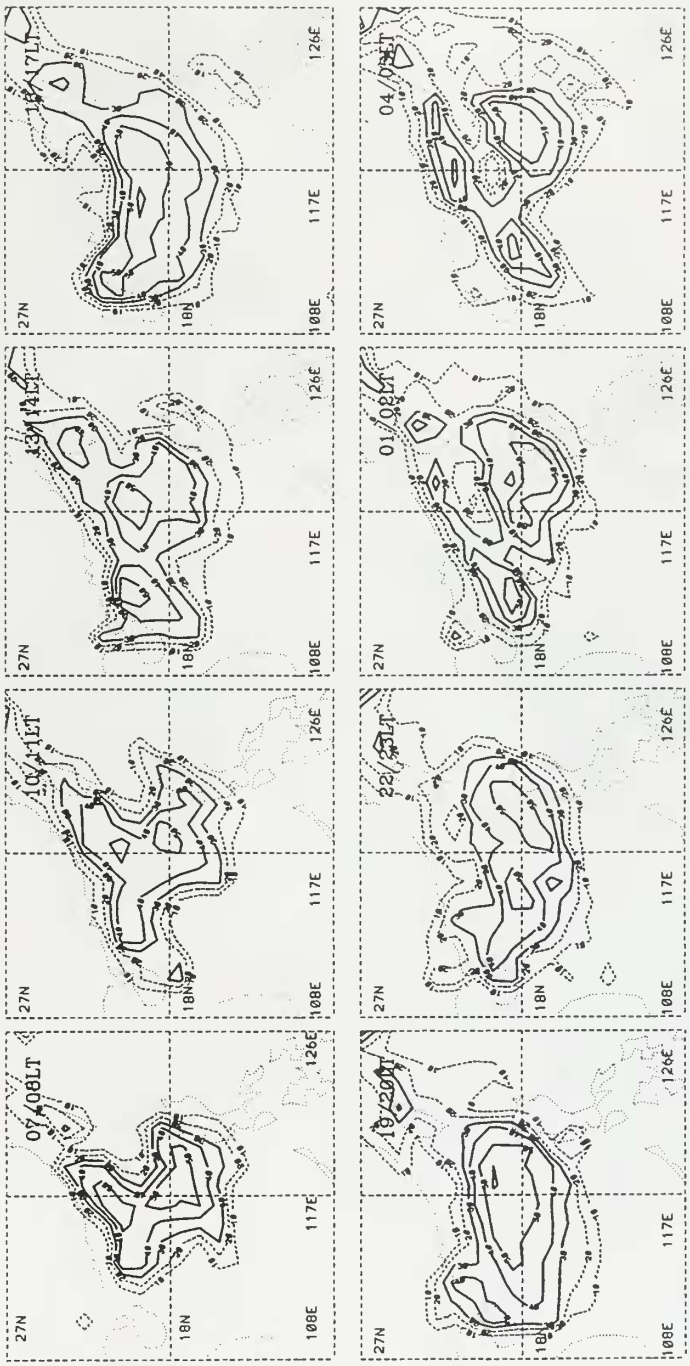

Figure 50d. As in Figure 50a except for June 22.

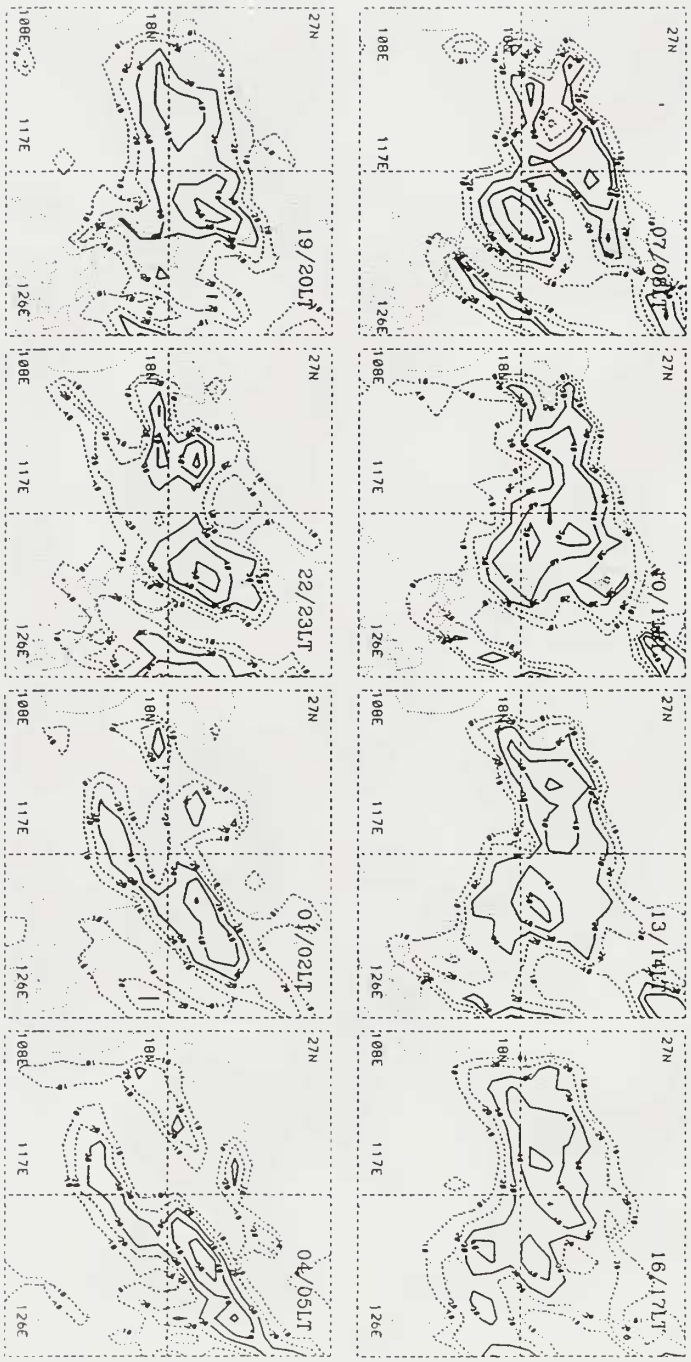

Figure 50e. As in Figure 50a except for June 23.

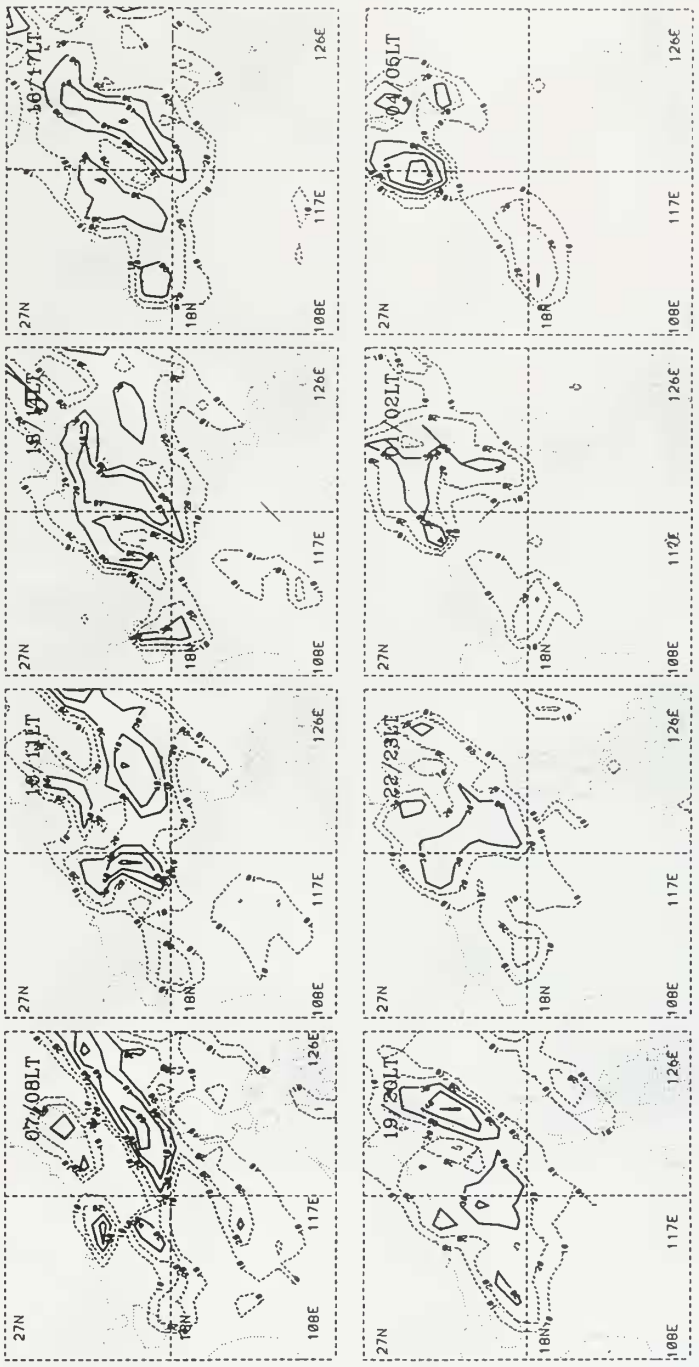

Figure 50f. As in Figure 50a except for June 24.

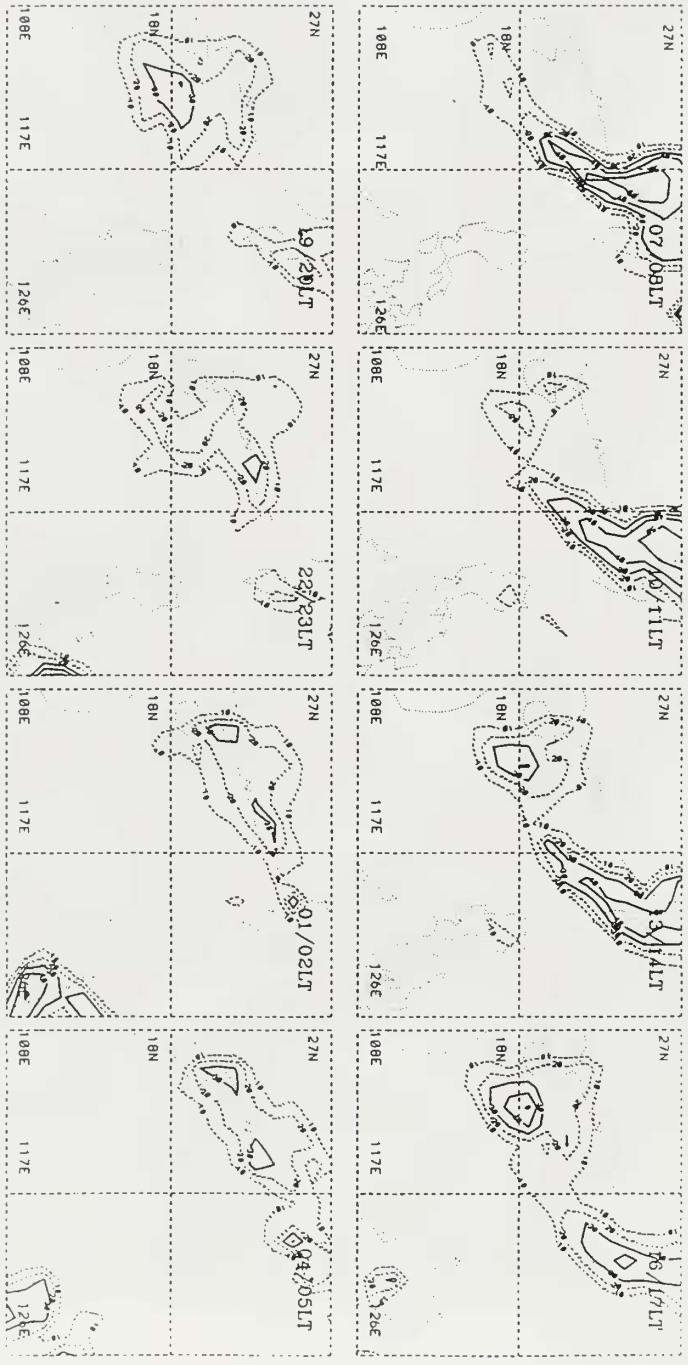

Figure 50g. As in Figure 50a except for June 25.

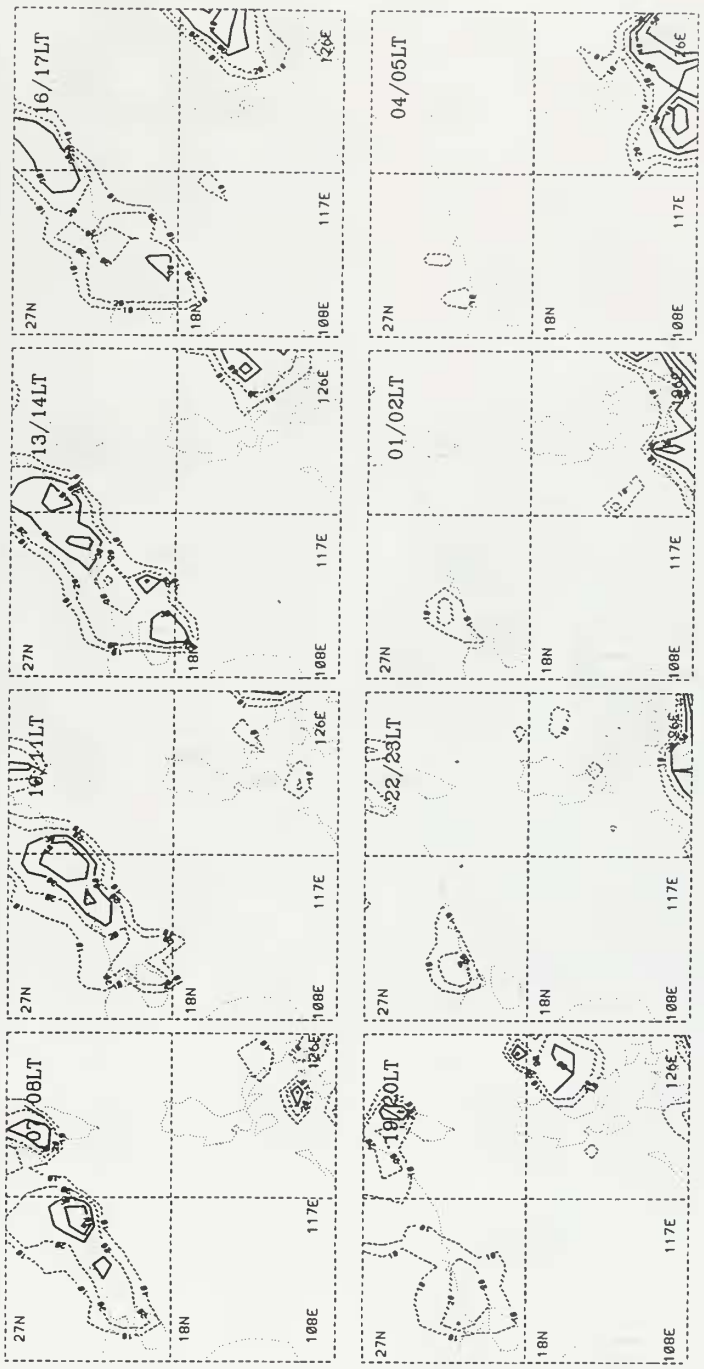

Figure 50h. As in Figure 50a except for June 26.

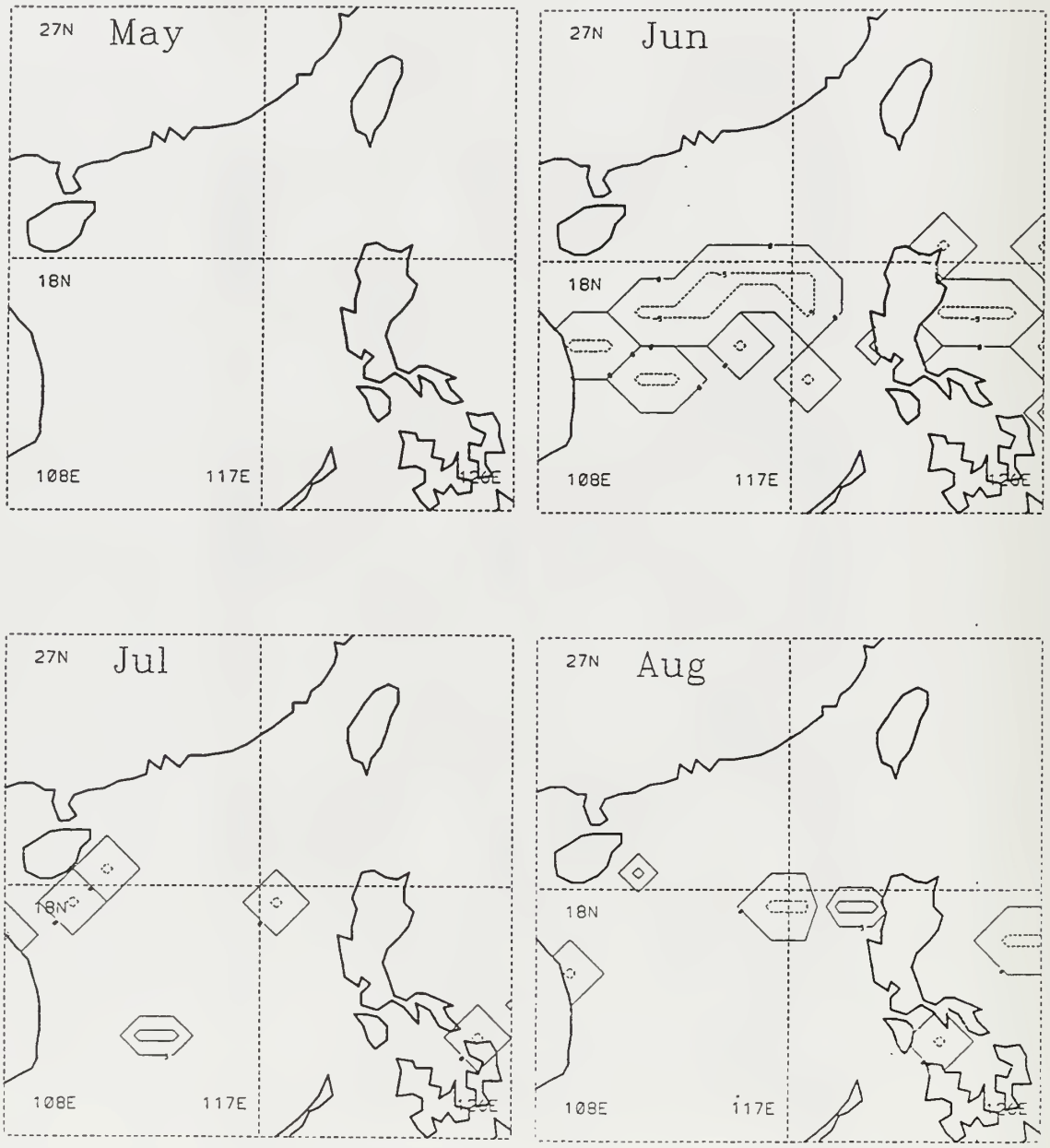

Figure 51. No. SCS Phase relationship between latent heat flux and CI greater then 10 °K for May, June, July and August 1991. Contour interval is 5 hours. Positive (negative) values are solid (dashed). Values less (greater) than -5 (+5) indicate flux leads (lags) convection. Values >5 indicate flux and convection are in phase. Values >10 indicate flux and convection are out of phase.

Month/Area	Points with CI>10 °K	Conv Leads	Conv In Phase	Conv Lags	Conv Out of Phase
May					
West India	40	19	5	8	8
Bay of Bengal	49	11	17	9	12
Indochina	41	13	14	7	7
June					
West India	106	27	34	27	18
Bay of Bengal	79	32	39	19	5
Indochina	40	11	15	12	2
N. S. China Sea	37	14	18	0	5
July					
West India	57	17	12	11	17
Bay of Bengal	76	21	34	18	3
Indochina	53	23	11	6	13
August					
India	20	1	6	10	3
Bay of Bengal	105	32	30	37	6
Indochina	27	5	10	9	3

Table 1. Summary of 850 hPa convergence lead/lag statistics indicating number of grid points where low-level convergence leads, is in phase with, lags, or is out of phase with CI when CI is greater than 10 °K.

Month/Area	Points with CI> 10 °K	Flux Leads	Flux In Phase	Flux Lags	Flux Out of Phase
May					
West India	17	2	4	9	2
Offshore India	9	0	0	5	4
Bay of Bengal	16	8	6	1	1
Indochina	16	10	5	0	1
June					
West India	58	12	30	15	1
W. Bay of Bengal	35	15	16	4	0
E. Bay of Bengal	7	0	6	0	1
Indochina	12	8	4	0	0
N. S. China Sea	32	9	18	0	5
July					
West India	5	0	2	2	0
W. Bay of Bengal	39	18	19	1	1
E. Bay of Bengal	19	6	7	6	0
Indochina	22	9	9	4	0
August					
India	0	0	0	0	0
W. Bay of Bengal	29	21	8	0	0
E. Bay of Bengal	20	16	4	0	0
Indochina	9	3	5	0	1
N. S. China Sea	6	4	2	0	0

Table 2. As in Table 1 except statistics are for the relationship between latent heat flux and CI when Ci is greater than 10 °K.

VII. SUMMARY AND CONCLUSIONS

The primary focus of this study has been to document the diurnal cycle of convection around the Indian sub-continent, Bay of Bengal, Indochina peninsula and South China Sea. Additionally, low-level divvergence and latent heat fluxes were computed to determine their relationship with active convection.

Using the combined GMS and INSAT high resolution (1° x 1°, eight times daily) infrared data set, a convective index (CI) was derived from the black body temperature to analyze the monthly mean and diurnal variation of convective activity over the Indian monsoon region. The satellite data is used with 850 hPa wind data from ECMWF global re-analyses available four times daily on a 1.125° x 1.125° grid. Sea surface temperature data available from NCEP, produced weekly on a 1° x 1° grid, was used with temperature, relative humidity, and surface wind fields from the ECMWF data set to derive latent heat fluxes. All data and derived fields are optimally interpolated in space to match the grid points of the ECMWF data set.

The results in most areas show that the diurnal variation of convection follows the basic land-sea breeze model. Convection over land is prevalent during the afternoon and evening as the land heats up and the sea breeze begins. Coastal convection is mostly an early morning phenomenon in response to a reversal of the pressure gradient and associated land breeze. Oceanic convection mostly prevails in the late morning and early afternoon as it too,

heats in response to solar radiation. In addition, local topography/coastline geometry and large-scale flow can modify the classic model.

Asnani (1993) discussed the diurnal variation of precipitation along the west coast of India during the northern summer monsoon, where maximum rainfall activity during late night and early morning was notable. He pointed out that the land breeze and downslope flow of the western Ghats oppose the low-level westerly monsoon winds and produces a convergence to give this coastal maximum. Our results show that while the land breeze and downslope winds do exist, the development of this coastal diurnal activity does not depend on the westerly monsoon wind. The late night and early morning low-level convergence due to the opposing westerly winds and the land breeze and downslope flow exists in July and may indeed enhance the coastal convection, but the westerly winds do not exist in pre-monsoon May and early June 1991 when the diurnal convection system was observed.

Rather, the coastal convection at night during May seems to be a result of the passage of a synoptic-scale convective system that diurnally develops in the interior of the Indian subcontinent in the afternoon due to maximum surface heating. After development, the convection is organized into a synoptic scale disturbance and the motion system is advected by the lower-middle to middle tropospheric winds to the west. This results in a westward propagation of the diurnal convection peaks towards the southeastern Arabian Sea/northern equatorial Indian Ocean. A similar propagation pattern is observed in June. Although in June the monthly mean lower and middle tropospheric winds are westerly in the southern India and equatorial Arabian Sea region, our inspection of the animation loops of the diurnal CI

anomalies show that the westward propagation occurs only in the first half of June, prior to onset of the monsoon.

Nitta and Sekine (1994) and Chen and Takahashi (1995) noted that the Bay of Bengal is a diurnally active region of complicated land-sea breeze circulations. Our results for 1991 support their studies. The most active regions are the western coast of the bay, the central bay, the Gulf of Martaban and the Andaman Sea. Overall, the convection over land generally peaks later and farther northeast with the prevailing southwesterly flow. Convective activity during May is moderate except for the Andaman Sea which follows the land sea model. The phase shift in this area is a result of large scale flow enhancing the land breeze. In June, The Gulf of Martaban follows the model but the west coast of the bay and Andaman Sea are both subject to convergence between the large-scale flow and the land breeze. Offshore migration over the head of the bay, from north to south is only seen in July when the large-scale flow enhances the land breeze. The Gulf of Martaban continues to follow the classic land sea model and the Andaman Sea is still subject to convergence. The winds change in August and the land breeze is enhanced by the large-scale flow over the Gulf of Martaban and the Andaman Sea is under a zone of convergent winds (the land breeze is not involved) over the open ocean.

Maximum CI over land is explained by southwesterly flow enhancing the sea breeze during the afternoon in all months but July when the winds were southerly, slightly weakening the onshore flow. The most complex area is the Gulf of Martaban/Andaman Sea due to the coastal geometry and topography modifying the diurnal convection. Generally speaking, the

entire domain can be described as complicated land-sea breeze domain in which convection occurs over land during afternoon and late evening, over coastal regions in early morning and over open ocean during late morning and early afternoon. The prevailing southwesterly monsoon flow and complex coastline and topography interact, providing two mechanisms for oceanic convection. The first mechanism is simply an enhancement of the land breeze that advects the convection off shore. The second mechanism is the convergence of the land breeze and opposing, prevailing large-scale flow. This mechanism was also proposed by Houze et al. (1981). Inspection of the animated satellite imagery shows the southward migration from the Gulf of Martaban is dominant.

The Indochina peninsula follows the land-sea breeze model as far as afternoon heating over land is concerned. The associated convection over the surrounding coasts is moderate. The Gulf of Thailand is the area of strong diurnal activity. This narrow body of water lies between the Indochina peninsula and the Malay peninsula, two strong land-sea breeze regimes within a small area. Since the southwestern monsoon flow is prevalent, it tends to enhance the land breeze off the Malay coast and oppose the land breeze from the Indochina coast, resulting in convergence and convective activity. The animated satellite imagery indicates several different flow directions. The most dominant pattern is convection over the Indochina peninsula moving west, then south over the Gulf of Thailand. There are also periods when convection moves eastward off the Malay peninsula and then southward over the Gulf. A mesoscale model is required to study the wind effects in this area since the resolution of the ECMWF data is far too coarse over this limited domain.

Overall, the quality of the ECMWF 850 hPa analysis is insufficient to detect a strong diurnal cycle that corresponds with the CI data. The primary reason is lack of radiosonde data over large open ocean regions and sparsely populated land areas. Since most of the convection within the coastal regime is a mesoscale phenomenon, circulations of interest are difficult to identify in large-scale wind fields. It is even more difficult to identify the diurnal cycle in divergence. Mean divergence fields were often in better agreement with mean CI fields than their diurnal counterparts. Although we found a weak to moderate diurnal signal in the divergence fields, there was rarely any realistic, corresponding convection. Thus, it appears that he diurnal signal we observed was more a result of model physics. For example, there were numerous cases where afternoon convergence was prevalent inland from the coast where intense afternoon heating is expected, but not always observed.

However, there were several instances in which convergence (often very weak), did occur prior to, or at the same time as intense convection over 10°K. These phase relationship statistics between low-level convergence and strong convection are summarized in Table 1. This table shows that low-level convergence often leads or coincides with the diurnal cycle of CI. This is consistent with the view that deep clouds with expanding cirrus continue to develop for a few hours after low-level convergence reaches a maximum

The influence of the strong southwesterly flow on evaporation is clearly seen in the relationship between latent heat fluxes and strong convective activity. The phase relationship statistics between latent heat flux and strong convection are summarized in Table 2. Latent heat fluxes generally lead or coincide with the diurnal cycel of CI in most of the areas except

for west India. It appears that wind has the strongest influence on the fluxes, although sea surface temperatures definitely play a role. SST variations can influence convective activity by modifying stability and the land sea temperature contrast. The sea surface temperatures may also respond to the convection as seen in June where the cooler SST was located below the area of maximum mean convection.

It is interesting to note that the lead/in-phase percentage is quite low over the west India sub-region during May as the prevailing winds are northerly and the monsoon onset has not yet occurred. Percentages are substantially higher in the other two sub-regions which are under the influence of southwesterly flow during May.

During June, the lead/in-phase percentages are quite high and have doubled in the west India sub-region. The percentage drops off in west India during July and August since the majority of convective activity has migrated to the northeast. Note that percentages are higher over the western Bay of Bengal than over the eastern Bay and Indochina. Perhaps this is due to the winds weakening slightly as they cross the bay. However, all three percentages are quite high in August.

The lead/in-phase percentages over the northern South China Sea are high in both June, the anomalous month, and August.

These flux-convection relationships agree with previous studies showing strong latent heat fluxes were associated with strong winds and lower pressure (associated vertical motion) convection.

Our study partially supports the findings of Chen and Takahashi (1995) since the diurnal signal is significantly enhanced over the east Arabian Sea during active convection. June, July and August make up the active period for the Bay of Bengal, resulting in enhanced diurnal convection over both ocean and land. The Indochina peninsula is also active during the monsoon period, but the small size of the Gulf of Thailand prevents us from drawing any solid conclusions based on active versus inactive phases due to the complicated land-sea breeze interactions. Over the northern South China Sea, the diurnal cycle was enhanced over water during two separate periods of interaction between large-scale fronts and tropical, oceanic convection.

LIST OF REFERENCES

Albright, M.D., E.E. Recker, R.J. Reed and R. Dang, 1985: The diurnal variation of deep convection and inferred precipitation in the central tropical Pacific during January-February 1979. *Mon. Wea. Rev.* **113**, 1663-1680.

Asnani, G. C., 1993: Diurnal variation of precitiptaion. In: *Tropical Meteorology*, G. C. Asnani, Indian Institute of Tropical Meteorology, 80.

Augustine, J.A., 1984: The diurnal variation of large-scale inferred rainfall over the tropical Pacific Ocean. *Mon. Wea. Rev.* **112**, 1745-1751.

Buck, J.S., 1981: Relationship between saturation vapor pressure to temperature for moist air. *J. Appl. Meteor.*, **20**, 1527-1532.

Chen, S.S. and R.A. Houze, Jr., 1997: Diurnal variation of deep convective systems over the tropical Pacific warm pool. *Quar. J. Royal Meteor. Soc.*, submitted.

Chen, T.-C, and K. Takahashi, 1995: Diurnal variation of outgoing longwave radiation in the vicinity of the South China Sea: Effect of intraseasonal oscillation. *Mon. Wea. Rev.* **123**, 566-577 .

Cornejo-Garrido, A.G. and P.H. Stone, 1977: On the heat balance of the Walker circulation. *J. Atmos. Sci.* **34**, 1155-1162.

Garratt, J.R., 1977: Review of drag coefficients over oceans and continents. *Mon. Wea. Rev.* **105**, 915-929.

Gray, W.M. and R.W. Jacobson, Jr., 1977: Diurnal variation of oceanic deep cumulus convection. *Mon. Wea. Rev.* **105**, 1171-1188.

Houze, R. A., Jr., S.G. Geotis, F.D. Marks and A.K. West, Jr., 1981: Winter monsoon convection in the vicinity of north Borneo. Part I: Structure and time variation of the clouds and precipitation. *Mon. Wea. Rev.* **109**, 1595-1614.

Kondo, J., 1975: Air-sea bulk transfer coefficients in diabatic conditions. *Bound. Layer Meteor.* **9**, 91-112.

McGarry, M.M., and R.J. Reed, 1978: Diurnal variations in convective activity and precipitation during Phases II and III of GATE. *Mon. Wea. Rev.* **106**, 101-113.

Murakami, M., 1983: Analysis of deep convective activity over the western Pacific and Southeast Asia. Part I: Diurnal variation. *J. Meteor. Soc. Jap.* **61**, 60-76.

Murakami, M., T. Inoue, N. Yamazaki, T. Nakazawa, H. Okamura, K. Takahashi and T. Harada, 1995: Study on air-sea-land interactions and their long-term variations. In: *Japanese Experiment on Asian Monsoon (JEXAM) Annual Report (April 1994-March 1995)*, Research and Development Bureau, Science and Technology Agency Japan, 13-19.

Murakami, M., T. Inoue, N. Yamazaki, K. Takahashi, T. Nakazawa and M. Tanaka, 1996: Analysis on the large scale convective activity and precipitation systems. In: *Japanese Experiment on Asian Monsoon (JEXAM) Annual Report (April 1995-March 1996)*, Research and Development Bureau, Science and Technology Agency Japan, 15-25.

Nitta, T., 1983: Observational study of heat sources over the eastern Tibetan Plateau during the summer monsoon. *J. Meteor. Soc Japan*, **61**, 606-618.

Nitta, T. and S. Sekine, 1994: Diurnal variation of convective activity over the tropical western Pacific. *J. Meteor. Soc Japan*, **72**, 627-641.

Oki, T. and K. Musiake, 1994: Seasonal changes of the diurnal cycle of precipitation over Japan and Malaysia. *J. Appl. Meteor.*, **58**, 448-461.

Pisharoty, P.R., 1965: Evaporation from the Arabian Sea and the Indian southwest monsoon. In: *Proceedings of the international symposium on meteorological results of the International Indian Ocean Expedition, Bombay India, 22-26 July 1965.* Kurawamis and Dumas, eds., Bombay Univ. Press. 43-54.

Pisharoty, P.R., 1981: Sea surface temperature and monsoon. In: *Monsoon Dynamics.* Lighthill and Pearce, eds., Cambridge Univ. Press. 238-251.

Ramage, C.S. and A.M. Hori, 1981: Meteorological aspects of the El Nino. *Mon. Wea. Rev.*, **109**, 1827-1835.

Rao, R.R., K.V. Sunderaramam, M.R. and M.R. Santa Devi, 1981: The energy budget at selected stations over the north Indian Ocean during Monsoon-77. In: *Monsoon Dynamics.* Lighthill and Pearce, eds., Cambridge Univ. Press. 509-521.

Rasmussen, E.M. and T.H. Carpenter, 1982: Variations in tropical sea surface temperature and surface wind fields associated with the Southern Oscillation/El Nino. *Mon. Wea. Rev.*, **110**, 354-384.

Reynolds, R.W. and D.C. Marsico, 1993: An improved real-time global sea surface temperature analysis. *J. Climate,* **6**, 114-119.

Reynolds, R.W., 1988: A real-time global sea surface temperature analysis. *J. Climate,* **1**, 75-86.

Rudolph, D.K. and C.P. Guard, 1991: Northern Indian Ocean Tropical Cyclones. In: *1991 Annual Tropical Cyclone Report of the Joint Typhoon Warning Center*. Rudolph and Guard, eds., National Technical Information Service Press. 150-158.

Schlatter, T.W., 1975: Some experiments with a multivariate statistical objective analysis scheme. *Mon. Wea. Rev.*, **103**, 246-257.

Wyrtki, K., 1965: Average annual heat balance of the north Pacific ocean and its relation to ocean circulation. *J. Geo. Res.*, **70**, 4547-4559.

Yasunari, T., 1979: Cloudiness fluctuations associated with the Northern Hemisphere summer monsoon. *J. Meteor. Soc. Jap.*, **57**, 227-262.

INITIAL DISTRIBUTION LIST

No. of copies

1. Defense Technical Information Center 2
   8725 John J. Kingman Rd.,STE 0944
   Ft. Belvoir, Virginia 22304-6145

2. Dudley Knox Library 2
   Naval Postgraduate School
   411 Dyer Rd.
   Monterey, California 93943-5101

3. Chairman (Code MR/Wx) 1
   Department of Meteorology
   Naval Postgraduate School
   Monterey, California 93943-5000

4. Chairman (Code OC/Bk) 1
   Department of Oceanography
   Naval Postgraduate School
   Monterey, California 93943-5000

5. Prof. Chih-Pei Chang (Code MR/Cp) 1
   Department of Meteorology
   Naval Postgraduate School
   Monterey, California 93943-5000

6. Prof. Peter Chu (Code OC/Cu) 1
   Department of Oceanography
   Naval Postgraduate School
   Monterey, California 93943-5000

7. LT Greg M. Jimenez 2
   503 Belem Drive
   Chesapeake, VA 23320